Application of microwave plasma technology to convert CO_2 into high value products

Fernandez de la Fuente, Javier

DOI
10.4233/uuid:bed854a8-e4bc-4d23-b90c-00d68c5f6517

Publication date
2017

Document Version
Final published version

Citation (APA)
Fernandez de la Fuente, J. (2017). *Application of microwave plasma technology to convert CO_2 into high value products*. [Dissertation (TU Delft), Delft University of Technology].
https://doi.org/10.4233/uuid:bed854a8-e4bc-4d23-b90c-00d68c5f6517

Application of microwave plasma technology to convert CO_2 into high value products

Proefschrift

ter verkrijging van de graad van doctor
aan de Technische Universiteit Delft,
op gezag van de Rector Magnificus prof. ir. K.C.A.M. Luyben,
voorzitter van het College voor Promoties,
in het openbaar te verdedigen op donderdag 16 november om 15:00 uur

door

Javier F. DE LA FUENTE
Master of Science in Chemical Engineering
University of Valladolid, Spain
geboren te Valladolid, Spain

This dissertation has been approved by the promotors:
Prof. Dr. Ir. A. I. Stankiewicz and **Prof. Dr. Ir. G. D. Stefanidis**

Composition of the doctoral committee:

Rector Magnificus	Chairman
Prof. Dr. Ir. A.I. Stankiewicz	Delft University of Technology, promotor
Prof. Dr. Ir. G.D. Stefanidis	KU Leuven, promotor

Independent members:

Prof. Dr. Ir. M.C.M. van de Sanden	University of Eindhoven/DIFFER
Dr. J. Lang	Evonik Industries, Germany
Prof. Dr. Ir. M. Jasinski	Polish Academy of Sciences, Poland
Prof. Dr. D.J.E.M. Roekaerts	Delft University of Technology
Prof. Dr. Ir. W. de Jong	Delft University of Technology (reserve member)

Other members:

Prof. Dr. Ir. A.A. Kiss	University of Twente/AkzoNobel

ISBN: 978-94-6299-761-5

The research was carried out within the European Community's Seventh Framework Programme under grant agreement no. FP7-NMP-2012-309874 and the project "ALTEREGO: Alternative Energy Forms for Green Chemistry".

Cover designed by Javier Fernandez & Alexandra Arranja

Published by Javier F. de la Fuente, Delft

Printed in The Netherlands by Ridderprint

[1]Author email address: javier.f.delafuente@gmail.com

Dedicated to my beloved parents Angel & Julia

my brother Jesus Manuel and my sister Mª Angeles

and especially to my soulmate Alexandra Arranja

Angel y Julia, estaré eternamente agradecido por todo lo que habéis hecho por mí, os quiero mucho y siempre estaréis en mi corazón.

CARPE DIEM

Summary

The global energy challenges along with global warming are regarded as the most important issues faced by humankind in the 21st century. A fossil fuels-based energy economy cannot support the rapidly increasing world energy demand in a sustainable manner. Hence, the development and implementation of alternative solutions to the use of fossil fuels have become a top priority for goverments, industries and academia. In this regard, a collaborative project (ALTEREGO) – funded by the European Union with the involvement of four industrial partners and four academic institutions, was carried out to develop novel forms of energy for intensified chemical manufacturing. In this thesis, the application of microwave plasma technology to convert carbon dioxide (CO_2) into added-value products was studied with a twofold purpose: the storage of electricity into chemicals and the chemical recycling of CO_2.

This thesis is divided into four different sections where fundamental and engineering aspects of microwave plasma and its application to CO_2 transformation are investigated. The first section tries to determine whether microwave plasma reactors can outperform conventional thermal chemical reactors, particularly when CO_2 is part of the feedstock. The second section explores further optimization of microwave plasma reactors by combining experimental and modelling work. The third section tackles the problem of implementation of complex kinetic models, exemplified for CO_2 dissociation, into multidimensional multiphysics simulations. The last section discusses scale up of microwave plasma technology, potential applications in the chemical industry and the milestones on the way to implementation of the technology to commercial scale.

In this doctoral work, a bench-scale microwave plasma reactor was built to investigate two key chemistries: the reduction of CO_2 with hydrogen (H_2) and the splitting of pure CO_2. In *Chapter 2*, we prove that microwave plasma can outperfom conventional thermal reactors; a chemical CO_2 conversion as high as ~80% was attained under microwave plasma conditions, compared to ~60% via thermal processes. High microwave power input, high H_2 content in the feed and low operating pressure favoured the attaitment of high CO_2 conversions. *Chapter 3* shows that two-dimensional multiphysics models with simple chemistries (e.g. argon) allow to study different reactor configurations in order to find the optimum performance.

Thus, modelling results were used to develop a modified downstream section of the microwave plasma reactor that led to the improvement of chemical CO_2 conversion (from 40 to 60%) at low H_2 content in the feed, which is beneficial given the current limited scalability of the microwave plasma technology. In *Chapter 4*, a new simplification approach of state-to-state kinetic models in microwave plasma conditions is presented for the CO_2 molecule. By means of chemical lumping, significant reduction in the number of species and reactions, 13 and 44 respectively, was achieved as opposed to its benchmark state-to-state kinetic model that required about 100 species and 10000 reactions. Lastly, *Chapter 5* summarizes the current state-of-the-art applications of the microwave plasma technology, along with the existing possibilities for scale up. Additionally, a detailed description of the scientific and engineering challenges towards the commercialization of this technology is given. In the last chapter (*Chapter 6*), the major conclusions of the project are summarized and recommendations for continuation of the research are provided.

Samenvatting

De energie uitdagingen in de wereld samen met de opwarming van de aarde worden beschouwd als de belangrijkste problemen die de mensheid in de 21e eeuw geconfronteerd heeft. Een economie op basis van fossiele brandstoffen kan niet op een duurzame wijze de snel groeiende vraag naar energie ondersteunen. Om deze reden hebben de ontwikkeling en implementatie van alternatieve oplossingen voor het gebruik van fossiele brandstoffen, de hoogste prioriteit gekregen binnen de overheid, industrie en wetenschap. In dit verband is een samenwerkingsproject (ALTEREGO), gefinancierd door de Europese Unie met de betrokkenheid van vier industriële partners en vier academische instellingen, uitgevoerd om nieuwe vormen van energie te ontwikkelen voor de chemische industry. In dit proefschrift werd de toepassing van microgolf-plasma technologie om kooldioxide (CO_2) om te zetten in waardeproducten bestudeerd met een tweeledig doel: de opslag van elektriciteit in chemicaliën en de chemische recycling van CO_2.

Dit proefschrift is verdeeld in vier verschillende afdelingen waar fundamentele en technische aspecten van microgolfplasma en de toepassing ervan op CO_2-transformatie worden onderzocht. De eerste deel focust zich in het bepalen of microgolf-plasma reactoren beter kunnen presteren dan conventionele thermische chemische reactoren, met name wanneer CO_2 deel uitmaakt van de grondstof. In de tweede deel wordt verdere optimalisatie van microgolf-plasma reactoren onderzocht door experimenten en modellen te combineren. In het derde deel wordt het probleem van de implementatie van complexe kinetische modellen, met specifieke verheldering van CO_2-dissociatie, aangepakt in multidimensionale multiphysische simulaties. In het laatste deel wordt de opschaling besproken van de microgolf plasma-technologie, potentiële toepassingen in de chemische industrie en de mijlpalen richting de implementatie van de technologie op commerciële schaal.

In dit doctoraal rapport, werd een labschaal plasma-reactor op basis van een microgolfplasma opgebouwd om twee belangrijke chemie te onderzoeken: de CO_2-reductie met waterstof (H_2) en het splitsen van zuiver CO_2. In hoofdstuk 2 bewijzen we dat microgolfplasma de conventionele thermische reactoren kan overtreffen; Een chemische CO_2-omzetting zo hoog als ~ 80% werd bereikt onder microgolf plasma omstandigheden, vergeleken met ~

60% via thermische processen. Hoge microgolf energie invoer, hoge H_2-concentratie in de voeding en lage druk, begunstigd het behalen van hoge CO_2-conversies. Hoofdstuk 3 laat zien dat tweedimensionale multiphysica modellen met eenvoudige chemieën (bijvoorbeeld argon) gebruikt kunnen worden om verschillende reactorconfiguraties te bestuderen om zo de optimale prestatie te vinden. Zo werden modelleringsresultaten gebruikt om een gemodificeerde vervolgprocess deel van de microgolfplasma-reactor te ontwikkelen die leidde tot de verbetering van de chemische CO_2-omzetting (40 tot 60%) bij een laag H_2-gehalte in de toevoer. Dit is gunstig gezien de huidige beperkte schaalbaarheid van de microgolf plasma-technologie. In hoofdstuk 4 wordt voor het CO_2-molecuul, een nieuwe vereenvoudigingsaanpak van state-to-state kinetische modellen in microgolf-plasmaomstandigheden voorgesteld. Door middel van chemische klontering werd aanzienlijke vermindering van het aantal soorten en reacties respectievelijk 13 en 44 bereikt, in tegenstelling tot state-to-state standaard kinetische model dat ongeveer 100 soorten en 10000 reacties vereiste.

Ten slotte wordt in hoofdstuk 5 de huidige state-of-the-art toepassingen van de microgolf-plasma-technologie samengevat, samen met de bestaande mogelijkheden voor opschaling. Daarnaast wordt een gedetailleerde beschrijving gegeven van de wetenschappelijke en technische uitdagingen voor de commercialisering van deze technologie. In het laatste hoofdstuk (hoofdstuk 6) worden de belangrijkste conclusies van het project samengevat en worden aanbevelingen voor het voortzetten van het onderzoek verstrekt.

Table of content

1

Introduction

1.1. The need for a sustainable economy

Climate change, growing energy demand, and sustainable development are the most important challenges of the 21st century. The increasing concentration of CO_2 in the atmosphere (> 400 ppm) together with the rise in the average global temperature (>2 °C increase by 2100) will have severe consequences worldwide [1, 2], such as extreme weather conditions (more intense heat waves and hurricanes) and glaciers shrinkage (accelerated sea-level increase). If no immediate actions are taken to reverse global warming, coastal cities may face the risk of flooding sometime in the future. In addition to that, the rapidly growing global population, expected to reach 9 billion people by 2050 [1], along with the projected increase in the worldwide energy demand (25-50% higher by 2050) [1, 3, 4], are facts that challenge the entire society.

Concerning global energy demand, fossil fuels represented in 2013 ~78% of the total world energy consumption share [5], as shown in Fig. 1.1.

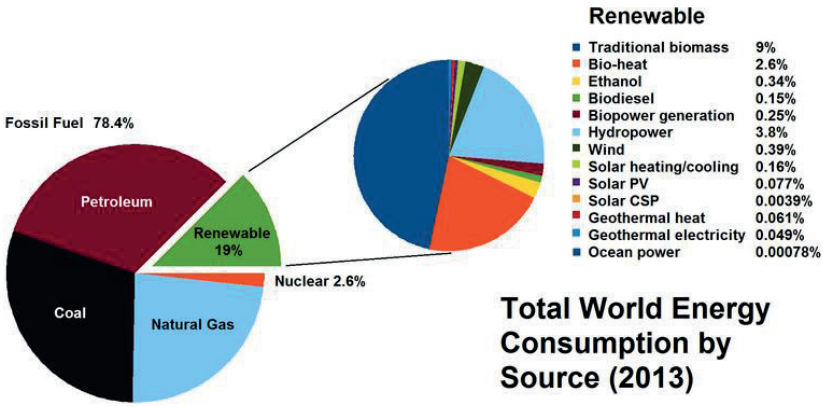

Fig. 1.1. Estimated energy share of total global energy consumption, 2013 [6].

Although some promising scenarios have been reported on the generation of electricity exclusively from renewable energy sources in countries such as Costa Rica (June-August 2016), Portugal (4 days, May 2016), and Scotland (1 day, August 2016), the main energy consumers per capita (China, USA, India, and Russia) [7] still depend strongly on fossil fuels. There is a big debate on how long fossil fuels (oil, natural gas and coal) will last; however, it is estimated that we will not run out of either coal or gas for at least the coming 200 years according to the latest outlook for energy published by Exxon Mobil [3] and also the U.S. Energy Information Administration [8]. In this regard, atmospheric levels of CO_2 will certainly continue to rise in the future unless

carbon emissions are significantly decreased through technological or legislative means. Therefore, in order to fight global warming and ensure future energy security, an urgent transformation of the world's energy infrastructure from an unsustainable fossil fuels-based economy to a renewable-based energy system producing minimum (zero) emissions is required. Nevertheless, there is a long way to go before that transition can become reality. Nowadays, according to the Energy Information Administration, the gains made by renewable energy sources such as wind, solar, and hydro energy remain largely confined to electricity generation for household and industrial applications [9].

It is indisputable that in the future there will be a need for high-energy density fuels, mostly for transportation purposes, i.e. road freight, shipping, and air transport, which together represent as much as 20-25% of the actual global energy demand [2, 5]. Hence, the next step for renewable energy sources is to expand their use in the transportation, industrial, and building sectors where enormous potential for growth exists. To promote the transition to a sustainable energy system, development and implementation of innovative fossil-free technologies appears to be the most promising and realistic short-term solution. In particular, these technologies should enable not only the manufacturing of high-energy density fuels but also the production of specialty and commodity chemicals via the use of renewable electricity. This concept is generally termed Power-to-X, with X standing for gas, liquid, or chemicals [10]. We should also note that the future energy mix will consist of a combination of all forms of fuels, which include hydrocarbons, natural gas, biofuels, solid fuels (coal, biomass), hydrogen and electricity. It is certain that no single solution can meet our society's future energy needs; instead, the solution will most likely come from a family of diverse energy technologies that share the common goal of mitigating climate change and reducing our dependence on fossil fuels. *Humankind did not leave the stone age because of running out of stones* (Eric Rignot, Senior Research Scientist at NASA)*;* the same applies now, society should leave the fossil fuels age because of the negative effect of burning fossil fuels on the climate.

In this thesis, we aim at exploring the applicability of the microwave plasma technology to conversion of the greenhouse gas CO_2 into high-value chemicals (syngas – mixture of CO and H_2) that can potentially be used as sustainable energy sources.

1.2. Power-to-chemicals technologies

While the conversion of greenhouse gases (e.g. CO_2) or other non-fossil feedstocks via renewable electricity into liquid fuels/chemicals seems to be an appealing solution to mitigate climate change and secure future energy demand, the usage of renewable energy sources have a number of limitations that need to be addressed. The decentralized production and inherent intermittency associated with renewable energy sources are identified as the main constraints. Renewable electricity generation is directly linked to the local conditions of a particular geographical area affected mainly by weather patterns. This results in a real challenge to match electricity supply and demand on the grid outside peak hours, which affects the frequency of the AC (alternating current) voltage and thus it might damage electrical equipment plugged into the grid [11]. To make effective use of renewable electricity, technologies that can mitigate power fluctuations must be developed, i.e. suitable technologies to either store energy or make use of it within short-time scales when surplus electricity periods are presented. According to the Eurostat, the energy consumption within the EU-28 in 2014 was around 3030 TWh [12], and ~900 TWh [13] was generated from renewable energy sources (hydropower, wind turbines, solar, biomass, and geothermal). Slight surplus of electricity is encountered when less than 25% of the total electricity generation comes from renewable energy sources. For the purpose of showing what the potential of surplus electricity is, a value of 5% over the total generated electricity from renewable sources is assumed herein [14, 15]. However, we should note that in a situation with 100% electricity supply generated by renewable sources, surplus electricity can increase up to 26% of the total demand [16]. Hence, a value of 45 TWh (5% of the total generated renewable electricity in Europe) can be assumed to be lost due to the lack of effective storing/utilizing technologies. In order to understand the potential presented by the employment of surplus electricity, one should notice that 45 TWh can supply sufficient electricity to more than 6.5 million people in Europe, assuming an annual electricity consumption of 7000 kWh per person [7].

Therefore, given the foreseen increase in the contribution of renewable sources to the future energy mix, it is imperative to find efficient processes to make use of surplus electricity. Storage of energy can be realized in several ways: (1) thermal, (2) mechanical (pumped hydro), (3) electrochemical (batteries) and electromagnetic, and (4) chemical (syngas, methanol, hydrogen) [17-19]. The chemical pathway is the most efficient way for storage and transport of energy due to the high energy density both by volume and by weight of the products,

but also in terms of cost-effectiveness [2, 15]. As mentioned, our society is and will be largely based on the use of liquid hydrocarbons, mostly in the transportation sector, given that the density in typical fuels is about two orders of magnitude larger than in batteries [15]. Thus, the main focus hereafter is on further developing the power-to-chemicals (P2C) approach. In this context, a number of novel technologies can be highlighted, such as 1) electrolysis, 2) photolysis, 3) microwave-assisted process and 4) plasma-assisted process. To date, these technologies have not yet shown competitive production costs compared to conventional technologies, mainly due to relatively low energy efficiencies and limited scalability; in fact, most of these technologies are at pilot-scale, which hinders the benefits from economies of scale. Therefore, notable effort on design, development and implementation of these technologies at commercial-scale is required to push the transition to a sustainable energy system. A brief description of the alternative technologies that can play an important role in power-to-chemicals processes is given below.

Electrolysis: Water electrolysis is a process whereby water splits into hydrogen and oxygen by the application of electric current through electrodes immersed in water. The process takes place in so-called electrolysis cells, which can be connected in parallel or in series to form the electrolyzer module. The hydrogen produced must be cooled, purified, and compressed in order to be stored. In addition, the feeding water needs to be pre-treated to minimize mineral decomposition and undesired parallel reactions [20]. Typical energy efficiencies lie in the range 50-80% depending mainly on the type of electrolyzer [21]. Remarkably, only 4% of the global hydrogen production is carried out via electrolysis [20, 22]. Hence, in order to utilize H_2 as a hydrogen source for the production of liquid fuels or even as an energy carrier to power fuel cell vehicles, this figure (4%) should significantly increase given that the remaining 96% hydrogen production comes from fossil fuels. Besides H_2O splitting, there is a second approach, which makes use of solid oxide electrolysis cells (SOEC) to produce syngas at high temperature (800-900 ^oC) by co-electrolysis of H_2O and CO_2 [23], although it has received much less attention compared to pure H_2O electrolysis [5].

Photolysis: Solar (photonic) energy is converted to chemical energy through photons, which break down chemical compounds. Two of the most studied photolytic processes are photocatalysis and photoelectrochemical processes. The solar light that is harvested by a photocatalyst or a photoelectrode (e.g. TiO_2), which must be a semiconductor, generates an electric charge that can be utilized to dissociate molecules [24, 25]. Not only do these processes still

remain at laboratory-scale, but also they show very low energy efficiencies and hence represent the most expensive power-to-chemicals approach [21, 24].

Microwave-assisted process: Microwaves are a form of electromagnetic radiation situated between the radio and the infrared frequencies – that is, between 300 MHz and 300 GHz. Microwave-assisted processes are widely used for process activation, given that molecules with a permanent dipole moment (e.g. water) can experience rotational or translational motion under a rapidly alternating electric field, resulting in heating of the medium. Common industrial applications of microwaves include preheating of materials, drying, cooking, and sterilization. In the context of power-to-chemicals (P2C), there are a number of processes that have been explored in microwave-assisted reactors. Fidalgo et al. [26] studied the dry reforming of methane for syngas production in a catalytic microwave-assisted reactor and also in a conventional heating device. They showed that conversion of reactants (CO_2 and CH_4) was improved when using microwave heating instead of conventional heating. Zhang et al. [27] investigated methane oxidation as well as methane cracking reactions using microwave heating for the production of C_2 hydrocarbons and syngas. In the case of methane cracking, reaction products were formed at lower temperatures with microwave heating (about 250 ^{o}C lower) compared to conventional heating. More information on other relevant microwave-assisted processes can be found in [28]. Nevertheless, application of microwave heating to P2C processes has not yet been spread at commercial scale. This is due to several factors, such as electricity cost, energy utilization efficiency, unstable operation in large scale units due to complex microwave propagation, and low scalability potential of the technology [28, 29].

Plasma-assisted process: Plasma is an ionized gas, also known as the fourth state of matter. Free electrons, i.e. electrons that are not bound to an atom or molecule, convert atoms and molecules into positively charged ions. These free electric charges make plasma electrically conductive and strongly responsive to electromagnetic fields. From an industrial point-of-view, the plasma state offers a number of features that are highly attractive for chemical manufacturing applications: (1) high energy density that can exceed that of conventional thermal processes, (2) very chemically reactive medium (electrons, ions, radicals and atoms, excited molecules), (3) operational flexibility regarding feedstock and switching the reactor on and off instantly, (4) fast reaction times, and (5) operation far from thermodynamic equilibrium with high concentration and temperature of chemically active species, while keeping the bulk gas near room temperature [30]. Various applications

relevant to power-to-chemicals processes can be found at industrial-scale, such as biomass gasification (thermal arc and microwave discharges), ozone production (dielectric barrier discharge DBD), and methane cracking (thermal arc discharge) [30]. Exciting results have been reported at laboratory-scale on energetically efficient CO_2 splitting, reaching up to 80-90% energy efficiency under supersonic (microwave plasma) conditions [31]. In addition, dry reforming of methane (using two greenhouse gases, CO_2 and CH_4, as reactants) in microwave plasma conditions has also shown promising results at pilot-scale in the context of power-to-hydrogen [32]. Despite of several decades of research though, the industrial implementation of this technology is still limited to few particular chemical applications, mostly related to waste treatment and electric cracking of hydrocarbons [30, 33].

In this thesis, due to the strong interest in exploring possibilities to utilize CO_2 as feedstock in the chemical industry, the conversion of this molecule to added-value products via microwave plasma technology is studied. In the following section, a short discussion on CO_2 recycling possibilities is given.

1.3. Challenges of CO_2 chemical recycling

The only way to mitigate global warming is by either producing lesser amount of CO_2 or by avoiding its emission to the atmosphere. The former option seems highly unlikely, at least in the short-term [1], because of reasons already discussed: (1) increasing energy demand as a consequence of a larger global population, and (2) projections of future energy mix still remain highly dependent on fossil fuels [3, 5, 9]. Concerning the latter option, we can identify two major mechanisms available: Carbon Capture & Storage (CCS) and Carbon Capture & Utilization (CCU). CCS can promote the global projected reduction of CO_2 emissions (about 20% [15]) by storing CO_2 in geological reservoirs. However, this approach does not comply with the mission/vision of sustainability because CO_2 is still treated as a waste. CCS is a costly solution. More specifically, the capture step accounts for 0.2 tons of CO_2-equivalent energy, and an additional 0.4 tons of CO_2 (per ton of CO_2 sequestrated) for transport and storage [15]. Therefore, it is unprofitable to simply store it instead of transforming CO_2 (carbon source) into valuable products that can generate revenue to offset the capture costs [34]. CCU will thus be the key to foster sustainable development in our society. In fact, CO_2 can become a strategic molecule for the introduction of renewable energy sources into the chemical industry and energy chain, thus reducing the consumption of fossil

fuels. Nonetheless, the currently available CO_2 utilization technologies present some disadvantages: (1) treatment capacity: only a very small fraction (0.3-0.4 Gt y^{-1}) of the total anthropogenic CO_2 emissions (roughly 35 Gt y^{-1}) can be processed [15, 35, 36], and (2) molecule stability: CO_2 is a highly stable molecule with a very low energy content, which means that the activation of CO_2 generally demands rather extensive energy input. Thus, the important question is: *can we develop a range of novel technologies that allows processing of high CO_2 flow streams in an energy-efficient manner?*

To answer this question, there are a number of aspects to be considered, such as fossil fuels price, incentives in limiting CO_2 emissions (carbon taxes), renewable electricity cost, and technological development. The price of fossil fuels is expected to exponentially increase as a result of its depletion, given that the demand-supply ratio will most likely rise, i.e. growing energy demand with fewer fossil resources. With respect to renewable electricity cost, the capital cost of solar and wind energy has substantially decreased in the last decade, while the cumulative installed capacity has increased due to much larger production volumes, which has the evident benefit of economies of scale [37]. When these facts are combined with innovation and technology development to improve the energy efficiency of fossil-free technologies, a shift towards electrification of the industry may occur aiming at an economically viable low-carbon circular economy.

One of the most profitable pathways to recycle CO_2 in a future low-carbon economy lies either in its direct use (enhanced oil recovery, calcium carbonate, polyols, food use), or in its conversion to high value products (indirect use). In the former, the demand for low-energy products (polycarbonates and inorganic carbonates) is relatively limited, which barely impacts on the reduction of CO_2 emissions [36]. In the latter, even though the cleavage of the C-O bond is energy intensive and often requires reducing agents (e.g. H sources), the demand for hydrocarbons is much larger (~14 times) than that for non-fuel chemicals [15, 36]. The ideal scenario then consists of the reduction of CO_2 with solar H_2, which is generated via water electrolysis, where solar fuels (oxygenates, hydrocarbons) are produced via the reverse water-gas shift (RWGS) reaction. The main product of this reaction is syngas, which is the key intermediate product for the generation of a large variety of added-value chemicals, see Fig. 1.2. This pathway requires much less input of energy (41 kJ/mol) compared to other commonly studied chemical routes: (1) pure CO_2 splitting (280 kJ/mol) and (2) dry reforming of methane (247 kJ/mol). The second step can be performed through the Fischer Tropsch (FT) process [38].

The nature of the catalyst determines the product generated, as shown in Fig. 1.2. Some of the most interesting products include methanol (feedstock for olefins and aromatics), ethanol, formic acid, dimethyl ether (DME), light olefins (ethylene and propylene), and substituted natural gas (SNG). Alcohols are preferred over hydrocarbons because their synthesis requires less hydrogen per unit of product, which notably reduces the operational cost (OPEX) [15]. The main constrain from an economic point-of-view to convert CO_2 into fuels is in fact the production cost of renewable H_2 [15, 36]. In conclusion, while the production of solar fuels enables carbon-neutral chemical recycling of CO_2, as well as the storage and transportation of solar energy using currently existing energy infrastructure, solar fuels from CO_2 are still not competitive to those made from fossil fuels.

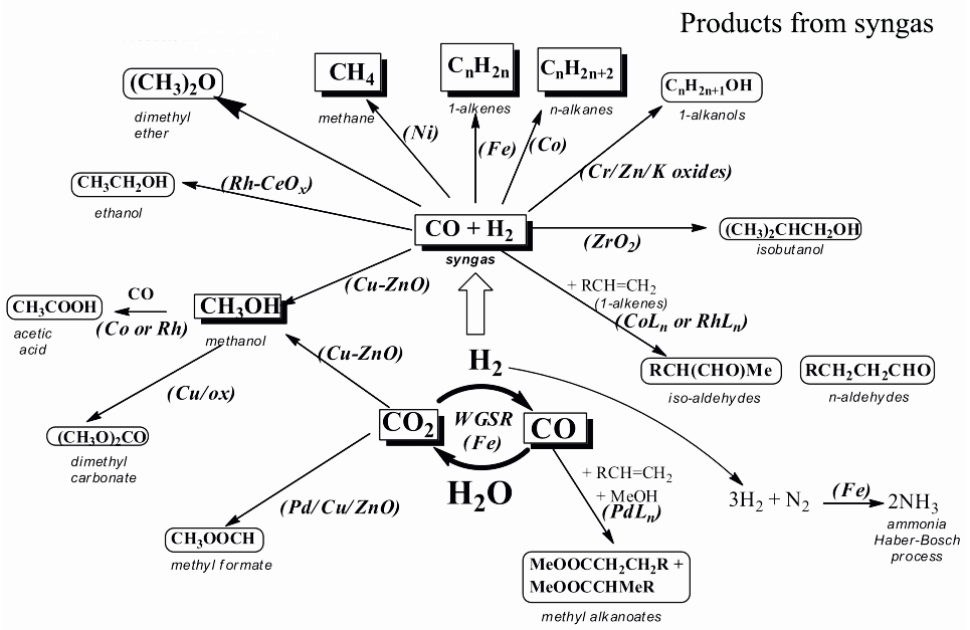

Fig. 1.2. Scheme showing various organic compounds that are obtained from syngas based on the nature of the metal catalyst [38].

1.4. The reverse water-gas shift (RWGS) reaction

The world of tomorrow will clearly need hydrocarbons as part of the global energy mix, mostly as transportation fuels. To date, no other type of energy storage has outperformed the usability of liquid fuels. Given the existing infrastructure for storage and delivery of liquid fuels, the development of other alternatives (e.g. H_2 economy) is notably hindered. The generation of syngas

from renewable energy sources (power-to-gas) via the RWGS reaction is a rather appealing solution in the short-term, as the products of this reaction can be handled via the available infrastructure. This reaction has been explored in different systems including: (1) thermal catalytic reactors, (2) photocatalytic reactors, (3) electrochemical reactors and (4) plasma-assisted reactors.

With regard to conventional thermal catalytic reactors, supported metal catalysts, such as copper (Cu), platinum (Pt), rhodium (Rh), nickel (Ni), and also oxide catalysts, such as zinc oxide (ZnO) and NiO have been widely investigated [39]. The best catalyst performance as to the conversion of CO_2 to CO (~60%) was found to be given by a Cu/Al_2O_3 catalyst. Other catalyst-based reactors – photocatalytic and electrochemically-assisted catalytic reactors have been explored, although the reported CO_2 conversions are relatively low (see Table 1.1). Additionally, very few research studies have assessed the RWGS reaction in plasma-assisted reactors. Table 1.1 summarizes the most relevant studies on reduction of CO_2 with H_2. As seen in Table 1.1, the highest CO_2 conversions (~80%) achieved to date were under microwave plasma conditions. More information on this topic is presented in Chapter 2.

Table 1.1. Comparison of different reactors in which the RWGS reaction is studied. X_{CO2} stands for conversion of CO_2.

	Catalyst	Plasma type	T (°C)	P (bar)	H_2:CO_2 ratio	X_{CO2} (%)	Ref.
Catalytic reactor	Cu/Al_2O_3	-	500	1	1:9	60	[40]
	NiO/SBA-15	-	900	1	1:1	55	[41]
	Rh/SiO_2	-	200	50	3:1	52	[42]
	Ni/Ce-Zr-O	-	750	1	1:1	50	[43]
Photocatalytic reactor	ß-Ga_2O_3	-	800	1	1.5:1	3	[44, 45]
Electrochemically -assisted catalytic reactor	Ni/YSZ/Au	-	225	1	4:1	27	[46]
Plasma-assisted reactor	-	Microwave	-	0.02	3:1	80	[47]
	-	Glow discharge	-	0.003	4:1	26	[48]
	$CuO/ZnO/Al_2O_3$	DBD	-	8	3:1	14	[49]

1.5. Microwave plasma technology

Plasma technology is one of the electricity-based technologies with the highest potential for scalability, and, as such, it represents a promising solution for integration of large volume usage of renewable electricity with CO_2 chemical recycling for the production of solar fuels. There are a broad variety of plasmas, such as those found in nature and also those man-made. In Fig. 1.3, an overview of both types of plasmas is presented. The comparison of the different plasmas is made with reference to electron temperature and electron density. One of the most important parameters that characterize plasma is the temperature of the species (electrons, ions, and neutrals), although the electron temperature is the driving factor for chemical reactions taking place in the plasma. At this point, it is important to mention the existence of two different operating (plasma) regimes, namely non-equilibrium and equilibrium plasmas. Non-equilibrium plasma is characterized by electron temperature (kinetic energy) much higher than heavy species temperature, whereas plasmas in which the heavy species temperature approaches the electron temperature are termed thermal plasmas. This classification is important to consider when deciding on the type of plasma to be used for a given application. For example, CO_2 splitting [31] or methane pyrolysis [33] have shown much higher energy efficiency under non-thermal plasma conditions, as discussed in Chapter 4, while processes such as gasification or dry reforming perform better under thermal plasma conditions, as addressed in Chapter 5.

The density of particles, in particular the electron density, is another relevant property of plasmas. When energy is supplied to a gas in the form of an electromagnetic field, the alternating electric field heats the electrons, which become the primary energy carriers transferring energy to heavy species via collisions. Plasma is thus ignited when the applied electric field strength overcomes the breakdown voltage of the gas, so-called electric breakdown. The degree of ionization of a gas, i.e. the ratio between the electrically charged number density and the neutral particle number density, determines the existence of plasma. Chemical processing applications are typically studied in plasmas with a degree of ionization in the range 10^{-7} – 10^{-4} (weakly ionized plasma), whereas a degree of ionization close to 1 is found in nuclear fusion (fully ionized plasma).

As already stated, plasma technology offers various benefits compared with other electricity-based technologies: (1) high energy density, (2) highly reactive medium, (3) operational flexibility, (4) fast reaction times, and (5) operation far

from thermal equilibrium. In addition, the principal advantage of microwave plasma technology over other plasma reactor types is that it does not require the use of an inner electrode, which would otherwise need frequent maintenance (hundred hours range) in order to replace the electrode due to erosion [50]. This is necessary if this technology is to be applied to the chemical industry, as most of the processes run in continuous operation.

As a final remark, the development of modular microwave plasma units, which can be assembled in containers and installed in the vicinity of where renewable electricity is generated, would allow the direct use of surplus electricity for powering microwave plasma reactors to generate liquid fuels and promote distributed manufacturing. Moreover, this approach will facilitate the challenging task of matching electricity supply and demand on the grid.

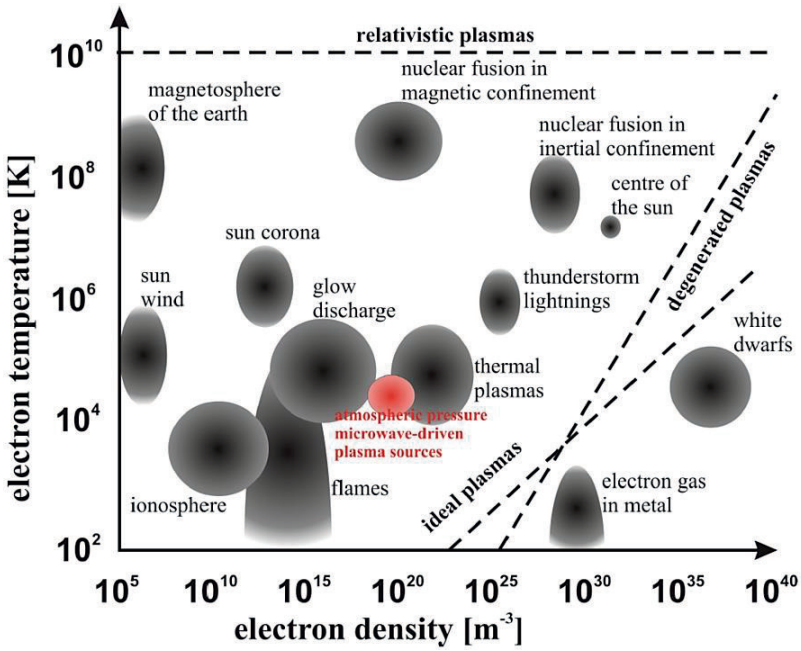

Fig. 1.3. Overview of the different plasmas found in nature as well as man-made plasmas, with microwave plasmas highlighted in red [51].

1.6. Scope of the thesis

This thesis aims to evaluate the application of microwave plasma technology as an alternative energy form to convert carbon dioxide (CO_2) into value-added products. Particularly, two different chemistries, pure CO_2 splitting and the

reduction of CO_2 with hydrogen (H_2), also known as reverse water-gas shift (RWGS) reaction, have been explored. Special attention is given to the latter chemistry, given that the production of liquid fuels from CO_2 takes place through the RWGS reaction. To date, rather limited research can be found in the literature on the RWGS reaction under plasma conditions, despite the fact that it has some advantages over other chemistries dealing with CO_2 as feedstock. These advantages include mild endothermicity, simple separation of the products formed and high CO_2 conversion per pass. Given the current progress in reducing the production cost of solar H_2 via water electrolysis, this conversion step may become an important process in the power-to-chemicals approach.

The main motivation of this thesis is driven by the need to fill the gap between plasma chemistry and chemical engineering, so-called plasma chemical engineering. Plasma discharges for chemical industrial purposes have been used for decades; however, most of the physical and chemical processes taking place in the discharge are seldom sufficiently understood. Due to the complexity of plasma chemistry and its interplay with the flow and electromagnetic fields, development of a rigorous plasma reactor design approach is challenging. In this context, the research questions that have been tackled in this thesis are grouped below:

1. Can microwave plasma technology convert carbon dioxide (CO_2) into high value products in a resource- and energy-efficient manner? How does it compare to conventional processes?
   [Chapter 2, 3, 5]

2. Which are the important modelling challenges, operating parameters and design aspects when developing and optimizing a microwave plasma reactor for CO_2 conversion?
   [Chapter 2, 3, 4]

3. What are the scientific and engineering challenges in the development of microwave plasma technology that can render it a key enabling technology for certain electrification processes in the chemical industry?
   [Chapter 5]

1.7. Outline of the thesis

To the best of our knowledge, this thesis is the first attempt to study the reverse water-gas shift (RGWS) reaction in non-equilibrium microwave plasma conditions for the production of synthesis gas. In addition, a technological roadmap of the microwave plasma technology is presented in which major issues, such as scale-up approaches along with technical and engineering challenges are discussed to empower the transition of this technology to commercial scale. This thesis is divided into six chapters, which cover fundamental, practical and engineering elements to further develop microwave plasma technology.

In *Chapter 1*, a general introduction to the perspectives on current and future energy demand is given. In this chapter, the societal need for developing strategies to supply enough energy to a constantly growing population in a sustainable manner is discussed. The concept of using electricity produced from renewable energy sources and carbon dioxide (CO_2) as feedstock to generate transportation fuels and/or chemicals is presented as one of the most promising options. The advantages and drawbacks of microwave plasma compared to other technologies are herein assessed, particularly for the reverse water-gas shift (RWGS) reaction. Lastly, the research questions regarding the development and implementation of microwave plasma technology are formulated.

Chapter 2 presents a parametric study on the RWGS reaction for the production of syngas in a bench-scale non-equilibrium microwave plasma reactor. The most important operating parameters when designing this type of plasma reactor were experimentally evaluated. The optimum process conditions were mainly dictated by the input microwave power and feed gas composition. This chapter also introduces an isothermal zero-dimensional chemical model for the RWGS reaction that qualitatively describes the performance of the reactor at high temperatures. Furthermore, the details of experimental measurement of important plasma parameters, including electron density and electron temperature, are also addressed.

In *Chapter 3* a follow-up study of the work in Chapter 2 is presented. The effect of an alternative microwave plasma reactor configuration on the chemical (CO_2) conversion is herein investigated. Moreover, the feasibility of a novel optimization methodology, which combines modelling and experimental work, is put forward in this chapter. Other process parameters that influence CO_2

conversion (e.g. cooling flow rates) are evaluated in detail. Additionally, it is shown that thermal imaging techniques can be used to explore the effect of process parameters on microwave discharges.

After demonstrating the feasibility of modelling an argon microwave plasma discharge in Chapter 3, *Chapter 4* addresses the challenges associated with more complex plasma chemistries, in particular CO_2 microwave plasmas. A novel methodology (chemical lumping) to reduce complex kinetic models in microwave discharges is described in this chapter. By significantly reducing the number of species and reactions, it was shown that the implementation of complex plasma chemistries in multidimensional multiphysics simulations can be attained.

Chapter 5 outlines a technological roadmap of microwave plasma. This chapter briefly summarizes the current state-of-the-art applications of microwave plasma technology, along with the existing possibilities for scale up. Additionally, a detailed description of the scientific and engineering challenges relevant to the implementation of microwave plasma technology to industrial scale is given. Lastly, in Chapter 5, the potential of microwave plasma to be used for commercial chemical applications, such as the production of fuels/chemicals and waste gas treatment, is assessed.

Chapter 6 summarizes the findings of the work and gives recommendations for future research on the application of microwave plasma technology in the chemical industry.

> *Plasma chemical technology is the technology of tomorrow, but today we have only a vague idea of the truly boundless possibilities for utilization of low-temperature plasmas in chemical and other branches of the industry;*
> (Vurzel et al. 1970 [33])

References

[1] Randers J. 2052: A Global Forecast for the Next Forty Years: Chelsea Green Publishing 2012.
[2] Jiang Z, Xiao T, Kuznetsov VL, Edwards PP. Turning carbon dioxide into fuel. Philos T R Soc A. 2010;368:3343-64.
[3] ExxonMobil. Outlook for Energy: A view to 2040. http://corporateexxonmobilcom/en/energy/energy-outlook. 2017.
[4] Shell. Shell energy scenarios to 2050. 2011.
[5] MacElroy JMD. Closing the carbon cycle through rational use of carbon-based fuels. Ambio. 2016;45:5-14.
[6] Renewable Energy Policy Network for the 21st Century. Renewables 2013 Global Status Report. 2013.
[7] Schlogl R. Systemic aspects of the transition to sustainable energy. Lectures Notes - Joint Eps-Sif International School on Energy - Course 2 Energy: Basic Concepts and Forefront Ideas. 2015;98.
[8] Energy Information Administration. What is the role of coal in the United States. https://wwweiagov/energyexplained/indexcfm?page=coal_use. 2011.
[9] U.S. Energy Information Administration. Annual Energy Outlook 2017 with projections to 2050. wwwieagov/aeo. 2017.
[10] Mennicken L, Janz A, Roth S. The German R&D Program for CO2 Utilization-Innovations for a Green Economy. Environ Sci Pollut R. 2016;23:11386-92.
[11] Sean Leavey. Mitigating power fluctuations from renewable energy sources. 2012.
[12] Eurostat. Electricity production, consumption and market overview. http://eceuropaeu/eurostat/statistics-explained/indexphp/Electricity_production,_consumption_and_market_overview. 2015.
[13] Eurostat. Electricity generated from renewable energy sources. http://eceuropaeu/eurostat/statistics-explained/indexphp/Renewable_energy_statistics. 2016.
[14] Wagner F. Considerations for an EU-wide use of renewable energies for electricity generation. Eur Phys J Plus. 2014;129.
[15] Centi G, Perathoner S. Green carbon dioxide: Advances in CO2 utilization: Wiley; 2014.
[16] Wagner F. Surplus from and storage of electricity generated by intermittent sources. The European Physical Journal Plus. 2016;131:445.

[17] Sabihuddin S, Kiprakis AE, Mueller M. A Numerical and Graphical Review of Energy Storage Technologies. Energies. 2015;8:172-216.
[18] Hameer S, van Niekerk JL. A review of large-scale electrical energy storage. Int J Energ Res. 2015;39:1179-95.
[19] Mahlia TMI, Saktisandan TJ, Jannifar A, Hasan MH, Matseelar HSC. A review of available methods and development on energy storage; technology update. Renew Sust Energ Rev. 2014;33:532-45.
[20] Shandarr R, Trudewind CA, Zapp P. Life cycle assessment of hydrogen production via electrolysis - a review. J Clean Prod. 2014;85:151-63.
[21] Dincer I, Acar C. Review and evaluation of hydrogen production methods for better sustainability. Int J Hydrogen Energ. 2015;40:11094-111.
[22] Wang MY, Wang Z, Gong XZ, Guo ZC. The intensification technologies to water electrolysis for hydrogen production - A review. Renew Sust Energ Rev. 2014;29:573-88.
[23] Ebbesen SD, Knibbe R, Mogensen M. Co-Electrolysis of Steam and Carbon Dioxide in Solid Oxide Cells. J Electrochem Soc. 2012;159:F482-F9.
[24] Boyjoo Y, Su HQ, Liu J, Pareek VK, Wang SB. A review on photocatalysis for air treatment: From catalyst development to reactor design. Chem Eng J. 2017;310:537-59.
[25] Ismail AA, Bahnemann DW. Photochemical splitting of water for hydrogen production by photocatalysis: A review. Sol Energ Mat Sol C. 2014;128:85-101.
[26] Fidalgo B, Dominguez A, Pis JJ, Menendez JA. Microwave-assisted dry reforming of methane. Int J Hydrogen Energ. 2008;33:4337-44.
[27] Zhang XL, Lee CSM, Mingos DMP, Hayward DO. Oxidative coupling of methane using microwave dielectric heating. Appl Catal a-Gen. 2003;249:151-64.
[28] Stefanidis GD, Munoz AN, Sturm GSJ, Stankiewicz A. A helicopter view of microwave application to chemical processes: reactions, separations, and equipment concepts. Rev Chem Eng. 2014;30:233-59.
[29] Durka T, Stefanidis GD, Van Gerven T, Stankiewicz AI. Microwave-activated methanol steam reforming for hydrogen production. Int J Hydrogen Energ. 2011;36:12843-52.
[30] Fridman A. Plasma Chemistry: Cambridge: Cambridge University Press; 2008.
[31] van Rooij G, van den Bekerom D, den Harder N, Minea T, Berden G, Bongers W, et al. Taming microwave plasma to beat thermodynamics in CO2 dissociation. Faraday Discuss. 2015;183:233-48.
[32] Jasinski M, Czylkowski D, Hrycak B, Dors M, Mizeraczyk J. Atmospheric pressure microwave plasma source for hydrogen production. Int J Hydrogen Energ. 2013;38:11473-83.

[33] Vurzel FB, Polak LS. Plasma Chemical Technology - Future of Chemical Industry. Ind Eng Chem. 1970;62:8-&.
[34] Styring P, Jansen D. Carbon Capture and Utilisation in the green economy. The centre for Low Carbon Futures 2011.
[35] Perez-Fortes M, Schoneberger JC, Boulamanti A, Tzimas E. Methanol synthesis using captured CO2 as raw material: Techno-economic and environmental assessment. Appl Energ. 2016;161:718-32.
[36] Lim XZ. How to make the most of carbon dioxide (vol 526, pg 628, 2015). Nature. 2016;529:141-.
[37] International Renewable Energy Agency. Renewable power generation costs in 2014. 2015.
[38] Peter M. Maitlis, Arno de Klerk. Greener Fischer-Tropsch processes for fuels and feedstocks: Wiley; 2013.
[39] Daza YA, Kuhn JN. CO2 conversion by reverse water gas shift catalysis: comparison of catalysts, mechanisms and their consequences for CO2 conversion to liquid fuels. Rsc Adv. 2016;6:49675-91.
[40] Chen CS, Cheng WH, Lin SS. Mechanism of CO formation in reverse water-gas shift reaction over Cu/Al2O3 catalyst. Catal Lett. 2000;68:45-8.
[41] Lu BW, Kawamoto K. Preparation of the highly loaded and well-dispersed NiO/SBA-15 for methanation of producer gas. Fuel. 2013;103:699-704.
[42] Kusama H, Bando KK, Okabe K, Arakawa H. CO2 hydrogenation reactivity and structure of Rh/SiO2 catalysts prepared from acetate, chloride and nitrate precursors. Appl Catal a-Gen. 2001;205:285-94.
[43] Sun FM, Yan CF, Wang ZD, Guo CQ, Huang SL. Ni/Ce-Zr-O catalyst for high CO2 conversion during reverse water gas shift reaction (RWGS). Int J Hydrogen Energ. 2015;40:15985-93.
[44] Izumi Y. Recent advances in the photocatalytic conversion of carbon dioxide to fuels with water and/or hydrogen using solar energy and beyond. Coordin Chem Rev. 2013;257:171-86.
[45] Teramura K, Tsuneoka H, Shishido T, Tanaka T. Effect of H(2) gas as a reductant on photoreduction of CO(2) over a Ga(2)O(3) photocatalyst. Chem Phys Lett. 2008;467:191-4.
[46] Ruiz E, Cillero D, Martinez PJ, Morales A, San Vicente G, de Diego G, et al. Bench-scale study of electrochemically assisted catalytic CO2 hydrogenation to hydrocarbon fuels on Pt, Ni and Pd films deposited on YSZ. J Co2 Util. 2014;8:1-20.
[47] de la Fuente JF, Moreno SH, Stankiewicz AI, Stefanidis GD. Reduction of CO2 with hydrogen in a non-equilibrium microwave plasma reactor. Int J Hydrogen Energ. 2016;41:21067-77.

[48] Kano M, Satoh G, Iizuka S. Reforming of Carbon Dioxide to Methane and Methanol by Electric Impulse Low-Pressure Discharge with Hydrogen. Plasma Chem Plasma P. 2012;32:177-85.

[49] Eliasson B, Kogelschatz U, Xue BZ, Zhou LM. Hydrogenation of carbon dioxide to methanol with a discharge-activated catalyst. Ind Eng Chem Res. 1998;37:3350-7.

[50] Fincke JR, Anderson RP, Hyde T, Wright R, Bewley R, Haggard DC, et al. Thermal conversion of methane to acetylene final report. Idaho National Engineering and Environmental Laboratory. 2000.

[51] Martina Leins. Development and spectroscopic investigation of a microwave plasma source for the decomposition of waste gases. PhD thesis, Stuttgart University. 2010.

2

Reduction of CO_2 with hydrogen in a non-equilibrium microwave plasma reactor

This chapter is published as:

de la Fuente JF, Moreno SH, Stankiewicz AI and Stefanidis GD, Reduction of CO_2 with hydrogen in a non-equilibrium microwave plasma reactor. *International Journal of Hydrogen Energy* **41**: 21067-21077 (2016).

Abstract

In the context of converting electricity into value-added chemicals, the reduction of carbon dioxide (CO_2) with hydrogen (H_2) in a surface-wave-induced microwave plasma discharge, so-called surfatron, was investigated. The effect of different input variables such as gas flow rate, feed gas composition ratio (H_2:CO_2) and specific energy input (SEI) on the reactor performance, i.e. the CO_2 conversion and energy efficiency, was assessed. A maximum CO_2 conversion of 85% is obtained when the feed gas mixture ratio (H_2:CO_2) was equal to 3. Moreover, a trade-off between CO_2 conversion and energy efficiency was clearly noticed when varying the supplied microwave power. High SEI resulted in high conversions and low energy efficiencies and vice-versa. Furthermore, the saturation of the carbon monoxide (CO) production was found at high SEI. These results were rationalized by means of a simplified reaction scheme and by optical emission spectroscopy analysis, which showed that the formation of hydrogen (H) and oxygen (O) atoms in the plasma are the dominant channels driving the reaction pathway. We also observed higher electron densities and temperatures at higher H_2 content, which may explain the high conversions achieved in the plasma reactor at high H_2:CO_2 ratios. H_2 is then not only capable of acting as a "catalyst" for CO_2 decomposition but also modifies the plasma properties, which seems to greatly enhance the potential of chemical reactions and thus the dissociation rates.

2.1. Introduction

To enable the transition from the current unsustainable energy economy, which is based on the exploitation of fossil fuels, to a future energy economy supported by the use of renewable forms of energy, two critical barriers should be overcome: 1) the development of technologies that allow for efficient storage of electricity to match generation and consumption and 2) the identification of profitable pathways to reduce greenhouse gas (GHG) emissions [1]. The main contributor to GHG emissions is carbon dioxide (CO_2) with an annual contribution of 35 Gt, accounting for 60% of the total GHG emissions. The Carbon Capture & Utilization (CCU) approach can be considered one of the most promising concepts to mitigate CO_2 emissions. In contrast to Carbon Capture & Storage (CCS), CCU does not treat CO_2 as a waste, but rather as a chemical feedstock for the synthesis of added value chemicals [2, 3]. In the context of CCU, plasma processing may address both of the aforementioned limitations, i.e. renewable energy storage and GHG conversion into valuable products (power-to-chemicals). Plasma represents a high energy density source that enables high chemical conversion in compact reactors with fast response time to the inlet conditions [4, 5].

The use of hydrogen (H_2) as feedstock to generate electricity by means of proton-exchange-membrane fuel cells (PEMFCs) [6, 7] as well as the production of H_2 from (oxygenated) hydrocarbon fuels have been largely researched in the literature [8-10]. Concerning the use of CO_2 as chemical feedstock, CO_2 dissociation [11-14] and methane (CH_4) dry reforming [15-19] have been widely studied under different plasma conditions. The hydrogenation of CO_2 into CH_4 (Sabatier reaction) was also explored in a hybrid plasma-catalytic system [20]. The simultaneous dissociation of CO_2 with water (H_2O) [21-23] and the reduction of CO_2 with H_2 [24-26] have been much less investigated. In this work, the reduction of CO_2 with H_2, also known as the reverse water-gas shift (RWGS) reaction, is explored as it represents the key intermediate step in the indirect route of production of methanol (CH_3OH) from CO_2. CO_2 hydrogenation to CH_3OH through the reverse-water-gas-shift reaction, named as CAMERE process, was investigated in [27, 28]. The process consists of two steps: 1) CO_2 and H_2 are converted to CO and H_2O (main products), and 2) after H_2O has been condensed out, CH_3OH synthesis is carried out via CO hydrogenation.

We investigated the RWGS reaction in a bench scale microwave plasma reactor to evaluate the reactor performance and possible process limitations.

Microwave plasma does not require electrodes, implying low maintenance cost, and has a high electric energy utilization efficiency (up to 85% conversion of electric to microwave energy at 915 MHz) [29]. Besides, in comparison to conventional thermal catalysis [27], a microwave plasma reactor does not require: a) catalyst, b) an expensive and bulky furnace to raise the reactor temperature to 650 °C-750 °C.

In this work, the effect of throughput (gas flow rate), feed composition and specific energy input (SEI) on the reactor performance, characterized by the CO_2 conversion and energy efficiency, is experimentally evaluated. The microwave-induced plasma reactor is also compared to other types of plasma reactors, and benchmarked against the thermal catalytic process. Optical emission spectroscopy was used to get insight into plasma-related parameters (electron density and temperature) and the dominant dissociation channels, which drive the chemical reactions.

2.2. Materials and methods

2.2.1. Reactor configuration

CO_2 hydrogenation was investigated in a non-thermal microwave discharge. The experimental setup used in this work is shown in Fig. 2.1. A solid-state microwave generator (MiniFlow 200SS, Sairem) with a maximum available power of 200 W at a frequency of 2.45 GHz is used to supply the microwave energy to the plasma reactor. In combination with the microwave generator, an electromagnetic surface-wave launcher (surfatron 60, Sairem) enables the ignition and sustenance of the non-equilibrium plasma. The microwave discharge is sustained in quartz tubes with fixed inner and outer diameters of 4 and 5 mm respectively. The length of the tubes is varied from 200 mm to 500 mm. Alumina tubes were also explored for this purpose, but due to a worse ignition capability and lack of visibility of the plasma column, quartz tubes were preferred over alumina tubes for the experiments. The ignition chamber as well as the outer wall of the quartz tube within the chamber is cooled by a system that consists of compressed air at 20 °C blowing inside the cavity and cooling water at 5 °C circulating around the surfatron's body. For further information on the device, the reader is referred to ref. [30, 31]. The reactants are injected into the plasma reactor from the left-hand side (Fig. 2.1) in the axial direction by means of mass-flow controllers (Bronkhorst). The operating gas flow rates are then adjusted in the range of 50 to 400 millilitres per minute

(ml/min). A vacuum pump (SC920, KNF) with an ultimate vacuum of 2 mbar absolute is connected in the downstream section to regulate the operating pressure of the system. The plasma operating pressure can be varied from 7 to 200 mbar, although most of the experiments are performed in the pressure range of 20 to 30 mbar.
Two analytical techniques are employed to characterize the plasma performance in-situ: mass spectroscopy (QGA Quantitative Gas Analyser, Hiden Analytical) and optical emission spectroscopy (HR2000+CG, Ocean Optics). Gas chromatography (CP4900, Varian Analytical) is used off-line for validation purposes. Mass spectroscopy and gas chromatography enable the quantification of the product gas composition, whereas optical emission spectroscopy allows the identification of the dominant reactive species present during plasma-assisted gas phase reactions. Temperature on the plasma reactor wall is measured by three thermocouples placed at various axial positions, as displayed in Fig. 2.1. A temperature data-recording device (OM-USB-TEMP 8 Channel, Omega) records the temperature evolution when plasma is switched on and off.

The first step in the experimental procedure is the plasma initiation. A low gas flow rate of argon (40 ml/min), which acts as a plasma igniter, is fed into the reactor while applying the maximum microwave power (200 W) to facilitate ignition. The operating pressure at this stage lies between 2 and 10 mbar. Once plasma is ignited, the reactants (CO_2 and H_2) are injected into the reactor. The argon flow rate is then set to zero, as argon is not required to sustain the plasma. By means of short-circuit tuning wheels integrated in the surfatron device, the reflected power is minimized so that microwave energy deposition into the plasma is maximized. Following the optimization of the input microwave power, mass spectroscopy and optical emission spectroscopy measurements are performed. Lastly, the gas needed to perform off-line gas chromatography measurements is collected using a sampling bag.

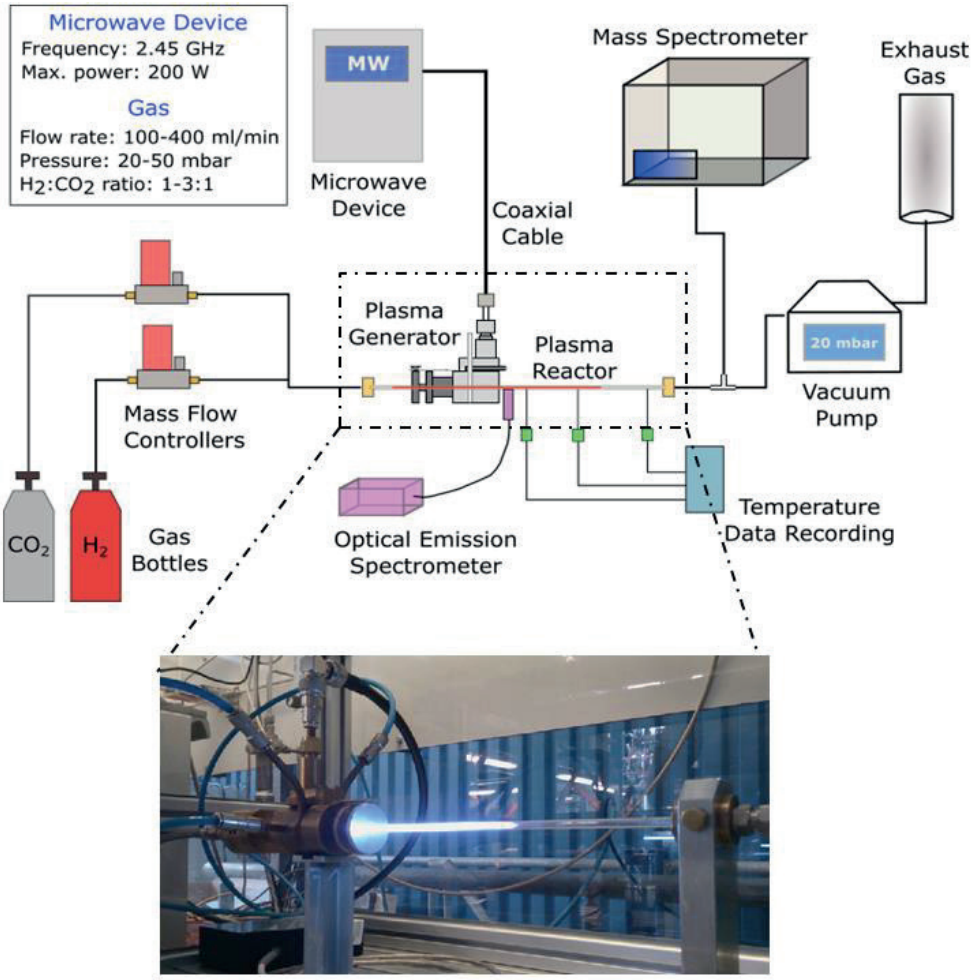

Fig. 2.1. Schematic of the bench scale surface-wave-induced microwave plasma setup.

2.2.2. Mass spectroscopy analysis

The quantification of the product gas composition is carried out by ionizing the gas molecules (ionization chamber QGA) and subsequently separating the species based on the mass/charge ratio. To perform a reliable measurement, the calibration of the equipment should be done according to the expected gas mixture in the product. In this case, a mixture of products (CO and H_2O) and unprocessed reactants (CO_2 and H_2) was considered. In order to detect the possible formation of secondary products [26] such as CH_4, acetylene (C_2H_2), ethylene (C_2H_4), CH_3OH, formaldehyde (CH_2O) and formic acid (CH_2O_2),

different atomic mass units (a.m.u.) were tracked during the experiments, measuring concentrations down to the ppm level. In this regard, the formation of carbon-bearing products, notably C_2H_4 at a.m.u.=27 with a concentration of about 200 ppm and CH_3OH at a.m.u. = 31 with concentrations in the range of 10-20 ppm, was found (Fig. 2.2). Markedly, there was no formation of CH_4 as observed by the constant trend of the red solid line in Fig. 2.2, which opposes to the results reported in [24-26]. The generation of CH_2O and CH_2O_2 was not quantified due to the overlapping of CO (0.2% at a.m.u.=30) and CO_2 (0.4% at a.m.u.=46). In conclusion, the concentration of the gas species containing carbon (excluding CO and CO_2) can then be considered negligibly small.

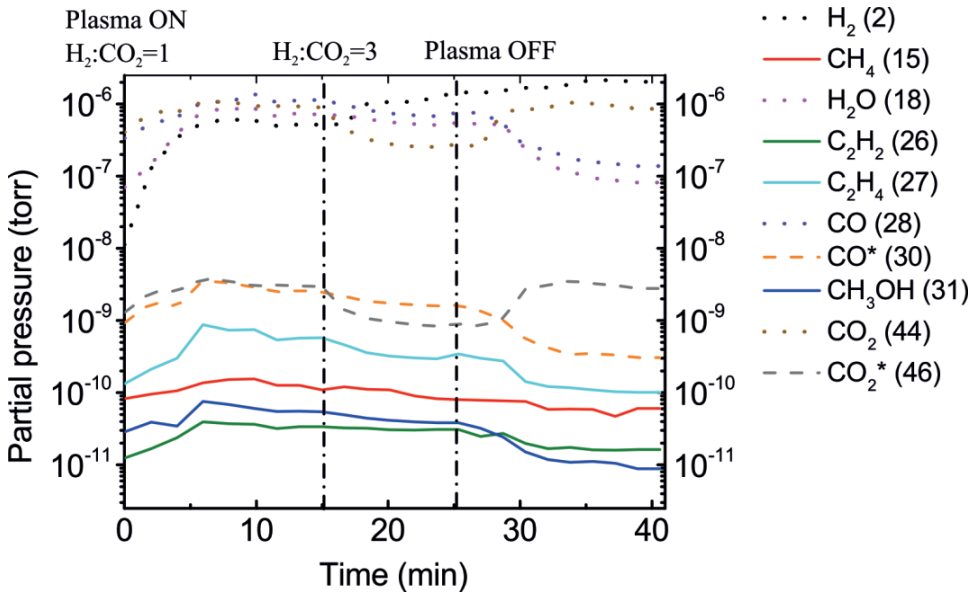

Fig. 2.2. Evolution of the intensity of the most relevant a.m.u. in time with the plasma on and off at two different inlet gas mixture ratios (H_2:CO_2=1 and 3). The dot lines show the most abundant species (CO, H_2O, CO_2 and H_2), the dash lines correspond to the contributions of CO at a.m.u.=30 (0.2%, orange dash line) and CO_2 at a.m.u.=46 (0.4%, grey dash line), and the solid lines represent the species with the lowest concentration (ppm level). Initially, the plasma was sustained with a feed gas mixture H_2:CO_2=1 and then changed from 1 to 3 at 16 min. The plasma was stopped at 26 min. Note that it took about 5 min to reach steady state as for measuring the concentration of the product gas when the conditions in the reactor are modified. Note also that the relative sensitivity of each molecule to be ionized is not considered in the data reported in this figure.

Concerning the calibration procedure, the following steps were applied to calibrate the device: 1) get data from the scan – a.m.u. of interest, 2) remove the background signal if present, 3) subtract the contribution of the molecules which present peaks at different a.m.u. – e.g. CO_2 has peaks at a.m.u. of 12, 16, 22, 28, 44, 45, 46) include the relative sensitivity of each molecule to be ionized, which changes depending on the gas mixture 5) add up all the partial pressures to calculate the total pressure $\sum pp_i = p_T$ and lastly 6) determine the gas composition as $Y_i = {pp_i}/{p_T}$

2.2.3. Reaction performance evaluation

The parameters used to describe the process performance are defined as follows:

$$CO_2(H_2)\ conversion = \chi_{CO_2}(\chi_{H_2}) = \frac{moles\ of\ CO_2(H_2)\ converted}{moles\ of\ CO_2(H_2)\ in\ feed} \quad (1)$$

$$Specific\ energy\ input = SEI\ (J\ cm^{-3}) = \frac{Power}{Input\ flow\ rate} \quad (2)$$

$$SEI\ (eV/mol) = \frac{SEI\ (J\ cm^{-3})}{3.92} \quad (3)$$

$$Total\ conversion = \chi_T = y_{CO_2\ in}.\chi_{CO_2} + y_{H_2\ in}.\chi_{H_2} \quad (4)$$

$$Energy\ efficiency\ (RWGS) = \eta = \frac{\chi_T\ \cdot\ \Delta H_r\ (0.425\ eV/mol)}{SEI\ (eV/mol)} \quad (5)$$

$$Energy\ efficiency\ (CO_2\ splitting) = \eta = \frac{\chi_{CO_2}\ \cdot\ \Delta H_r\ (2.9\ eV/mol)}{SEI\ (eV/mol)} \quad (6)$$

2.3. Results and discussion

Fig. 2.3 shows the mass spectra at different feed gas ratios (H_2:CO_2) in the presence and absence of plasma. Plasma triggered the dissociation of CO_2 and H_2, thus stimulating the RWGS reaction in which CO and H_2O were formed as the main products. For a feed gas mixture ratio of 3 (Fig. 2.3c), the relative intensity of CO_2 approached zero, which in turn resulted in the highest CO_2 dissociation rate.

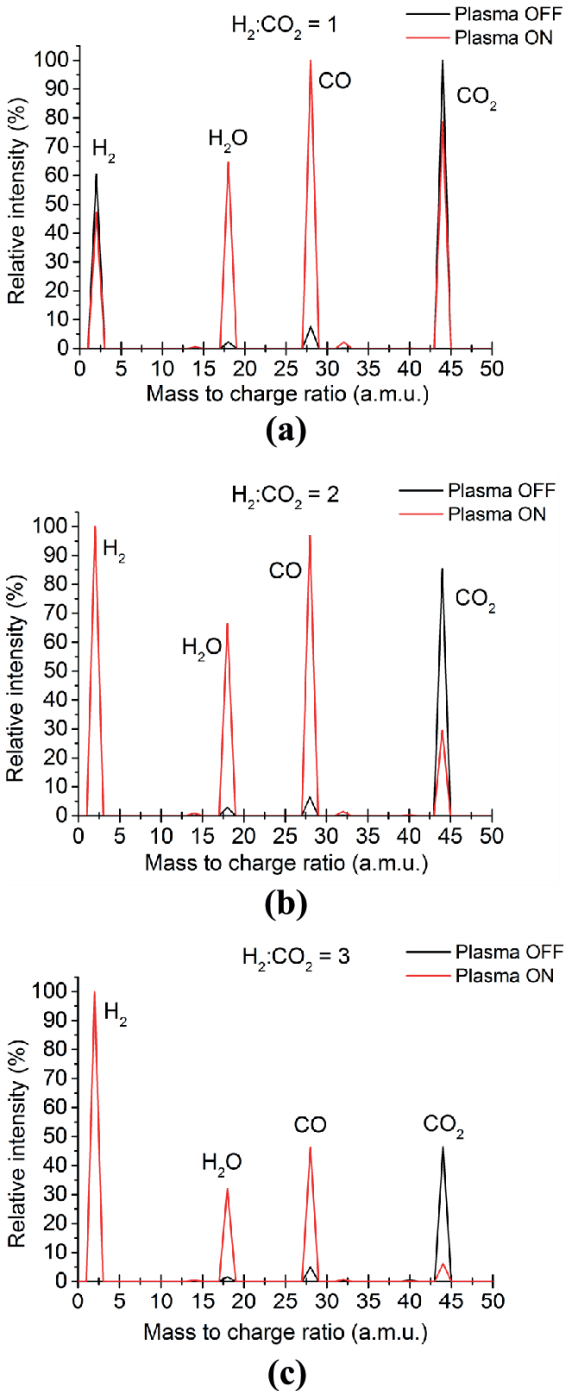

Fig. 2.3. Mass spectra with the plasma on and off at different H_2:CO_2 ratios. Note that in (b) and (c) the H_2 peaks with plasma off/on are overlapped (intensity normalized over the maximum).

2.3.1. Effect of inlet gas flow rate at varying inlet H_2:CO_2 ratio

Plasma was sustained purely by the reactants (CO_2 + H_2), without the need of an inert gas, which is commonly used in plasma-based reactors. The inlet gas flow rate was varied from 100 to 400 ml/min. At higher flow rates, it was not possible to sustain the plasma with the available microwave power. For a given inlet flow rate, the feed H_2:CO_2 ratio was varied in the range from 1 to 3. In the set of experiments presented in this section, the following parameters were maintained fixed: operating pressure (20 mbar), net input power (150 W), reactor volume (V_r = 6 ml, quartz tube of 500 mm length and 4 mm inner diameter), cooling rate (cooling water at 5 ^oC and air at 20 ^oC and flow rate of 20 l/min). The residence time of the reactants in the plasma medium, i.e. contact time of the gas mixture with plasma, varied from 0.1 to 0.4 s. The plasma column had a plasma radius of 1 mm and an average length of 200 mm, which slightly shortened with increasing gas flow rate. The specific energy input (SEI) ranged from 5.8 to 22.9 eV/mol.

Both the RWGS reaction and the splitting of CO_2 were investigated. In Fig. 2.4, the effect of the flow rate and H_2:CO_2 ratio on CO_2 conversion and energy efficiency are presented. The H_2:CO_2 ratio had noticeable impact on the CO_2 conversion. Fig. 2.4a shows that the highest CO_2 conversion (~85%) was obtained for a H_2:CO_2 ratio of 3, whereas for (a lower) H_2:CO_2=1, CO_2 conversion reached only ~40%. For the activation of pure CO_2, a maximum dissociation rate of 65% was obtained at the lowest gas flow rate (100 ml/min). Hence, H_2 acts as a "catalyst" for CO_2 decomposition.

The inlet flow rate for any given H_2:CO_2 ratio had a rather minor effect, nearly negligible, on CO_2 conversion, in the case of the RWGS reaction (Fig. 2.4a). The same observation was also made in [32], where changing the flow rate was shown to have no effect on the species concentrations. Contrariwise, as for the splitting of CO_2, a drastic decrease in the CO_2 dissociation was observed when increasing the gas flow rate. The same conclusion was drawn in [11], where a maximum CO_2 conversion efficiency of 90% was achieved at the lowest studied gas flow (15 sccm).

With regard to the energy efficiency (Fig. 2.4b), the best performance was obtained for CO_2 splitting with a maximum efficiency of 8% in the event of the lowest gas flow rate. As for the RGWS reaction, the maximum energy efficiency was 6% at the highest gas flow rate (400 ml/min) and H_2:CO_2 = 3. Concerning the effect of the inlet flow on the energy efficiency, Fig. 2.4b shows that an

increase in the flow rate results in higher energy efficiencies for the RWGS reaction and lower energy efficiencies for the dissociation of pure CO_2.

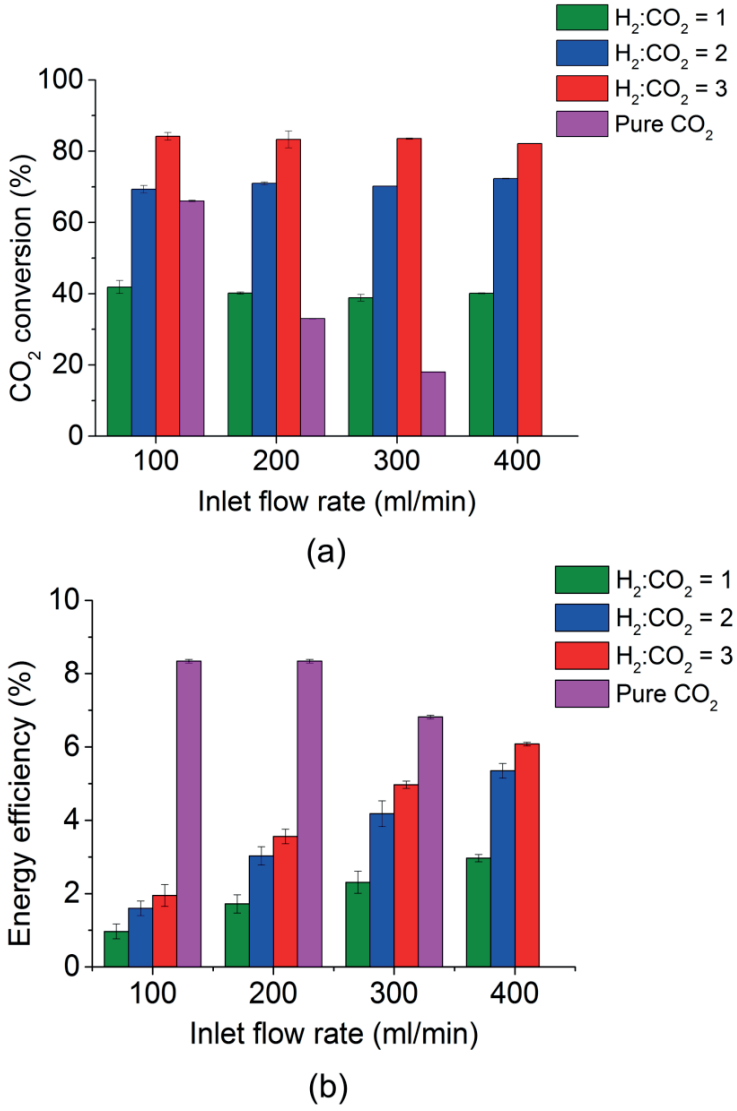

Fig. 2.4. Effect of the inlet gas flow for different H_2:CO_2 ratios on (a) CO_2 conversion and (b) energy efficiency. The following parameters were kept constant: pressure (20 mbar), net input power (150 W), reactor volume (V_r = 6 ml), cooling rate (cooling water at 5 °C and air at 20 °C and flow rate of 20 l/min).

The literature on the RWGS reaction in plasma conditions is limited. Previously reported results on this process together with the results of this work are presented in Table 2.1. Compared to previously reported studies on plasma-assisted RWGS, use of low-pressure microwave plasma (this work) seems to give the highest CO_2 conversion and energy efficiency (Table 2.1). As stated in section Mass spectroscopy analysis, in the present work the selectivity of CO_2 to CO is nearly of 100%, meaning that the formation of secondary carbon-bearing products is found negligibly small. In contrast, other works [24-26] report the formation of CH_4 at low concentrations (~0.1%). Even relatively small amounts of CH_4 in the product are undesirable if the produced gas is to be fed to a downstream reactor for further hydrogenation of CO to CH_3OH production via the CAMERE process.

Table 2.1. Overview of reported experimental data on plasma-assisted RWGS including this work.

OPERATING CONDITIONS				
Plasma type	**Operating pressure**	**Input power (W)**	**Gas flow (ml/min)**	**Inlet H_2:CO_2 ratio**
This work	20 mbar	150	400	3
DBD[25]	8 atm	500	500	3
Glow Discharge[24]	2.4 torr	10	10	4
Microwave[26]	2 torr	80-175	15	2

REACTOR PERFORMANCE		
Plasma type	**CO_2 conversion (%)**	**Energy efficiency (%)**
This work	82 ± 0.3	6.1 ± 0.2
DBD[25]	13	0.37
Glow Discharge[24]	26	0.72
*Microwave[26]	70	0.17-0.36

* The given values are based on readings from Fig. 2 in [26] where counts, in arbitrary units, are shown.

In Table 2.2, the performance of the herein studied microwave plasma reactor is compared to a conventional reactor in which a Ni/Ce-Zr-O catalyst is used [33]. It is shown that CO_2 conversion is much higher under plasma conditions, nearly 85% at H_2:CO_2 = 3 and 400 ml/min versus 50% in the conventional

reactor. More importantly, it should be noted that the conventional process requires high temperatures of ~750 °C, and consequently the use of bulky and costly gas-fired furnaces, as well as the use of catalyst with the potential associated issues of thermal degradation and coking at high temperatures [34].

As far as the energy cost is concerned, the conventional thermal catalytic process [33] requires an energy input of 1.6 eV/mol CO (1.2 eV/mol CO of sensible heat of reactants plus 0.4 eV/mol CO of heat of reaction considering the process conditions reported in [33]) versus 9.1 eV/mol for the microwave plasma reactor. This means that the plasma-based process consumes roughly six times more energy than the catalytic process. It is known that plasma-based processes are energy expensive; hence this remains the biggest challenge to address in this technology.

Table 2.2. Comparison of the microwave plasma reactor of this work with a conventional catalytic reactor [33].

Reactor type	Operating temperature (°C)	Gas flow (ml/min)	Operating pressure (bar)	H_2:CO_2 ratio	CO_2 conversion (%)
Microwave plasma	Cold plasma*	400	0,02	3	82 ± 0.3
Conventional (catalytic)[33]	750	50	1	1	50

* The outer wall temperature was monitored and ranged between 50 and 90 °C. The inner wall temperature can be assumed to be nearly the same considering the thin reactor wall thickness (0.5 mm). However, the temperature of the heavy particles in the plasma core was much higher (T_g>2000K) as discussed in section Optical emission spectroscopy (OES) analysis.

2.3.2. Effect of specific energy input (SEI)

The gas flow rate and the SEI – ratio of the discharge power over the gas flow rate through the discharge – are the most relevant input variables for process scale up. In this set of experiments, the net input power was varied to study the effect of the SEI on CO_2 conversion and energy efficiency. The inlet gas flow (200 ml/min), the feed gas composition (H_2:CO_2 = 1), and the operating pressure (16 mbar) were kept constant throughout the experiments, while the SEI was varied from 1 up to 12 eV/mol. Fig. 2.5 shows the effect of the SEI on CO_2 conversion and energy efficiency. These parameters show a trade-off: when

raising the SEI, CO_2 conversion increases but the energy efficiency drops and vice-versa. A similar behaviour was observed in [18] for the dry reforming of CH_4. Under the aforementioned operating conditions, a maximum energy efficiency of 8% was reached at a SEI = 1.5 eV/mol and CO_2 conversion = 23%. On the contrary, CO_2 conversion increased monotonically with SEI, with a decreasing slope, up to ~50% asymptotic level at SEI > 8 eV/mol. Above 8 eV/mol, the microwave energy input is mainly converted into thermal energy instead of chemical energy. This is in accordance with the temperature measurements at the reactor wall. A rather low temperature increase was measured when SEI increased from 1 to 8 eV/mol (60-65 °C), whereas when SEI increased from 8 to 12 eV/mol, the wall temperature increased from 65 to 90 °C. This phenomenon can also be observed in Fig. 2.6, where the concentration of reactants and products underwent small variations at a net power input above 100 W, compared to the lower power range (10-100 W).

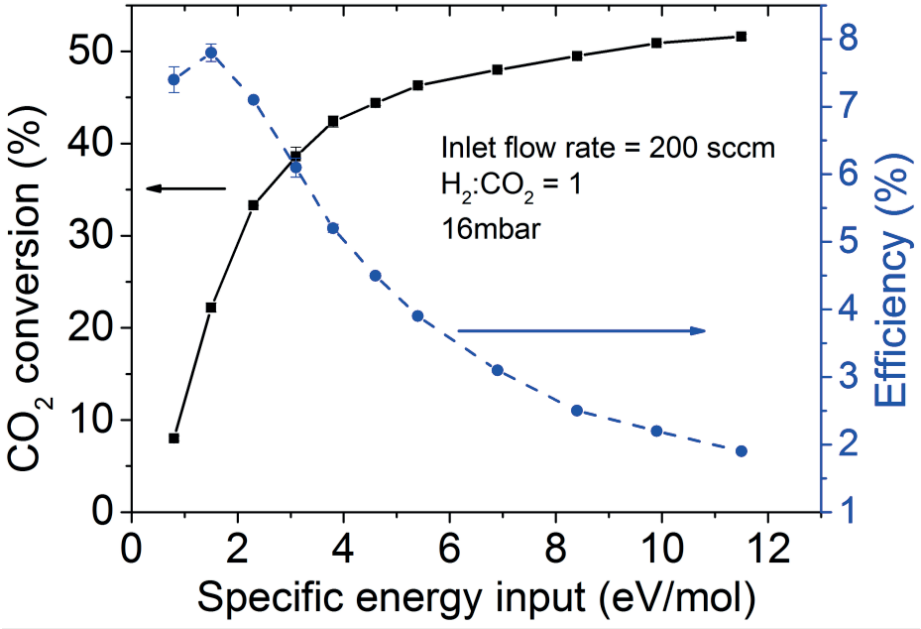

Fig. 2.5. Effect of the specific energy input (SEI) on CO_2 conversion and energy efficiency.

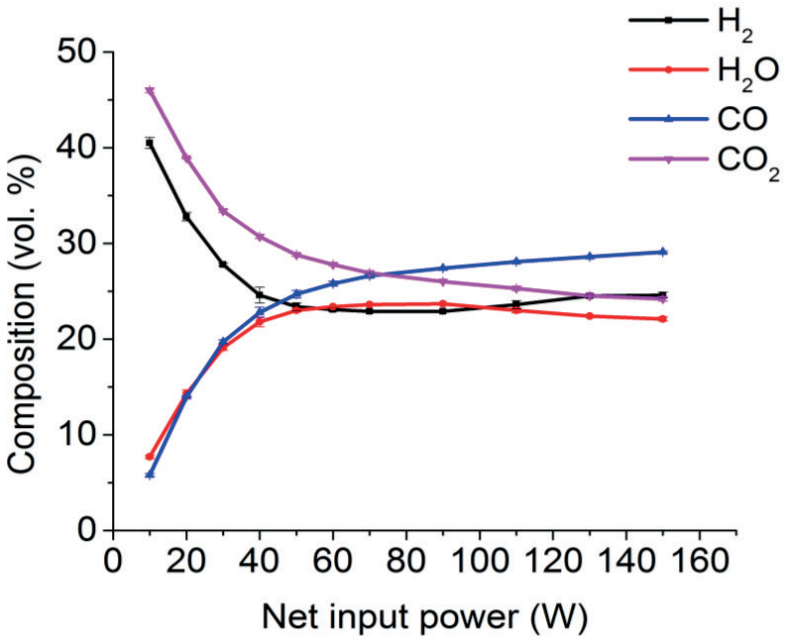

Fig. 2.6. Composition of the main species in the product gas as function of the net input power. The applied experimental conditions were the same as the ones mentioned in Fig. 2.5.

2.3.3. Reaction scheme for the dissociation of CO_2 and H_2

A simplified reaction scheme for the dissociation of CO_2 and H_2 is herein proposed to investigate the effect of the gas temperature on the product composition. The microwave discharge is regarded as a source of reactive species that initiate chemical reactions. This takes place by collisions of highly energetic electrons generated in the plasma with the gas molecules, which predominantly produce H and O atoms. This model is based on a similar approach taken in [32]. The microwave plasma can be considered as a localized high temperature medium, enabling high temperature chemistry in a relatively cold environment. The reaction scheme is summarized in Table 2.3 and consists of 19 reactions among 8 species. The chemical reaction engineering module of COMSOL Multiphysics 5.1 [35] was used to solve an isothermal zero-dimensional (0-D) reactor model in which heavy species mass balances are computed at different gas temperatures using the rates constants presented in Table 2.3.

As suggested in [32], the hydroperoxy radical (HO_2) may have significant influence on the product gas; therefore, 5 reactions (reactions 3, 6, 7, 8 and 13 from ref. [32]) were initially added to the proposed scheme. However, it was found that the effect of the HO_2 concentration on the product species concentrations was practically negligible. This is due to the low reaction rates involving HO_2 for a simulation time up to 0.2 s (Fig. 2.7), which corresponds with experiments at a flow rate equal of 200 ml/min. Therefore, these reactions were discarded from the reaction scheme. Besides, as discussed in section Mass spectroscopy analysis, CH_3OH concentration in the products was very low, in the range of 10-20 ppm; consequently, all the reactions related to CH_3OH formation were also neglected, as opposed to the model described in [25].

Table 2.3: Chemical reactions included in the simplified reaction scheme for the reaction of CO_2 with H_2.

Number	Reaction	Rate constant (cm^3 $molecule^{-1}$ s^{-1})	Ref.
1	$CO_2 + CO_2 \rightarrow CO + O + CO_2$	$4.39 \times 10^{-7} \exp(-65000/T)$	[36, 37]
2	$CO_2 + CO \rightarrow CO + O + CO$	$4.39 \times 10^{-7} \exp(-65000/T)$	[36, 37]
3	$CO_2 + O_2 \rightarrow CO + O + O_2$	$3.72 \times 10^{-10} \exp(-60200/T)$	[37]
4	$CO_2 + O \rightarrow CO + O_2$	$7.77 \times 10^{-12} \exp(-16600/T)$	[36]
5	$CO + O_2 \rightarrow CO_2 + O$	$1.23 \times 10^{-12} \exp(-12800/T)$	[36]
6	$O_2 + CO_2 \rightarrow O + O + CO_2$	$2.57 \times 10^{-9} \exp(-56150/T)$	[37]
7	$O_2 + CO \rightarrow O + O + CO$	$2.40 \times 10^{-9} \exp(-59500/T)$	[37]
8	$O_2 + O_2 \rightarrow O + O + O_2$	$8.14 \times 10^{-9} \exp(-59700/T)$	[37]
9	$O_2 + O \rightarrow O + O + O$	$2 \times 10^{-8} \exp(-57900/T)$	[37]
10	$CO_2 + H \rightarrow CO + OH$	$2.5 \times 10^{-10} \exp(-13300/T)$	[38]
11	$CO + OH \rightarrow CO_2 + H$	$1.12 \times 10^{-13} \exp(0{,}00091*T)$	[38]
12	$H_2 + H_2 \rightarrow H + H + H_2$	$1.43 \times 10^{-12} T^{-0,7} \exp(-52530/T)$	[39]
13	$O + H_2 \rightarrow OH + H$	$1.80 \times 10^{-20} T^{2,8} \exp(-2980/T)$	[38]
14	$OH + H_2 \rightarrow H_2O + H$	$1.06 \times 10^{-17} T^{2} \exp(-1490/T)$	[38]
15	$OH + H \rightarrow O + H_2$	$8.10 \times 10^{-21} T^{2,8} \exp(-1950/T)$	[38]
16	$OH + O \rightarrow H + O_2$	$7.50 \times 10^{-10} T^{-0,5} \exp(-30/T)$	[38]
17	$OH + OH \rightarrow H_2O + O$	$3.50 \times 10^{-16} T^{1,4} \exp(200/T)$	[38]
18	$H_2O + H \rightarrow H_2 + OH$	$1.03 \times 10^{-16} T^{1,9} \exp(-9265/T)$	[38]
19	$H_2O + O \rightarrow OH + OH$	$7.60 \times 10^{-15} T^{1,3} \exp(-8605/T)$	[38]

The mechanism of the RWGS reaction considering the proposed scheme starts with reaction 1, where CO and O are produced. The generation of O atoms predominantly leads to the production of OH radicals and H atoms via reaction 13. Consequently, the large concentration of H atoms renders reaction 10 the main path for CO production, whereas reaction 14 dominates the H_2O

formation path (via reactions 10 and 13 for OH radical generation). These reactions (10 and 14) have the highest reaction rates at the studied gas temperatures and residence time.

As reported in [21, 36, 40], an increase in the microwave power input gives rise to higher gas temperatures, implying that when the SEI is raised, the gas temperature also increases. It was observed experimentally that the saturation of the CO production was practically achieved at net input powers higher than 100 W (Fig. 2.6). This is also computed by the model as shown in Fig. 2.7, where the saturation of the CO_2 conversion occurs at gas temperatures above 2100 K. This fact may explain why experimentally an input power higher than 100 W caused barely no increase in the production of CO.

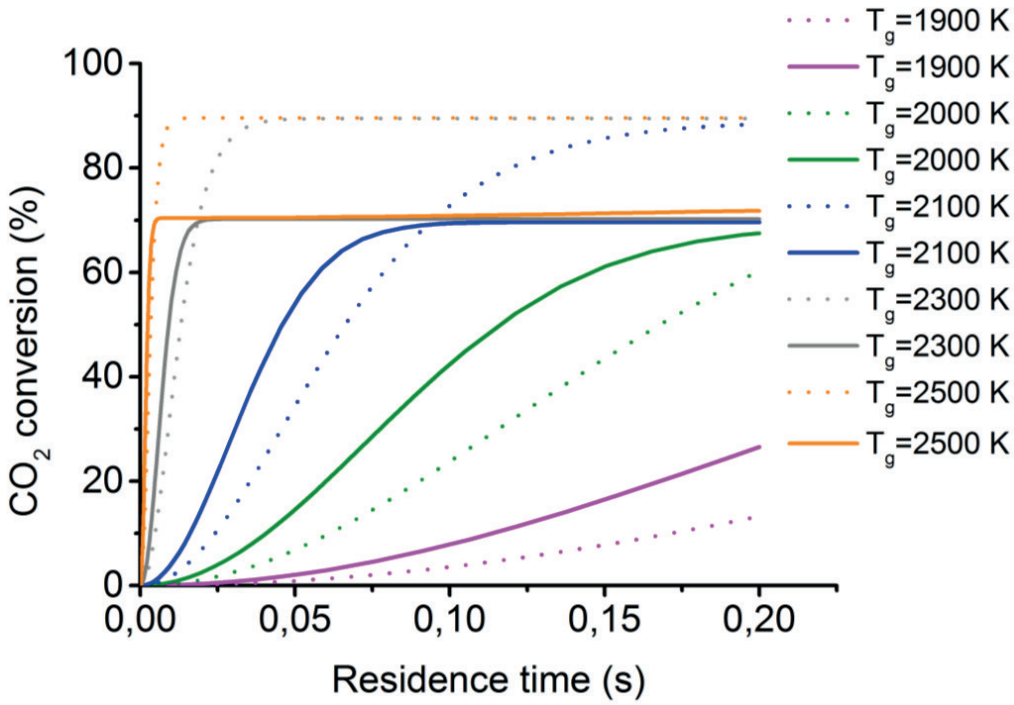

Fig. 2.7. Modeling results of CO_2 conversion *vs* residence time at different gas temperatures (T_g=1900-2500 K). Two different feed gas mixture ratios were considered in the calculations; H_2:CO_2=1 (solid lines) and H_2:CO_2=3 (dot lines).

The required gas temperature to reach the experimentally obtained CO_2 conversions, presented in Fig. 2.4a, was verified numerically. For a flow rate equal to 200 ml/min (equivalent residence time of 0.2 s) the measured CO_2

conversion ranged from 40 to 80 % at different H_2:CO_2 ratios (1-3). The 0-D model shows that similar conversion values are obtained at gas temperatures equal to 1950 K for H_2:CO_2=1 and 2100 K for H_2:CO_2=3. The calculated gas temperature, based on optical emission spectroscopy (following section Optical emission spectroscopy (OES) analysis), was ~2700 K in the plasma core. It is likely that this temperature is overestimated and most probably ranges from 2200 to 2400 K. The reader should take into account that the determination of the gas temperature is inaccurate, based on the calculation of the rotational temperature of the OH radical via Optical Emission Spectroscopy (OES). Commonly used temperature measurement devices cannot be used to measure the gas temperature in the plasma due to interferences with the microwave field. In this regard, a range of validity is given considering the results reported in [40, 41]. Moreover, it should be noted that some of the proposed rate constants in Table 2.3 are out of range (T_g<2000 K, [38]). Lastly, considering the simplicity of the herein proposed reaction scheme, the model calculations qualitatively match the trends observed experimentally as for the CO_2 conversion.

2.3.4. Optical Emission Spectroscopy (OES) analysis

Optical emission spectroscopy was employed to identify the main chemical species present in the plasma. It should be noted that the emitted light from the plasma was captured very close to the ignition zone, where the microwave plasma discharge shows the strongest light intensity. The main species driving the chemical reactions in the plasma are the H and O atoms (Fig. 2.8), and the OH radicals to a lesser extent. Fig. 2.8 shows that the intensity of the H_α and H_β emission lines is much higher compared to the other species (e.g. O atomic emission lines) even for a ratio H_2:CO_2 = 1. The intensity of the OH radical was quite low at both gas mixture ratios (H_2:CO_2 = 1 and 3), implying that the concentration of this species was rather low in the microwave discharge. A similar observation was reported in [32] as well, where the OH radical concentration was three and two orders of magnitude lower than the H and O concentrations, respectively. The dominant chemical reactions in the plasma zone, in particular close to the ignition source, are the generation of H and O atoms, which are the precursors for the formation of CO and H_2O via the reactions 10, 13 and 14 (Table 2.3). The microwave discharge was therefore identified as the source of H and O atoms. Lastly, the intensity of the O atoms in the case of H_2:CO_2 = 3 (Fig. 2.8b) is, as expected, much lower than in the case of an equimolar gas mixture ratio (Fig. 2.8a).

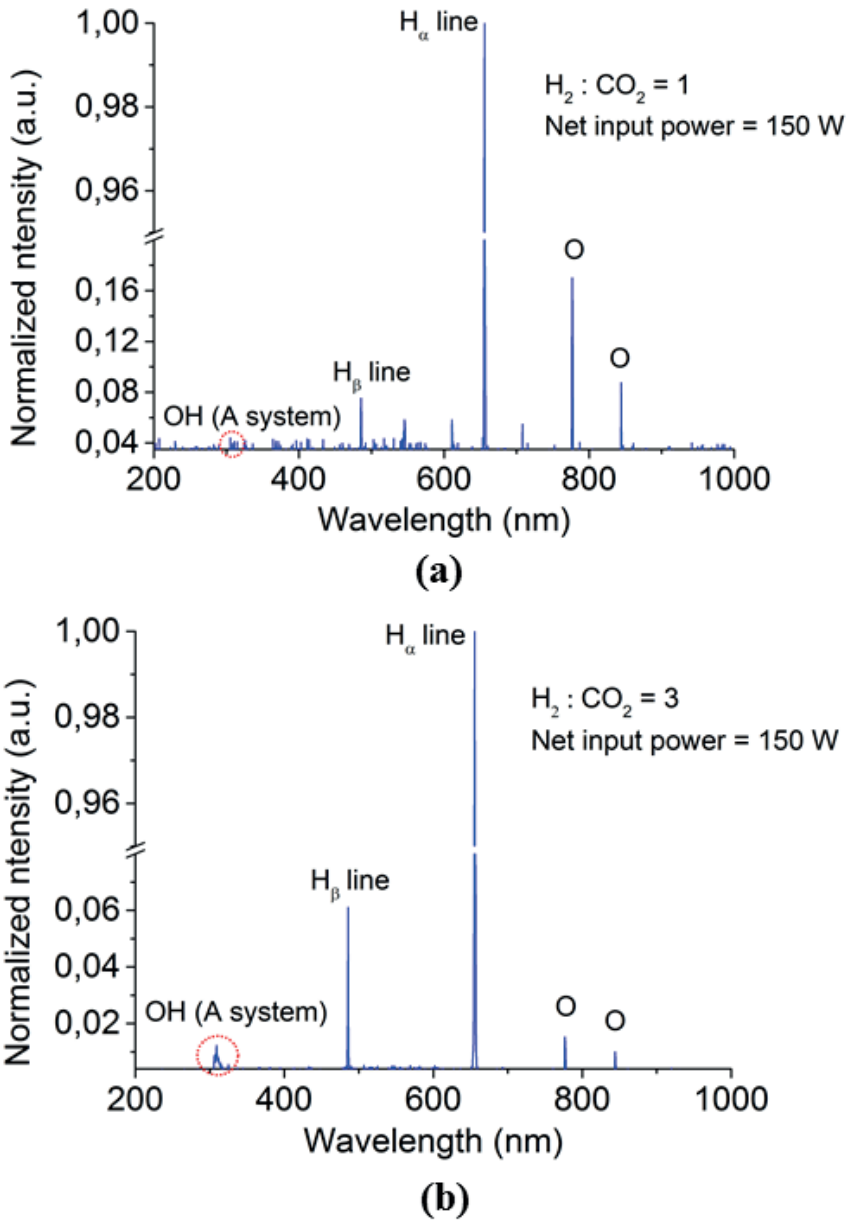

Fig. 2.8. Optical emission spectra measured experimentally at H_2:CO_2 feed ratios of 1 and 3.

2.3.4.1. Electron density determination

A commonly used method to determine the electron density (n_e) is by means of the hydrogen Balmer series, particularly the hydrogen-alfa (H_α) and hydrogen-beta (H_β) lines. In this work, the H_β line was used to compute n_e because the dependence of the Stark broadening on the electron temperature (T_e) and the effect of ionic dynamics on the H_β profile [42, 43] can be neglected. The expressions proposed by Gigosos et al. [44] and Laux et al. [45] for the H_β line were used to calculate the electron density. A previous step in which the Stark broadening width ($\Delta\lambda_s$) is computed by fitting the experimentally obtained H_β line via a Voigt function [10] is required to enable the determination of the Gaussian and Lorentzian components. The fitting results of the Voigt function to the experimental data for two different H_2:CO_2 ratios are shown in Fig. 2.9. At low gas mixture ratios the contribution of the H_β line was too weak to allow for good fitting, therefore only the feed mixture ratios of 3 and 4 are considered for this purpose. It is observed that when the amount of H_2 is increased the electron density also increases, indicating that the feed composition has direct influence on the plasma-related parameters. The dissociation energy of the H_2 molecule is lower compared to the CO_2 molecule (4.4 vs 5.5 eV), hence the probability to dissociate H_2 is higher, resulting in a larger fraction of H atoms through the reaction: $H_2 + e \rightarrow H + H + e$ [25].

The main production mechanism of energetic electrons in plasma is via ionization processes [14]. A larger fraction of H atoms, which present a slightly lower ionization energy compared to the CO_2 molecule and CO_2-related species, in combination with higher electron temperatures (see subsection Gas an electron temperatures), results in higher electron densities as displayed in Fig. 2.9. A twofold effect may occur: 1) a higher number of electrons is available to produce highly reactive species enhancing the potential of chemical reactions, and 2) improvement in the energy transfer mechanisms from the energetic electrons to the heavy particles, which raises the gas temperature. This twofold effect in combination with an increase in the H_2:CO_2 feed ratio (lower CO_2 partial pressure) improves notably the CO_2 conversion. It was also previously reported that the addition of 1% H_2 to a pure CO_2 feed improved the energy efficiency by 5% [12].

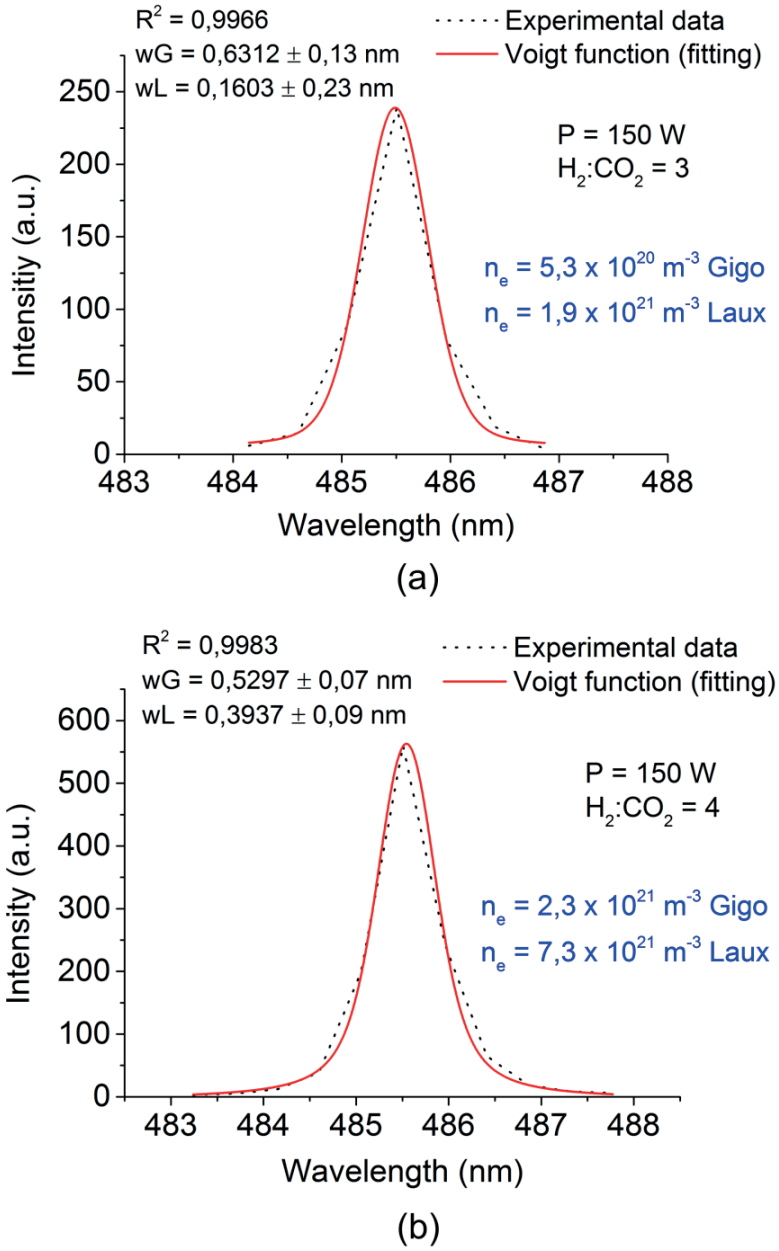

Fig. 2.9. H_β lines and Voigt function fitting at different feed gas compositions. OriginPro was used to determine the Gaussian and Lorentzian components [10]. The expressions proposed in [44, 45] were employed to calculate the Stark broadening width and the electron density.

2.3.4.2. Gas and electron temperatures

The detection of the OH radical ($A\,^2\Sigma^+ - X\,^2\Pi_\gamma$ transition) enabled the calculation of the rotational temperature T_{rot}, which can be approximated to the gas temperature [21, 45, 46]. The two atomic oxygen emission lines at 777 nm ($^5P \rightarrow {}^5S^0$ transition) and 844 nm ($^3P \rightarrow {}^3S^0$ transition) were used to evaluate the excitation temperature T_{ex}, which can be assumed equal to T_e when the plasma is in local thermodynamic equilibrium (LTE) [47]. T_e mostly affects the intensity of these emission lines [48, 49]. The software SPECAIR was used to compare experimental results to simulated spectra, giving gas and electron temperatures as outputs.

With regard to the rotational (gas) temperature, a value of about 2700 K is predicted as shown in Fig. 2.10. A rotational temperature of 2260 K was reported for the same plasma system at similar operating conditions (input power=150 W, flow rate=18 ml/min and operating pressure=7.5 torr (~10 mbar)) in [40]. In the present work, the measurement was obtained at an operating pressure of 25 mbar, a net input power of 150 W and a gas mixture ratio H_2:CO_2 = 4. At these conditions, the highest intensity of the OH radical peak was attained, which in turn improved the fitting. It is then expected to obtain a higher gas temperature than those reported in [40], considering that higher operating pressure (25 *vs* 10 mbar) brings the plasma closer to thermal equilibrium [14].

However, the computed gas temperature seems to be overestimated. Fig. 2.10 shows that the calculated P/R branch peak ratio (red dot line) is lower than the one observed experimentally (black line). The P/R branch peak ratio affects significantly the gas temperature as described in [45], where higher P/R ratios result in lower gas temperatures. Hence, we can conclude that the computed gas temperature by SPECAIR is overestimated due to the mismatch between the experimental and calculated P/R branch peak ratios. Therefore, the gas temperature most likely lies in the range 2200 – 2400 K based on the results reported in [40].

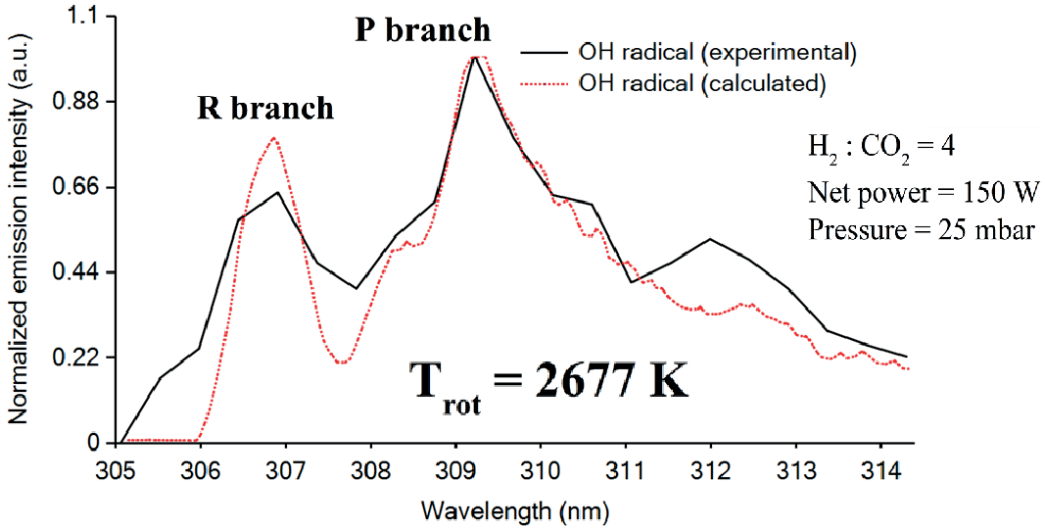

Fig. 2.10. Experimental and fitted spectra calculated using the software SPECAIR to determine the gas temperature based on the intensity of the R and P branches of the OH radical. A feed gas mixture ratio H_2:CO_2=4 was required to obtain a peak with intensity high enough for the fitting.

Concerning the excitation (electron) temperature, the experimental spectra at feed gas compositions H_2:CO_2=1 and 3 were analysed. As shown in Fig. 2.11, the electron temperature is also influenced by the H_2 content in the feed. Particularly, T_e increases at high H_2:CO_2 ratios. The increase in the H_2 content enables the formation of a larger fraction of H atoms in the plasma. Atoms cannot be excited vibrationally and/or rotationally by the electrons, meaning that less energy is consumed in these collisional processes, thus allowing these electrons to gain higher kinetic energies. This boost in the T_e results in higher ionization rates, which explains the observed increase in the electron density (Fig. 2.9). The computed values, 0.7 eV for H_2:CO_2 = 1 and 1.3 eV for H_2:CO_2 = 3 are found within the expected range for low-pressure microwave discharges ($T_e \approx 1$ eV) [14, 50].

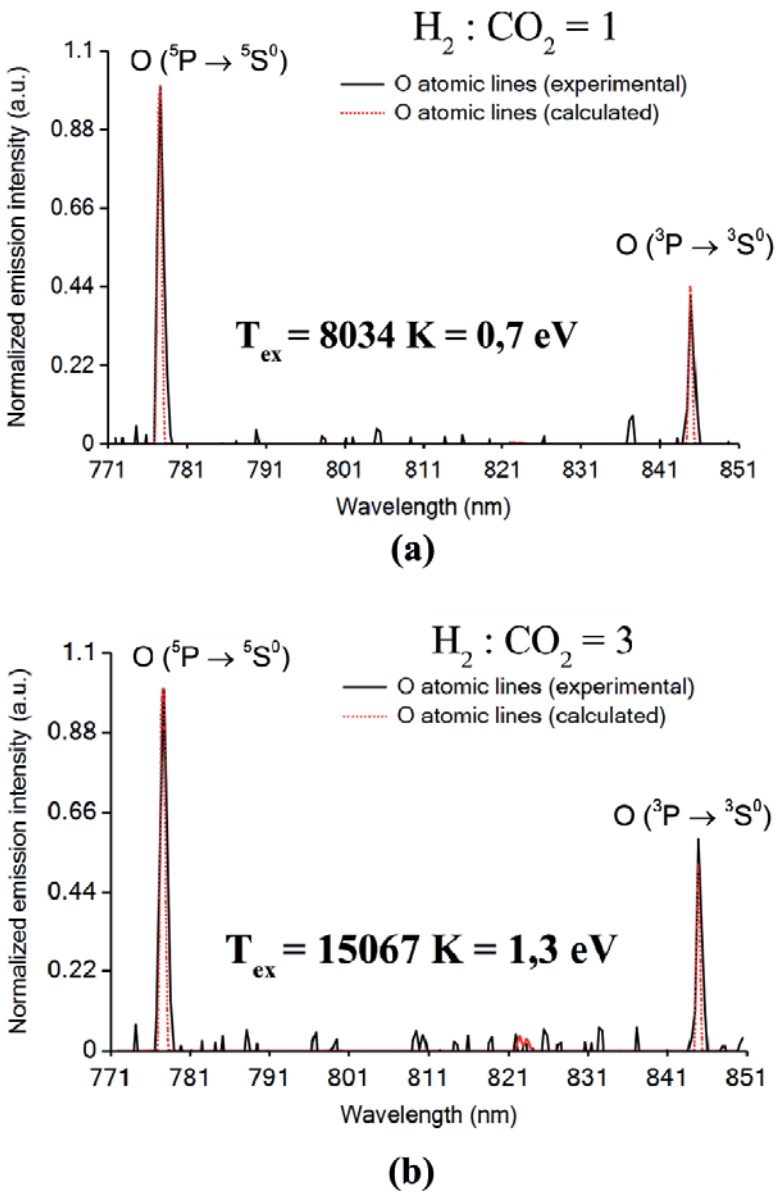

Fig. 2.11. Experimental spectra and fitted spectra calculated using the software SPECAIR to determine the excitation (electron) temperature based on the two O atomic lines at different H_2:CO_2 ratios.

2.4. Conclusions

We carried out experiments of simultaneous dissociation of CO_2 and H_2 in a non-equilibrium microwave plasma reactor. The effect of different operating conditions, such as the gas flow rate, specific energy input and gas feed composition (H_2:CO_2 ratio) on CO_2 conversion and energy efficiency were investigated. The best performance was obtained for a feed mixture ratio of H_2:CO_2 = 3 at which CO_2 conversion was nearly 85% at an energy efficiency of ~6%. To our knowledge, these are the highest values reported for plasma-assisted RWGS. Negligible amounts of C_2H_4 and CH_3OH at the product were measured, meaning that nearly 100% selectivity of CO_2 to CO was achieved. The activation of pure CO_2 in the microwave discharge was also explored; a maximum CO_2 dissociation rate of 65% with energy efficiency of 8% was obtained under the same operating conditions considered for the RWGS reaction.

A simplified reaction model qualitatively reproduced the experimental observations. The chemical reaction engineering module of COMSOL Multiphysics 5.1 was used to compute the species concentrations by solving an isothermal zero-dimensional reactor model. The model showed that the generation of H and O atoms were the dominant intermediate species, which was also proven by OES measurements. Further, at high H_2 content in the feed, electron density and temperature increased due to the large concentration of H atoms in plasma. The increase in the fraction of H atoms, which present a slightly lower ionization energy compared to the CO_2 molecule, results in intensification of the ionization processes occurring in the plasma, and as a result, in higher electron densities. Moreover, H atoms cannot be excited vibrationally and/or rotationally by electrons, which allows the electrons to gain higher kinetic energies increasing then the ionization reaction rates. Therefore, a twofold effect is attained by increasing the H_2:CO_2 molar ratio in the feed, namely decrease in the CO_2 partial pressure and increase in the electron density and temperature; both effects promote higher CO_2 conversions.

References

[1] Hameer S, van Niekerk JL. A review of large-scale electrical energy storage. Int J Energ Res. 2015;39:1179-95.
[2] Peter Styring DJ. Carbon Capture and Utilisation in the green economy. The centre for Low Carbon Futures 2011.
[3] Atsonios K, Panopoulos KD, Kakaras E. Investigation of technical and economic aspects for methanol production through CO2 hydrogenation. Int J Hydrogen Energ. 2016;41:2202-14.
[4] Patil BS, Wang Q, Hessel V, Lang J. Plasma N-2-fixation: 1900-2014. Catal Today. 2015;256:49-66.
[5] Sturm GSJ, Munoz AN, Aravind PV, Stefanidis GD. Microwave-Driven Plasma Gasification for Biomass Waste Treatment at Miniature Scale. Ieee T Plasma Sci. 2016;44:670-8.
[6] Khorasany RMH, Singh Y, Sadeghi Alavijeh A, Kjeang E, Wang GG, Rajapakse RKND. Fatigue properties of catalyst coated membranes for fuel cells: Ex-situ measurements supported by numerical simulations. Int J Hydrogen Energ. 2016;41:8992-9003.
[7] Alavijeh AS, Khorasany RMH, Nunn Z, Habisch A, Lauritzen M, Rogers E, et al. Microstructural and Mechanical Characterization of Catalyst Coated Membranes Subjected to In Situ Hygrothermal Fatigue. J Electrochem Soc. 2015;162:F1461-F9.
[8] Durka T, Stefanidis GD, Van Gerven T, Stankiewicz AI. Microwave-activated methanol steam reforming for hydrogen production. Int J Hydrogen Energ. 2011;36:12843-52.
[9] Pacheco J, Soria G, Pacheco M, Valdivia R, Ramos F, Frías H, et al. Greenhouse gas treatment and H2 production, by warm plasma reforming. Int J Hydrogen Energ. 2015;40:17165-71.
[10] Tsyganov D, Bundaleska N, Tatarova E, Ferreira CM. Ethanol reforming into hydrogen-rich gas applying microwave 'tornado'-type plasma. Int J Hydrogen Energ. 2013;38:14512-30.
[11] Spencer LF, Gallimore AD. Efficiency of CO2 Dissociation in a Radio-Frequency Discharge. Plasma Chem Plasma P. 2011;31:79-89.
[12] Nunnally T, Gutsol K, Rabinovich A, Fridman A, Gutsol A, Kemoun A. Dissociation of CO2 in a low current gliding arc plasmatron. J Phys D Appl Phys. 2011;44.
[13] Kwak HS, Uhm HS, Hong YC, Choi EH. Disintegration of Carbon Dioxide Molecules in a Microwave Plasma Torch. Sci Rep-Uk. 2015;5:18436.

[14] Fridman A. Plasma Chemistry: Cambridge: Cambridge University Press; 2008.
[15] Jasinski M, Czylkowski D, Hrycak B, Dors M, Mizeraczyk J. Atmospheric pressure microwave plasma source for hydrogen production. Int J Hydrogen Energ. 2013;38:11473-83.
[16] Ghorbanzadeh AM, Lotfalipour R, Rezaei S. Carbon dioxide reforming of methane at near room temperature in low energy pulsed plasma. Int J Hydrogen Energ. 2009;34:293-8.
[17] Tao XM, Bai MG, Wu QY, Huang ZJ, Yin YX, Dai XY. CO2 reforming of CH4 by binode thermal plasma. Int J Hydrogen Energ. 2009;34:9373-8.
[18] Snoeckx R, Zeng YX, Tu X, Bogaerts A. Plasma-based dry reforming: improving the conversion and energy efficiency in a dielectric barrier discharge. Rsc Adv. 2015;5:29799-808.
[19] Li DH, Li X, Bai MG, Tao XM, Shang SY, Dai XY, et al. CO2 reforming of CH4 by atmospheric pressure glow discharge plasma: A high conversion ability. Int J Hydrogen Energ. 2009;34:308-13.
[20] Nizio M, Albarazi A, Cavadias S, Amouroux J, Galvez ME, Da Costa P. Hybrid plasma-catalytic methanation of CO2 at low temperature over ceria zirconia supported Ni catalysts. Int J Hydrogen Energ. 2016;41:11584-92.
[21] Chen GX, Silva T, Georgieva V, Godfroid T, Britun N, Snyders R, et al. Simultaneous dissociation of CO2 and H2O to syngas in a surface-wave microwave discharge. Int J Hydrogen Energ. 2015;40:3789-96.
[22] Futamura S, Kabashima H. Production of synthesis gas from H2O and CO2 with nonthermal plasma. Abstr Pap Am Chem S. 2003;225:U862-U.
[23] Ihara T, Ouro T, Ochiai T, Kiboku M, Iriyama Y. Formation of methanol by microwave-plasma reduction of CO2 with H2O. B Chem Soc Jpn. 1996;69:241-4.
[24] Kano M, Satoh G, Iizuka S. Reforming of Carbon Dioxide to Methane and Methanol by Electric Impulse Low-Pressure Discharge with Hydrogen. Plasma Chem Plasma P. 2012;32:177-85.
[25] Eliasson B, Kogelschatz U, Xue BZ, Zhou LM. Hydrogenation of carbon dioxide to methanol with a discharge-activated catalyst. Ind Eng Chem Res. 1998;37:3350-7.
[26] Maya L. Plasma-assisted reduction of carbon dioxide in the gas phase. Journal of Vacuum Science & Technology a-Vacuum Surfaces and Films. 2000;18:285-7.
[27] Joo OS, Jung KD, Moon I, Rozovskii AY, Lin GI, Han SH, et al. Carbon dioxide hydrogenation to form methanol via a reverse-water-gas-shift reaction (the CAMERE process). Ind Eng Chem Res. 1999;38:1808-12.

[28] Joo OS, Jung KD, Jung YS. CAMERE Process for methanol synthesis from CO2 hydrogenation. Carbon Dioxide Utilization for Global Sustainability. 2004;153:67-72.
[29] Roth JR. Indutrial plasma engineering IOP Publishing Ltd: British Library; 1995.
[30] Moisan M, Zakrzewski Z, Pantel R. Theory and Characteristics of an Efficient Surface-Wave Launcher (Surfatron) Producing Long Plasma Columns. J Phys D Appl Phys. 1979;12:219-&.
[31] Selby M, Hieftje GM. Taming the Surfatron. Spectrochim Acta B. 1987;42:285-98.
[32] Levanov AV, Gromov AR, Antipenko EE, Lunin VV. The kinetics of chemical reactions in the products of dissociation of the CO2-H-2 gas mixture in microwave discharge. Russ Chem B+. 2000;49:669-73.
[33] Sun FM, Yan CF, Wang ZD, Guo CQ, Huang SL. Ni/Ce-Zr-O catalyst for high CO2 conversion during reverse water gas shift reaction (RWGS). Int J Hydrogen Energ. 2015;40:15985-93.
[34] Argyle MD, Bartholomew CH. Heterogeneous Catalyst Deactivation and Regeneration: A Review. Catalysts. 2015;5:145-269.
[35] Comsol Multiphysics v.5.1 Reaction Engineering Module User's Guide. COMSOL AB, Stockholm, Sweden. 2015.
[36] Kozak T, Bogaerts A. Evaluation of the energy efficiency of CO2 conversion in microwave discharges using a reaction kinetics model. Plasma Sources Sci T. 2015;24:015024.
[37] Machrafi H, Cavadias S, Amouroux J. CO2 valorization by means of Dielectric Barrier Discharge. Journal of Physics: Conference Series. 2011;275:012016.
[38] Tsang W, Hampson RF. Chemical Kinetic Database for Combustion Chemistry .1. Methane and Related-Compounds. J Phys Chem Ref Data. 1986;15:1087-279.
[39] Obrusnik A, Bonaventura Z. Studying a low-pressure microwave coaxial discharge in hydrogen using a mixed 2D/3D fluid model. J Phys D Appl Phys. 2015;48.
[40] Riviere B, Mermet JM, Deruaz D. Spectroscopic Evaluation of a Carbon-Dioxide and a Helium Carbon Dioxide Microwave-Induced Plasma (Surfatron). J Anal Atom Spectrom. 1988;3:551-5.
[41] Krzysztof J. Jankowski ER. Microwave Induced Plasma Analytical Spectrometry: RSC Publishing 2011.
[42] Yubero C, Garcia MC, Calzada MD. On the use of the H alpha spectral line to determine the electron density in a microwave (2.45GHz) plasma torch at atmospheric pressure. Spectrochim Acta B. 2006;61:540-4.

[43] Belmonte T, Noel C, Gries T, Martin J, Henrion G. Theoretical background of optical emission spectroscopy for analysis of atmospheric pressure plasmas. Plasma Sources Sci T. 2015;24.
[44] Gigosos MA, Gonzalez MA, Cardenoso V. Computer simulated Balmer-alpha, -beta and -gamma Stark line profiles for non-equilibrium plasmas diagnostics. Spectrochim Acta B. 2003;58:1489-504.
[45] Laux CO, Spence TG, Kruger CH, Zare RN. Optical diagnostics of atmospheric pressure air plasmas. Plasma Sources Sci T. 2003;12:125-38.
[46] Silva T, Britun N, Godfroid T, Snyders R. Optical characterization of a microwave pulsed discharge used for dissociation of CO2. Plasma Sources Sci T. 2014;23:025009.
[47] Calzada MD, Moisan M, Gamero A, Sola A. Experimental investigation and characterization of the departure from local thermodynamic equilibrium along a surface-wave-sustained discharge at atmospheric pressure. J Appl Phys. 1996;80:46-55.
[48] Spencer LF, Gallimore AD. CO2 dissociation in an atmospheric pressure plasma/catalyst system: a study of efficiency. Plasma Sources Sci T. 2013;22:015019.
[49] Leins M, Walker M, Schulz A, Schumacher U, Stroth U. Spectroscopic Investigation of a Microwave-Generated Atmospheric Pressure Plasma Torch. Contrib Plasm Phys. 2012;52:615-28.
[50] Jimenez-Diaz M, Carbone EAD, van Dijk J, van der Mullen JJAM. A two-dimensional Plasimo multiphysics model for the plasma-electromagnetic interaction in surface wave discharges: the surfatron source. J Phys D Appl Phys. 2012;45:335204.

3

On the improvement of chemical conversion in a surface-wave microwave plasma reactor for CO_2 reduction with hydrogen (The Reverse Water-Gas Shift reaction)

This chapter is published as:

de la Fuente JF, Moreno SH, Stankiewicz AI and Stefanidis GD, On the improvement of chemical conversion in a surface-wave microwave plasma reactor for CO_2 reduction with hydrogen (The Reverse Water-Gas Shift reaction). *International Journal of Hydrogen Energy* **42**: 12943-12955 (2017).

Abstract

A novel surface-wave microwave discharge reactor configuration to generate syngas via gaseous CO_2 reduction with H_2 (non-catalytic Reverse Water-Gas Shift reaction) is studied in the context of power-to-chemicals concept. Improvement of CO_2 conversion to maximize CO production is explored by adding an external cylindrical waveguide downstream of the plasma generation system. A 2D self-consistent argon model shows that power absorption and plasma uniformity are improved in the presence of the waveguide. We show experimentally that CO_2 conversion is increased by 50% (from 40% to 60%) at the stoichiometric feed ratio H_2:CO_2 equal to 1 when using the waveguide. At higher H_2:CO_2 ratios, the effect of the waveguide on the reactor performance is nearly negligible. Optical emission spectroscopy reveals that the waveguide causes significant increase in the concentration of O atoms at a ratio H_2:CO_2=1. The effects of the operating pressure and cooling rate are also investigated. A minimum CO_2 conversion is found at 75 mbar and ratio H_2:CO_2 = 1, which is in the transition zone where plasma evolves from diffusive to combined operation regime. The cooling rates have significant impact on CO_2 conversion, which points out the importance of carefully designing the cooling system, among other components of the process, to optimize the plasma effectiveness.

3.1. Introduction

There is an imminent need to reduce the societal dependence on fossil fuels and increase the usage of renewable electricity to mitigate climate change. According to the International Energy Agency (IEA), electricity accounts for less than 25% of the world total energy consumption [1] because sectors such as transportation and industry with high demand for energy still depend strongly on carbonaceous fuels. One solution to increase the share of electricity over the total energy consumption is based on the production of the same energy carriers through chemical pathways in which renewable electricity is used as the energy source. In this regard, three criteria must be satisfied: (1) the manufactured fuels must have a high energy density, (2) handling of fuels must be possible using the current infrastructure, and (3) the production cost must be comparable with or even lower than fossil fuels-based processes [2]. When liquid fuels, such as alcohols [3], gasoline or diesel, are produced, the first two of the aforementioned requirements are fulfilled because these liquid fuels can be easily transported and stored. The biggest challenge concerns the manufacturing cost of fuels produced via renewable energy; to date, none of the technologies under development has made a breakthrough to achieve competitive production costs compared to the processes using fossil fuels [4-7]. Therefore, further improvement on the overall efficiency of electricity-based systems is vital for the commercial implementation of power-to-chemicals approaches [8, 9]. It is particularly interesting to explore the production of solar fuels (oxygenates, hydrocarbons) from CO_2 and solar hydrogen, i.e. hydrogen produced via water electrolysis using electricity from renewable energy sources, due to the much larger demand (14 times) for hydrocarbons compared to other non-fuel chemicals [10, 11]. The Reverse Water-Gas Shift (RWGS) reaction is the key intermediate step to produce high added-value products using CO_2 as a feedstock. The main product of this reaction is synthesis gas (gas mixture of CO and H_2), which can be used to make a large variety of chemicals through the Fischer Tropsch process [12]. In this regard, plasma-assisted reactors are key players in the development of electricity-based technologies. Microwave plasma (MWP) is considered one of the most promising alternatives due to various benefits that have been widely discussed in the literature [13-17]. Particularly, travelling-wave-sustained discharges are investigated because of the flexible operation regimes (continuous wave and pulse), the broad attainable pressure range (10^{-5} torr – 1 atm) and wave-frequency range (f = 500 kHz – 10 GHz), as well as wide plasma reactor size range in cylindrical reactor configurations (R = 0.5 mm – 15 cm) [18]. Moreover, this type of discharge production systems can create large plasma

volumes and enable scale-up of MWP reactors for gas processing applications. To find the optimum chemical conversion and energy efficiency, various parameters should be considered in the optimization process: input power, throughput, feed composition, pressure, cooling rates and frequency along with the reactor material, geometry & size. Furthermore, it is essential to understand the interaction of electromagnetic waves with the plasma in order to enhance overall reactor performance. More information on surface-wave (SW) discharges can be found in [18-21].

Two approaches can be considered when aiming to improve the chemical conversion and/or energy efficiency of MWP reactors: (1) the invasive approach, such as the alteration of the plasma reactor geometry to attain certain flow regimes or the addition of (a) alkali metal coated surfaces or (b) catalysts [22] to optimize plasma conditions, and (2) the non-invasive approach, where external elements or fields are applied to the reactor in order to produce more uniform and stable plasmas [16]. One example of the former approach is given by Bongers et al. [23], where different reactor geometries and configurations (forward and reverse vortex, supersonic plasma expansion, quenching tube) were investigated to boost the energy efficiency of the CO_2 splitting process by rapidly cooling the molecules to avoid recombination reactions. Van Rooij et al. [24] proposed to add a coating of low ionization potential alkali metals (lithium or sodium) to, among other effects, lower the electron temperature in order to promote the dissociation of CO_2 molecules via vibrational excitation. Bhattacharya et al. [25] studied a similar concept for the use of microwaves to reduce the energy consumption for endothermic reactions by including a metallic coating on the reactor wall, which brought about significant energy savings. Concerning the second (non-invasive) approach, Spencer et al. [26] made use of two bronze waveguides upstream and downstream of the plasma ignition zone to investigate CO_2 splitting, but its effect on the reactor performance was not reported.

In this work, we present modelling and experimental results of a SW sustained microwave discharge in which the process performance of two different reactor configurations is assessed. A cylindrical waveguide attached to the downstream reactor section is implemented to evaluate its potential to increase the absorption of microwave power and enlarge the plasma reaction zone. A 2D self-consistent argon microwave plasma model gives insight into the spatially-resolved plasma and wave properties (electric field, electron density and temperature), which allows for evaluation of the plasma behaviour. Experimental results for the reverse-water-gas-shift (RWGS) reaction shows

the influence of the waveguide on the process performance. The work focuses on the improvement of CO_2 conversion in the RWGS reaction and on the understanding of the plasma-wave interplay and its effect on reactor performance.

3.2. Materials and methods

3.2.1. Novel reactor configuration

The RWGS reaction is explored in a modified version of the SW microwave discharge presented in our previous work [27]. The upgraded bench-scale setup and the gas supply unit are shown in Fig. 3.1. The core of the equipment is the same as the one previously used, and comprises: (1) solid-state microwave generator (MiniFlow 200SS, Sairem), (2) electromagnetic surface-wave launcher (surfatron 60, Sairem), (3) quartz tube (reactor) with inner and outer diameters of 4 and 5 mm respectively, and (4) vacuum pump (SC920, KNF). With respect to the analytical techniques, mass spectroscopy (QGA Quantitative Gas Analyser, Hiden Analytical), optical emission spectroscopy (OES; MAYA2000PRO, Ocean Optics) and infrared thermography (FLIR A645 SC infrared thermal camera) are used to qualitatively and quantitatively evaluate the plasma performance with two different reactor configurations. Both compressed N_2 and cooling water are used to cool down the surfatron body and the quartz tube outer wall. The operating conditions set in the experiments are: reactants flow rate = 0.1-0.4 l/min, pressure = 20-200 mbar, input microwave power = 60-200 W, feed gas composition H_2:CO_2 = 1-3, cooling N_2 flow rate = 0-40 l/h (T_{in} = 20 ^oC), cooling water flow rate = 0.3 l/min (T_{in} = 6 ^oC), argon flow rate = 5-50 ml/min. As regards the experimental procedure, the first step is plasma ignition, which is carried out at low operating pressures (6-10 mbar), maximum microwave power (200 W) and argon flow rate of 50 ml/min. After plasma is ignited, the reactants (CO_2 + H_2) and argon, as a carrier gas (5 ml/min), are fed to the reactor. Once the reflected power is minimized and plasma is stabilized, the final step involves measuring gas composition, emission spectrum, and infrared image.

In this work, attention was paid to the automation of the system. If MWP reactors are to be implemented at commercial scale for chemical manufacturing applications, several process aspects must be carefully evaluated; these include (1) safety; the operation of microwave discharges entail the consideration of hazards, such as reactor melting, microwave leakage, and toxic gas leakage

(e.g. CO), (2) controllability; operating MWP reactors implies the manipulation and control of a large number of process parameters, which in turn requires the development of highly automated systems, and (3) reproducibility; slight variations of operating conditions can lead to notable changes in the output product, meaning that the installation of accurate measurement devices with rather quick time response is needed to react to the inherently fast dynamics of microwave discharges. In this regard, a semi-automated SW MWP reactor is built, in which hardware such as pneumatic valves operated by compressed air (Fig. 3.1(a)), gas detection systems, a microwave leakage detector and several pressure and temperature measurement devices and interlocks are installed along the setup. All the aforementioned devices are connected to a CompactRIO controller (National Instruments), which controls real-time applications by means of a LabVIEW interface.

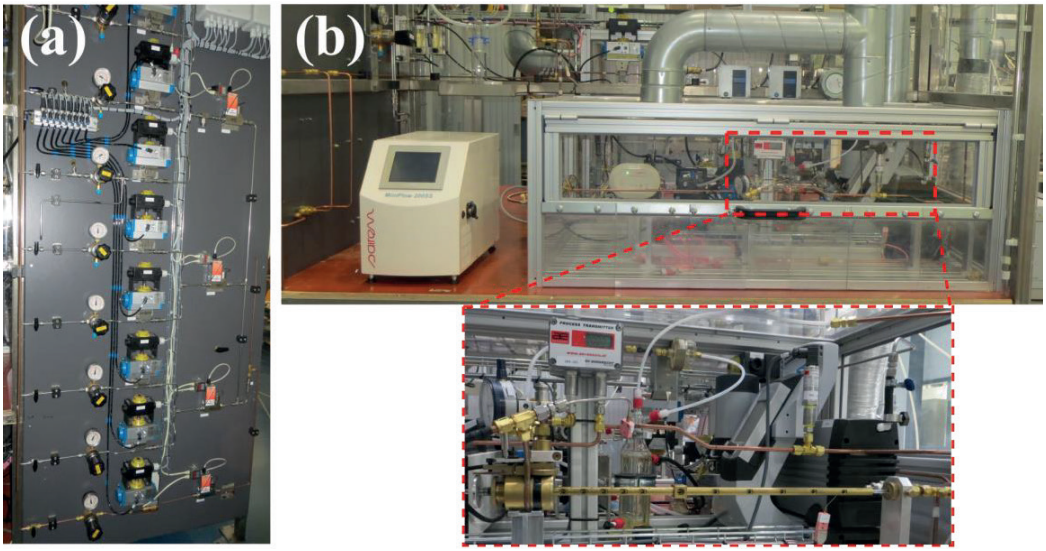

Fig. 3.1. Schematic of the (a) gas supply unit and (b) the semi-automated bench-scale SW microwave plasma setup.

In addition, an alternative method compared to the one considered in our previous work [27] is used to validate the measurements performed via mass spectroscopy. The method involves calculation of calibration curves by injecting a tiny amount of argon (5 ml/min) in combination with the gas of interest at different mass flow rates. This procedure allows finding a calibration factor that relates the ratio of the partial pressure of each gas to the partial pressure of argon. The effect of the addition of argon as carrier gas to the plasma is studied by OES, which turned out to have no influence on the intensity of key

excited species (OH radical, O and H atoms). For further information on this characterization method, the reader is referred to the references [26, 28].

3.3. Results and discussion

3.3.1. Modelling work

To evaluate the effect of an additional cylindrical waveguide on important process parameters such as electromagnetic field distribution, electron density, electron temperature and gas temperature, a 2D axisymmetric self-consistent argon microwave plasma (MWP) model is presented. This model illustrates the variations observed in wave and plasma properties when comparing two reactor configurations: (1) single discharge tube MWP reactor as the one assessed in our earlier work [27], and (2) secondary waveguide-based MWP reactor presented herein. As shortly discussed in the Introduction, several options to enhance the overall process performance in MWP reactors can be proposed. In this work, we opt to explore a non-invasive approach using a cylindrical waveguide to increase absorption of the microwave power. The waveguide redirects back to the discharge a fraction of the energy flux that would otherwise be dissipated to the surroundings [29, 30]. This concept is further evaluated in the following section "Modelling results". Furthermore, the installation of the waveguide not only prevents microwave leakage by encasing the discharge tube, but also facilitates the realization of spatially uniform measurements of emission spectra through 5 mm outer-diameter holes placed axially along the cylindrical waveguide, see Fig. 3.1(b).

Fig. 3.2 shows a schematic drawing of the surface-wave (SW) MWP reactor including the secondary waveguide along with the computational domain highlighted in the top section of Fig. 3.2. In the bottom section of Fig. 3.2, the 2D axisymmetric geometry used in the simulations is outlined. The computational domain consists of the plasma region (inside the dielectric tube), the quartz (dielectric) tube, the SW launcher (surfatron), where the wave propagation cavity and the microwave excitation port are located, the gas inlet and outlet and the waveguide placed downstream of the plasma generator.

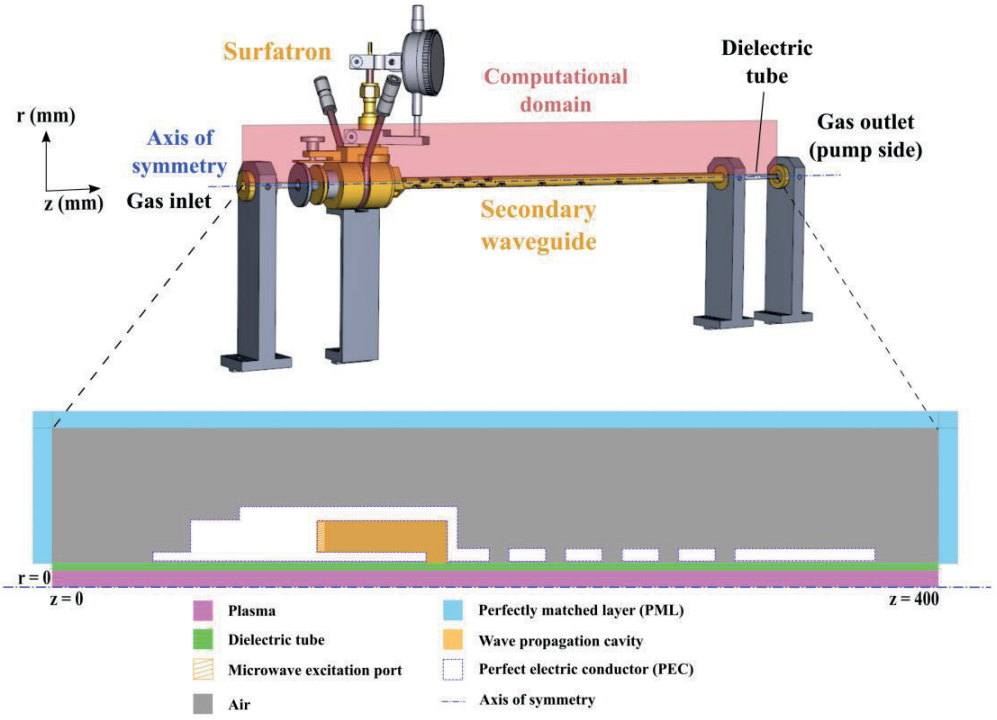

Fig. 3.2. Schematic drawing of the SW MWP reactor including the reactor configuration, the computational domain and the 2D axisymmetric geometry used in the numerical model.

3.3.1.1. Description of the model

The argon model of the SW microwave discharge is built in the commercial software COMSOL Multiphysics [31]. The total model accounts for microwave plasma, laminar flow and conductive heat transfer in fluids. The submodels, implemented in respective software modules, are solved self-consistently in a frequency-transient study, which calculates the electromagnetic field in the frequency domain and the remaining variables in the time domain. In this scheme, variations within the microwave cycles are not computed in order to attain steady state solutions in much shorter time. Solution times are in the order of 15-20 min. The multiphysics interface is fully coupled, meaning that it shares parameters or variables between the physics simultaneously. The microwave plasma interface can be considered as the core of the model. It solves the electromagnetic wave equation (including heating of the electrons), the drift-diffusion equations for the conservation of mass and energy of electrons, the heavy species transport equations and the ambipolar field due to

space charge separation. Regarding the electromagnetic field, the transverse electromagnetic (TEM) mode is assumed at the coaxial excitation port. The relative permittivity and permeability are taken from the materials specifications. For the drift-diffusion equations, a Maxwellian electron energy distribution function is specified and the electron transport properties are given in reduced form.

Cross section data is used to determine the electron impact reaction rate coefficients. The mixture-averaged model is used for the mass transport, in which the mixture diffusion coefficient for each species is computed based on the binary diffusion coefficients of the species in the mixture. The thermodynamic and transport properties of the gas mixture are calculated by means of the ideal gas mixture model. Ambipolar diffusion is considered for the charged species. All the reaction kinetics considered in the argon model are presented in Table 3.1 along with the corresponding references.

Table 3.1. Reactions included in the model.

No	Process	Reaction	ΔE [eV]	Rate constant	Sticking coefficient	Ref.
1	Elastic scattering	e + Ar→e + Ar	0	$f(E/N)$	N/A	[32]
2	Ground state excitation	e + Ar→e + Ars	11.50	$f(E/N)$	N/A	[32]
3	Superelastic	e + Ars→e + Ar	-11.50	$f(E/N)$	N/A	[a]
4	Ground state ionization	e + Ar→e + e + Ar^+	15.80	$f(E/N)$	N/A	[32]
5	Step-wise ionization	e + Ars→e + e + Ar^+	4.24	$f(E/N)$	N/A	[33]
6	Two-body quenching	Ars + Ar→Ar + Ar	-11.50	1807[b]	N/A	[34]
7	Penning ionization	Ars + Ars→e + Ar + Ar^+	-7.20	3.734 ·E8[b]	N/A	[35, 36]
8	Quenching[c]	Ars→Ar	N/A	N/A	1	N/A
9	Neutralization[c]	Ar^+→Ar	N/A	N/A	1	N/A

[a] Computed with the detailed balancing principle
[b] Units in [m^3/s ·mol]
[c] Surface reactions
N/A: Not applicable

The velocity and pressure fields used as input to the microwave plasma and heat transfer in fluids interfaces are solved by the laminar flow module. This is configured to calculate the Navier-Stokes and continuity equations for a compressible (Mach < 0.3) single-phase laminar flow with the thermodynamic and transport properties taken from the microwave plasma interface. Similarly, the temperature field is computed by the heat transfer in fluids module, which solves the energy conservation and the Fourier's law of heat conduction for a fluid with the thermodynamic and transport properties taken once again from the microwave plasma interface. Convection and radiation are neglected and the gas heating source is considered to be the sum of the heats of reactions solved by the microwave plasma interface. For additional information on the equations solved, the reader is referred to [19, 30, 37-40].

To date, this model cannot be applied to study the RWGS reaction itself as the available kinetic models for CO_2 and gas mixtures ($CO_2 + H_2$) do not allow the computation of spatial distributions of the main plasma parameters via 2D self-consistent simulations [41].

3.3.1.2. Modelling results

The presented model for argon microwave plasma at reduced pressure allows for assessment of the spatial distribution of the wave properties and the most relevant plasma parameters. Numerical calculations are carried out at the following process conditions: gas flow rate 0.1 l/min, inlet gas temperature 293 K, input microwave power 200 W, operating pressure 10 mbar, inner and outer radius of the reactor 0.002 m and 0.0025 m respectively, and reactor length 0.4 m, which match the operating conditions set experimentally for the plasma ignition phase. Fig. 3.3 displays the deposited power over time for both reactor configurations. Fig. 3.4 presents the gas temperature and radial power flow, whereas Fig. 3.5 shows the spatially-resolved electric field distribution, electron density and electron temperature. The results given on the left-hand side of Fig. 3.4 and Fig. 3.5 correspond to Case 1 (no waveguide), while the results on the right-hand side correspond to the reactor configuration with the waveguide.

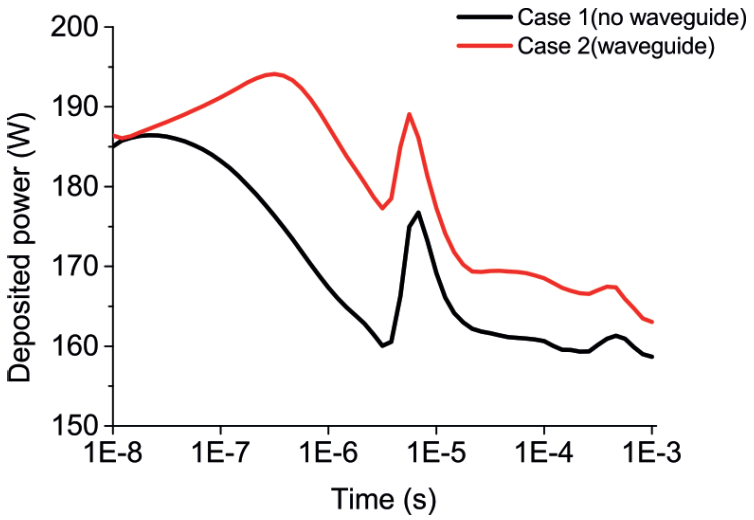

Fig. 3.3. Deposited microwave power over time for Case 1 (no waveguide) and Case 2 (waveguide).

Gas temperature: The main reactions responsible for heating of the gas in argon microwave plasma at reduced pressure are: (1) elastic scattering; electrons collide with neutral argon atoms causing no change in the internal energy of the colliding particles [42], and (2) two-body metastable quenching; excited argon atoms quench back to the ground state. Temperature gradients observed in the plasma volume are notably high due to very large L/R ratio (400/2 mm), where L is the length and R the radius of the reactor, as seen in Fig. 3.4(a); the temperature drops from ~1500 to 300 K within 30 mm. The maximum gas temperature calculated, although similar in both cases, is higher in Case 2 due to the higher deposited power (Fig. 3.3). This is also experimentally confirmed as discussed later in section "Optical Emission Spectroscopy analysis".

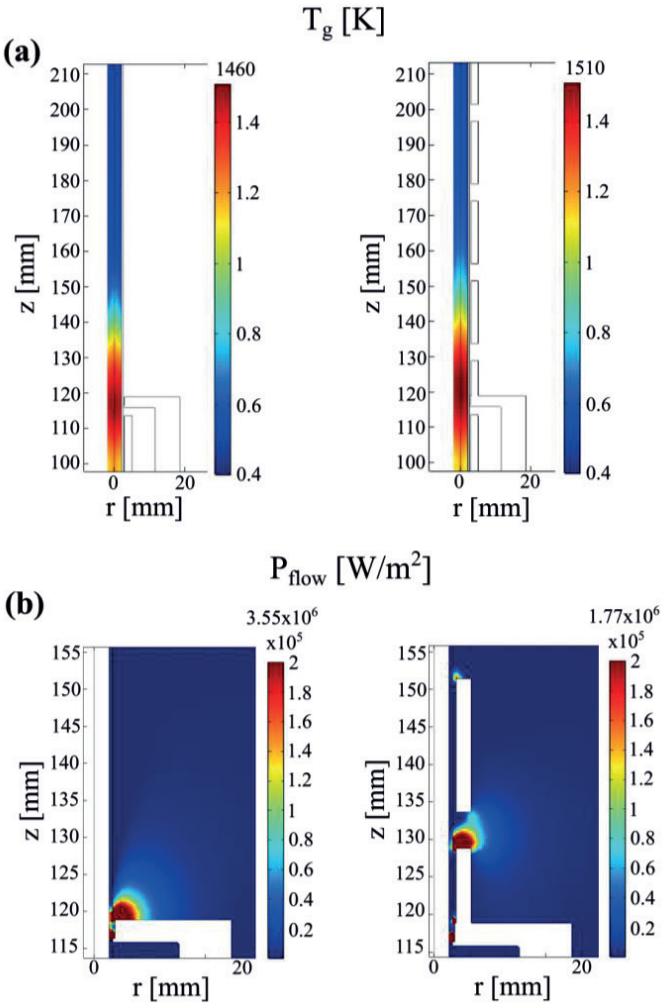

Fig. 3.4. Modelling results for both reactor configurations: Case 1, left-hand side (extended waveguide not included); Case 2, right-hand side (extended waveguide included). (a) gas temperature and (b) time-average (t = 0-1·10^{-3} s) radial power flow.

Electric field distribution: The electric field (wave) propagates along the z-direction due to the existence of the plasma; the plasma behaves as a waveguide, and simultaneously the plasma absorbs energy from the surface waves. As shown in Fig. 3.5(a-left), the electric field is concentrated in the free space surrounding the dielectric tube, right outside the wave launcher (z = 120 mm); this is also the region with the highest electron density [29] (see Fig. 3.5(b)). Regarding the case with the secondary waveguide (Case 2) in Fig. 3.5(a-right), the electric field is not concentrated at z = 120 mm, but rather at the

first port that is used to measure the emission spectrum. This effect is also observed for the radial power flow in Fig. 3.4(b). Fig. 3.4(b-right) also shows that the power flow in the radial direction decreases in Case 2 (waveguide reactor), which implies reduction in power losses. The introduction of the cylindrical waveguide changes the E field and improves the uniformity of the deposited power over the plasma volume and therefore enlarges the plasma column. The maximum electric field is also altered by the waveguide due to the redistribution of power. Hence, the variation of the E field largely influences the plasma parameters, as wave properties, electron density (n_e), and electron temperature (T_e) are self-consistently related to each other [30].

Electron density: In the process of wave-to-plasma power coupling, the wave energy flux and the electron density decay along the discharge. As the wave propagates, a fraction of the wave energy is absorbed by the plasma column for its sustenance as far as the condition $n_e \geq n_{cr}$ is maintained; the critical plasma density at 2.45 GHz is $n_{cr} = 7.5 \cdot 10^{16}$ [1/m^3] [15]. Fig. 3.5(b) shows that the maximum electron density is higher in Case 2, as a consequence of a larger power density [19, 43] (see Fig. 3.3). It is also observed that the area with high electron density ($n_e > 1.4 \cdot 10^{20}$ [1/m^3]) values in the plasma is enlarged in the presence of the waveguide due to the increase in power absorption.

Electron temperature: Electron heating through collisions in the plasma volume takes place predominantly through the E_z –field component [18, 30]. As a consequence, the maximum electron temperature in Case 1 is higher compared to Case 2. The electric field has a direct dependence on the electron temperature [42] under the considered chemistry and conditions in the model. Nevertheless, as seen in Fig. 3.5(c), the spatial distribution of the electron temperature is more uniform in Case 2 as a result of the enhanced electric field distribution.

In conclusion, the proposed argon microwave plasma model allowed us to investigate the effect of an extended waveguide on the electromagnetic field distribution, the net input (deposited) microwave power, the key plasma parameters (n_e and T_e) and the gas temperature. We believe that the improvement on electron density and temperature uniformity in the discharge in combination with the gas temperature increase has the largest impact on the experimental results reported in the following section "Experimental work" for the RGWS reaction. From the engineering point-of-view, practical models, as the one presented herein, are of importance for further development of the microwave plasma (MWP) technology in general and alternative reactor

configurations for improved process performance and scalability. The development of reduced kinetic models for key gas phase plasma chemistries, such as CO_2 splitting, RWGS (CO_2 + H_2) and dry reforming of methane (CH_4 + CO_2) is an important challenge in the plasma field [41].

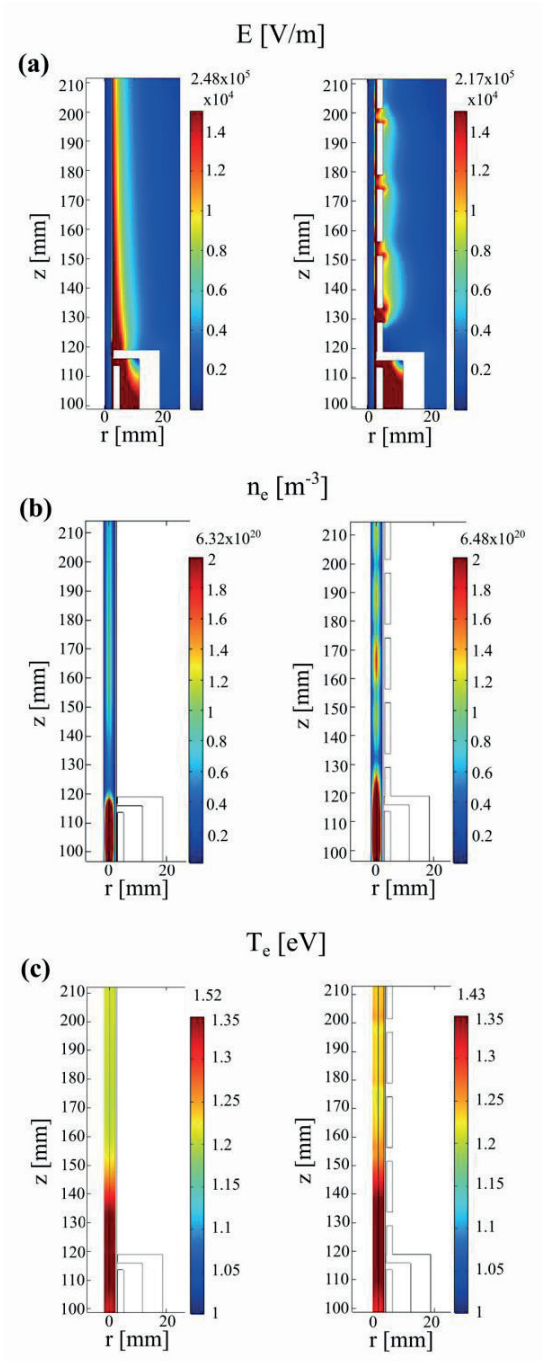

Fig. 3.5. Modelling results for both reactor configurations: Case 1, left-hand side (extended waveguide not included); Case 2, right-hand side (extended waveguide included). (a) electric field norm distribution, (b) electron density and (c) electron temperature.

3.3.2. Experimental work

In the previous section, a numerical model was proven to be a useful tool for the study of a process in alternative SW MWP reactor configurations. Research studies combining modelling and experimental work in MWP reactors are rather limited. In our previous work [27], we studied the RWGS reaction in a SW MWP reactor without an extended waveguide and reported CO_2 conversion up to 80% at a feed H_2:CO_2 ratio = 3. In this work, we carry out a detailed evaluation of the RWGS reaction in a novel reactor configuration involving an extended waveguide. To assess process performance, mass spectroscopy, optical emission spectroscopy and thermal imaging are used as analytical techniques, and the experimental results are presented in the following paragraphs.

3.3.2.1. Effect of the secondary waveguide on CO_2 conversion

With the aim of evaluating the RWGS reaction performance in two different reactor configurations, the operating conditions are kept constant in all the experiments. The inlet gas flow rate is maintained at 0.4 l/min, the net input microwave power at 150 W, and pressure at 25 mbar. The feed gas composition (H_2:CO_2) is varied from 1 to 3 (same as in our previous work [27]). The results presented in Fig. 3.6 shows that the addition of the waveguide leads to an improvement of about 50%, from 40% to 60%, on CO_2 conversion at a ratio H_2:CO_2 = 1. However, the effect is nearly negligible at higher ratios. To interpret the difference observed at ratio H_2:CO_2 = 1, the reader is referred to Fig. 3.7 in which the RWGS reaction is evaluated through a 0-D isothermal kinetic model [27]. At relatively low gas temperatures (1900-2100 K), the CO_2 conversion experiences large variations with small changes in gas temperature and/or the residence time. In Case 2, the waveguide increases the absorption of microwave power (Fig. 3.3 and Fig. 3.4) that leads to gas temperature rise (Fig. 3.4) and slight extension of the plasma column (residence time increase) (Fig. 3.4 and Fig. 3.5); this results in higher CO_2 conversion. The plasma generation system investigated in this work is a surface-wave launcher, so-called surfatron, which produces rather warm plasmas (2000-2500 K) within the category non-equilibrium discharges [44]. Even though the microwave discharge can be considered to be in non-equilibrium conditions due to the difference between electron temperature and gas temperature, presumably the dominant chemical reactions are thermally driven – that is, the CO_2 conversion improves when increasing the temperature of the bulk gas.

At higher ratios H_2:CO_2 ratios, this effect is no longer observed because in both cases, (i.e. with and without the waveguide), the gas temperature as well as the residence time are high enough to drive the CO_2 conversion to saturation on a shorter time scale, as displayed in Fig. 3.7 for H_2:CO_2 = 3. This finding is further evaluated in the following sections by means of OES.

When syngas is to be produced via the RWGS reaction, it is important to maximize the conversion of CO_2 to CO while using a minimum amount of H_2 as raw material, given that the production cost of H_2 is the main parameter driving the overall operating cost (OPEX) [10, 11, 45]. First, it is still expensive to manufacture H_2 via renewable energy-based production processes (electrolysis, plasma-assisted, photocatalysis) [46]. Second, low H_2:CO_2 feed ratios imply smaller MWP reactor volumetric footprint [47], which is beneficial given the current limited scalability of the MWP technology [48].

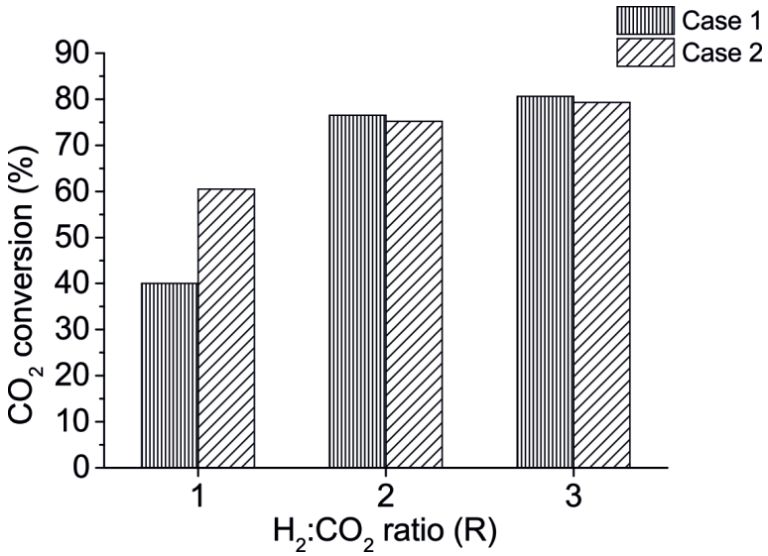

Fig. 3.6. Comparison of CO_2 conversion for two MWP reactor configurations: Case 1, extended waveguide not included; Case 2, extended waveguide included. Operating conditions: total gas flow rate = 0.4 l/min, net input microwave power = 150 W, operating pressure = 25 mbar.

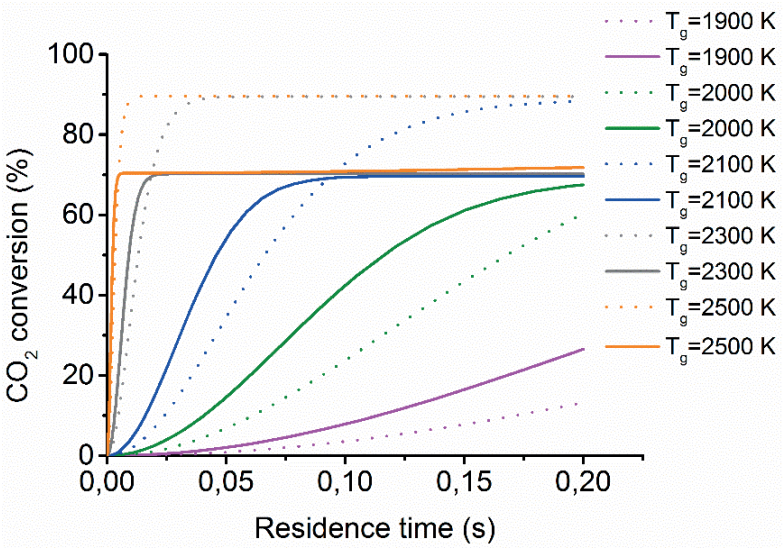

Fig. 3.7. Modelling results of RWGS reaction (CO_2 conversion) vs residence time at different gas temperatures (image reprinted with permission from [27]). Two feed gas mixture ratios are considered in the calculations; H_2:CO_2 = 1 (solid lines) and H_2:CO_2 = 3 (dot lines).

3.3.2.2. Optical Emission Spectroscopy (OES) analysis

To better understand the influence of the cylindrical waveguide on the SW microwave discharge, emission spectra obtained from the two MWP reactor configurations are analysed at different input microwave power values. Furthermore, the electron and gas temperatures are quantified by means of OES. In both cases, the measurements are taken 10 mm downstream from the surfatron launcher, where the first access port in the waveguide is located.

The emission line intensity is used to qualitatively measure the abundance of excited species present in the plasma [49-52]. Fig. 3.8 highlights the changes observed in the concentration of key excited species when considering the two reactor configurations. It is clear that raising the input microwave power increases the production of reactive species, mainly OH radical, H and O atoms, as discussed in [53]. Notably, the concentration of OH radicals is larger in Case 1 (without waveguide), whereas the concentration of O atoms largely decreases in Case 1 as compared to Case 2 (waveguide reactor). This indicates that the CO_2 conversion process occurs faster in Case 2 due to the higher gas temperatures reached in the plasma; the higher concentration of O atoms is directly related to the degree of CO_2 dissociation. Based on the results, one can

expect that the configuration of Case 2 (waveguide reactor) would lead to higher CO_2 conversions, which indeed occurs at a feed ratio of H_2:CO_2 = 1 as displayed in Fig. 3.6. Hence, it is shown that the inclusion of an external element can alter the concentration of key excited species that dominate the plasma chemistry due to variations in wave and plasma properties, eventually leading to better reactor performance.

To further evaluate changes in the plasma parameters when adding a cylindrical waveguide to the MWP reactor, the electron temperature (T_e) and gas temperature (T_g) are calculated. We intended to estimate the electron density as well, but due to the low optical resolution of the employed spectrometer (> 1 nm FWHM), it was not possible to capture the H_β line at all feed ratios with enough data points to perform accurate fitting. The same methods used in our earlier work [27] are herein considered too for the determination of these parameters. In particular, T_e is determined based on its dependence on the atomic oxygen lines [26, 54, 55]. However, it should be noted that this method only provides rough estimations of T_e, therefore it is used to assess trends as to how operating process conditions influence plasma parameters, and consequently, the reactor performance. Concerning T_g, the detected OH radical [56] is used in the calculation process. The results obtained for the two reactor configurations are presented in Table 3.2. The values of T_e show a change in trend when comparing both cases, meaning that Case 2 shows a higher T_e than Case 1 at feed H_2:CO_2 = 1, whereas at higher ratios, Case 1 has higher T_e values. The electrons can be energized to higher values when the dissociation rate of the molecules increases; higher dissociation of CO_2 and H_2 molecules results in larger concentration of atomic species in the plasma, which cannot be excited vibrationally and/or rotationally by electrons. Due to the lack of energy transfer via these collisional processes, electrons gain higher energies at a constant input microwave power, as seen in Table 3.2 for H_2:CO_2 = 1. The influence of the conversion rates on T_e for CO_2 splitting was also discussed by Kozak et al. [57], who showed that high power densities, which resulted in higher CO_2 conversions, led to lower T_e values due to variation in the species concentrations.

Table 3.2. Electron temperature (T_e) and gas temperature (T_g) for both reactor configurations. Operating conditions: total gas flow rate = 0.4 l/min, net input microwave power = 150, operating pressure = 25 mbar.

	CASE 1 = NON-WAVEGUIDE		CASE 2 = WAVEGUIDE	
T_e [Ev]	R = 1	1.43	R = 1	1.72
	R = 2	1.75	R = 2	1.73
	R = 3	1.96	R = 3	1.81
T_g [K]→(OH)	R = 1	2191	R = 1	2576
	R = 2	2382	R = 2	2687
	R = 3	2446	R = 3	2702

However, the opposite behaviour is observed at higher H_2:CO_2 ratios where the concentration of H_2 is well in excess of the concentration of CO_2. The gas mixture change makes the H_2 chemistry dominate over the CO_2-related chemical processes. As stated by Hassouni et al. [43], in pure H_2 microwave discharges, the energy transfer channels highly depend on the considered discharge conditions. At low-power density, the predominant energy dissipation channel is through electron-impact H_2 dissociation, whereas at high-power density, a large fraction of the energy is dissipated in elastic collisions (~3 times higher than that dissipated through H_2 dissociation). At high H_2:CO_2 ratios, the power density is higher when the waveguide is included (Fig. 3.3), meaning that more energy is lost via elastic collisions yielding lower T_e values compared to the single discharge tube case (see Table 3.2). As the gas temperature increases, especially at the highest ratio (H_2:CO_2 = 3), the variation of T_e in Case 2 (waveguide reactor; T_e = 1.81 eV) versus that in Case 1 (single plasma tube-no waveguide; T_e=1.96 eV) shows that the plasma evolves faster from non-equilibrium towards thermal plasma conditions when the waveguide is present. Additionally, we should note that the electron density strongly depends on the power density [30, 58] and the H_2 content [27, 59]. Hence, higher electron density values are expected in the waveguide case and at high H_2 feed concentrations.

Regarding gas temperature T_g, the waveguide enhances the absorption of microwave power, which results in bulk gas temperature rise [19, 60], as shown in Table 3.2. The gas temperatures reported herein are mainly intended to draw conclusions from a qualitative perspective considering that these values are likely overestimated due to the lack of sufficient data points for a good

fitting [27]. Nevertheless, the trends show that the largest difference is found at H_2:CO_2 = 1, where the thermal conductivity of the gas mixture has its minimum, i.e. the thermal conductivity of CO_2 is roughly 8 times lower than that of H_2. When H_2 is fed in excess (H_2:CO_2 > 1), the thermal conductivity of the plasma increases causing a more uniform gas temperature distribution and lower gas temperature differences between the two reactor configurations (18%, 13%, 10% for H_2:CO_2 = 1-3, respectively).

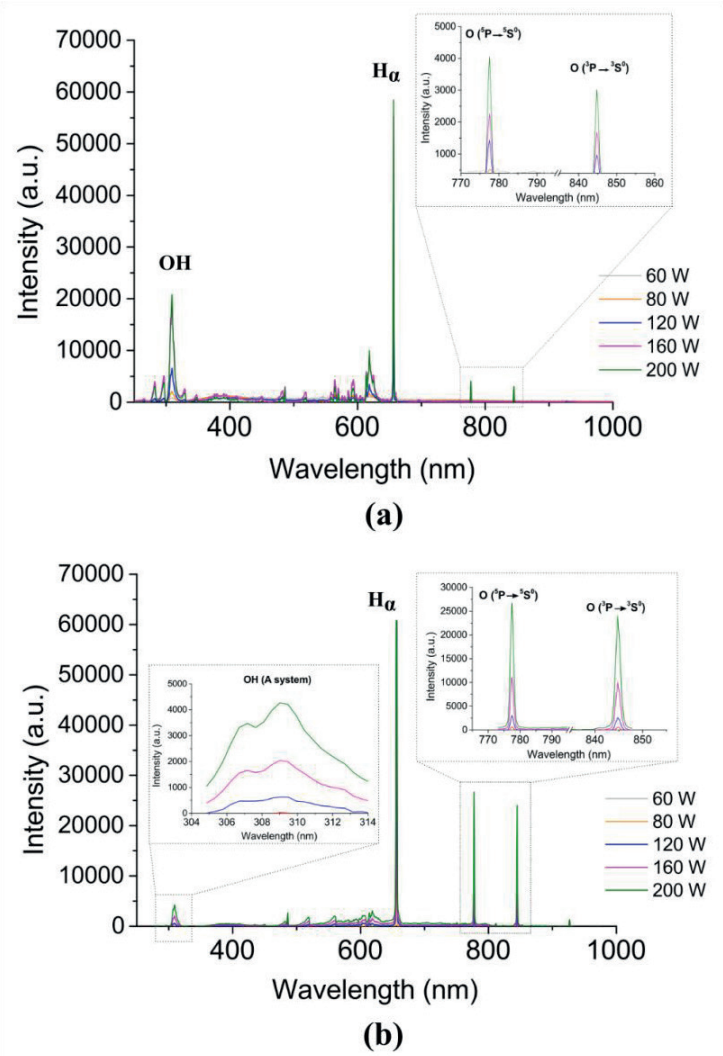

Fig. 3.8. Emission spectra at different input microwave power for (a) Case 1, waveguide not included and (b) Case 2, waveguide included. Operating conditions: total gas flow rate = 0.4 l/min, feed composition H_2:CO_2 = 1, operating pressure = 25 mbar.

3.3.2.3. *Infrared imaging*

Thermography or infrared thermal imaging is a commonly used plasma diagnostics technique in fusion research [41-43]. Infrared radiation (IR) is emitted by all objects, and the amount of radiation increases with temperature. The radiative properties of a body are denoted by the emittance or emissivity (ε), which changes with temperature. In this work, the IR camera is used for the identification of the plasma length along with the dissociation and recombination zones (Fig. 3.9). As stated by Fridman et al. [42], molecules are mostly dissociated into atoms in a zone with higher temperature and are much less dissociated in lower-temperature zones. Therefore, in Fig. 3.9, the IR camera enables us to visualize the effect of the feed H_2:CO_2 ratio on the plasma, i.e. the dissociation or high temperature zone (whitish) and the recombination or low temperature zone (bluish) [61, 62]. Fig. 3.9 shows clearly how the dissociation zone is enlarged and the recombination zone is shrunk when increasing the feed ratio H_2:CO_2 from 1 to 3. At feed ratio 4, the difference is barely noticeable. This also agrees with the fact that H_2 presents much larger thermal conductivity compared to CO_2; thus the increase in the H_2 content should result in enlargement of the high temperature zone in combination with greater plasma uniformity [42, 44, 59, 63]. This explains the higher CO_2 conversions obtained at high H_2:CO_2 ratios.

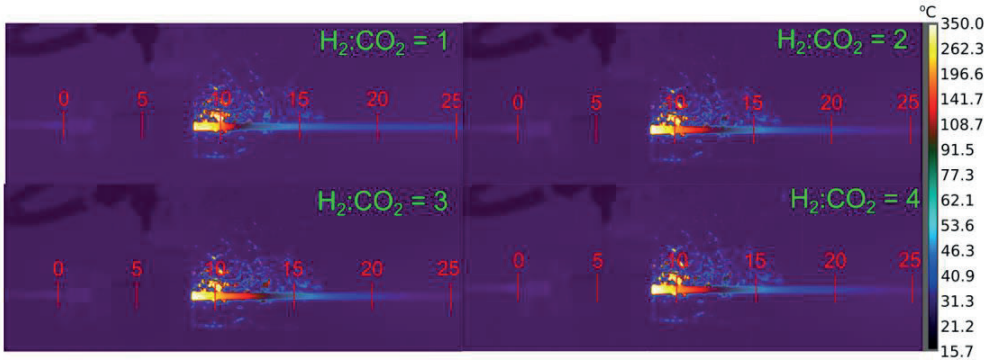

Fig. 3.9. Thermal images of the plasma reactor (Case 1, waveguide not included) at different feed H_2:CO_2 ratios. The dimensions specified in the figure (red colour numbers) are in cm scale. The temperature scale on the left is calculated considering an emissivity of quartz equal to 0.9. These values do not represent the gas plasma temperature, but rather a rough estimation of the surface plasma/inner reactor wall temperature. Operating conditions: total gas flow rate = 0.4 l/min, net input microwave power = 150, operating pressure = 25 mbar.

3.3.2.4. Effect of other parameters on CO_2 conversion

The effects of operating pressure and cooling N_2 flow rate on CO_2 conversion are assessed. The operating pressure defines how close or far from thermal equilibrium plasma is, as it influences directly the electron-neutral collision frequency and therefore the energy transferred from the electrons to the bulk gas. As reported by Fridman et al. [42], the optimum pressure range for plasma-chemical applications in microwave discharges lies in the range 20-200 mbar. At relatively low pressures (20-70 mbar), the diffusive regime prevails in the plasma; the discharge is attached to the wall (expanded-like plasma), whereas at intermediate pressures (70-200 mbar), the combined regime takes place in which a contraction of the discharge is observed (contracted-like plasma). The experimental results in Fig. 3.10(a) show that there is a minimum CO_2 conversion at ~75 mbar. It appears that this minimum is presented at the transition point, where the plasma evolves from a diffusive to a combined regime.

We measured the emission spectra at three different pressures within the diffusive regime (22, 44, 66 mbar) to gain insight into how the operating pressure influences the chemical species present in the plasma. Fig. 3.10(b) shows that increase in pressure (up to 66 mbar) decreases the concentration of reactive species (OH radical, H and O atoms), which drive the RWGS reaction in the plasma. As already mentioned, the generation of O atoms is directly linked to the CO production rate. Belete et al. [53] studied the direct dissociation of CO_2 and H_2O for syngas production in a microwave plasma reactor, showing that a higher operating pressure in the diffusive regime results in lower generation of excited species, as seen in Fig. 3.10(b) for the RGWS reaction.

Another important parameter is the cooling N_2 flow rate. The effect of the cooling water is also evaluated, although it has no measurable effect on the reactor performance. The cooling N_2 flow rate, meant to cool down the quartz tube, affects significantly the CO_2 conversion as outlined in Fig. 3.11. While CO_2 conversion is ~35% at low N_2 flow rates, it drops down to ~15% when the N_2 flow rate is increased to 40 l/h. This is also noticed visually during the experiments, where the increase in the N_2 flow rate shrinks the dissociation (brightest) zone in the plasma. Note that to sustain plasma with no N_2 cooling, the input microwave power has to be lowered considerably in order not to melt the quartz tube. This represents a compromise between the integrity of the MWP reactor and its performance. Therefore, careful design of the cooling

system to avoid reactor melting while optimizing the plasma potential is required when developing MWP technology.

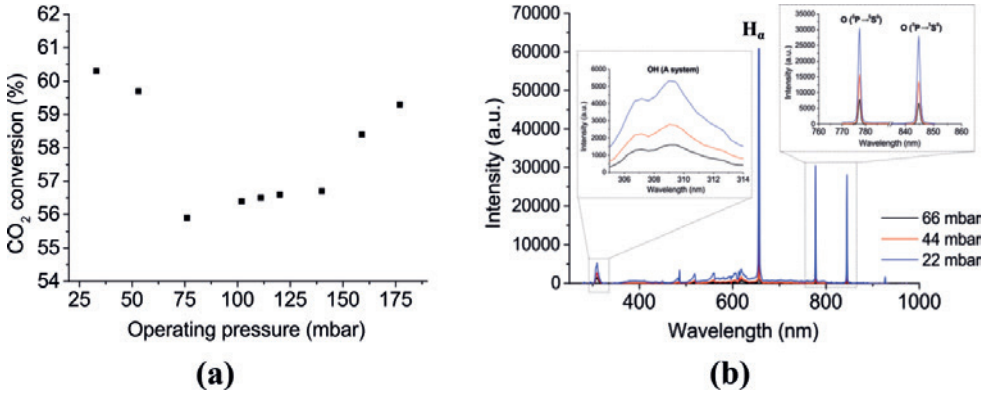

Fig. 3.10. (a) Effect of operating pressure on CO_2 conversion and (b) the emission spectra at three different pressures, for Case 2 (waveguide included). Operating conditions: total gas flow rate = 0.4 l/min, feed gas composition H_2:CO_2 = 1, net input microwave power = 150 W.

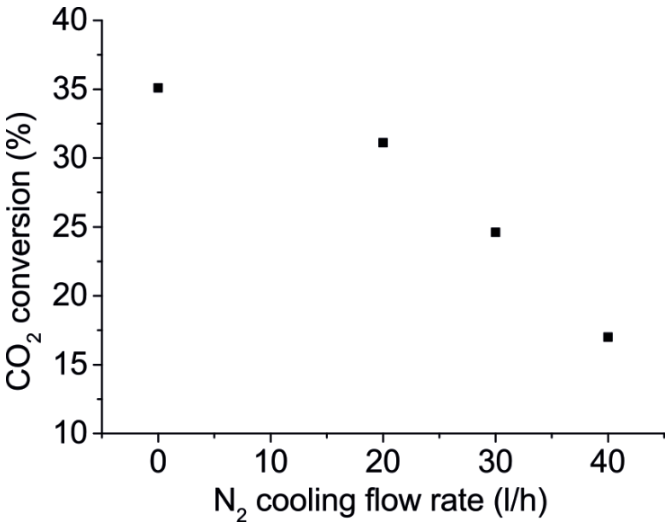

Fig. 3.11. Effect of the cooling N_2 flow rate on CO_2 conversion for Case 2 (waveguide included). Operating conditions: total gas flow rate = 0.4 l/min, feed composition H_2:CO_2 = 1, net input microwave power = 80 W, operating pressure = 25 mbar.

3.4. Conclusions

A novel surface wave-sustained microwave discharge reactor configuration was numerically and experimentally investigated to improve CO_2 conversion to CO through the reverse water gas-shift reaction in gas phase. We developed a 2D axisymmetric self-consistent model of argon microwave plasma to study the influence of a cylindrical waveguide on the electric field distribution, key plasma parameters, and gas temperature. The modelling results show that the waveguide increases the absorption of microwave power by the plasma, which in turn increases the gas temperature. The spatial uniformity of the electron density and electron temperature is improved as well in the presence of the waveguide. We proved experimentally that the waveguide changes the plasma reactor performance. CO_2 conversion increase by 50%, from 40% to 60%, is achieved for the stoichiometric feed gas composition ratio H_2:CO_2 = 1 when the waveguide is present. At higher feed ratios, the effect of the waveguide is nearly negligible. Increase in H_2 content in the feed (H_2:CO_2 > 1) causes a rise in gas temperature and residence time, which drive the dissociation of CO_2 to saturation on a shorter time scale as compared to the case of H_2:CO_2 = 1. Furthermore, the formation of other carbon-bearing products (e.g. methane, methanol) was analysed throughout all the experiments. It was observed that negligible amounts of these species are formed, meaning that nearly 100% selectivity of CO_2 to CO is achieved.

We also studied how the operating pressure in the range 20-200 mbar and the cooling N_2 flow rate influence the reactor performance. The CO_2 conversion presents a minimum at ~75 mbar, which might be related to the change in the plasma operating regime from diffusive to contracted mode. The effect of the cooling N_2 flow rate on CO_2 conversion is remarkably high, meaning that careful design of the cooling system is required to optimize plasma efficiency.

References

[1] International Energy Agency (IEA) Energy Balances U.S. Final Energy Consumption 2012.
[2] Pearson RJ, Eisaman MD, Turner JWG, Edwards PP, Jiang Z, Kuznetsov VL, et al. Energy Storage via Carbon-Neutral Fuels Made From CO2, Water, and Renewable Energy. P Ieee. 2012;100:440-60.
[3] Goeppert A, Czaun M, Jones JP, Prakash GKS, Olah GA. Recycling of carbon dioxide to methanol and derived products - closing the loop. Chem Soc Rev. 2014;43:7995-8048.
[4] Varne M, Dey GR, Das TN. Evaluation of optimum conditions for hydrogen generation in argon-water vapor dielectric barrier discharge. Int J Hydrogen Energ. 2016;41:22769-74.
[5] Banerjee S, Musa MN, Jaafar AB. Economic assessment and prospect of hydrogen generated by OTEC as future fuel. Int J Hydrogen Energ. 2016.
[6] Du C, Ma D, Wu J, Lin Y, Xiao W, Ruan J, et al. Plasma-catalysis reforming for H2 production from ethanol. Int J Hydrogen Energ. 2015;40:15398-410.
[7] Levin DB, Chahine R. Challenges for renewable hydrogen production from biomass. Int J Hydrogen Energ. 2010;35:4962-9.
[8] Kranenburg Kv, Schols E, Gelevert H, Kler Rd, Delft Yv, Weeda M. Empowering the chemical industry: Opportunities for electrification. 2016:1-32.
[9] Mennicken L, Janz A, Roth S. The German R&D Program for CO2 Utilization-Innovations for a Green Economy. Environ Sci Pollut R. 2016;23:11386-92.
[10] Lim XZ. How to make the most of carbon dioxide (vol 526, pg 628, 2015). Nature. 2016;529:141-.
[11] Centi G, Perathoner S. Green carbon dioxide: Advances in CO2 utilization: Wiley; 2014.
[12] Peter M. Maitlis, Arno de Klerk. Greener Fischer-Tropsch processes for fuels and feedstocks: Wiley; 2013.
[13] Czylkowski D, Hrycak B, Miotk R, Jasiński M, Dors M, Mizeraczyk J. Hydrogen production by conversion of ethanol using atmospheric pressure microwave plasmas. Int J Hydrogen Energ. 2015;40:14039-44.
[14] Jasiński M, Czylkowski D, Hrycak B, Dors M, Mizeraczyk J. Atmospheric pressure microwave plasma source for hydrogen production. Int J Hydrogen Energ. 2013;38:11473-83.
[15] Schulz A, Buchele P, Ramisch E, Janzen O, Jimenez F, Kamm C, et al. Scalable Microwave Plasma Sources From Low to Atmospheric Pressure. Contrib Plasm Phys. 2012;52:607-14.

[16] Lebedev YA. Microwave discharges: generation and diagnostics. 25th Summer School and International Symposium on the Physics of Ionized Gases - Spig 2010. 2010;257.
[17] Ferreira CM, Moisan M. Microwave Discharges Fundamentals and Applications: NATO ASI Series; 1993.
[18] Schluter H, Shivarova A. Travelling-wave-sustained discharges. Phys Rep. 2007;443:121-255.
[19] Georgieva V, Berthelot A, Silva T, Kolev S, Graef W, Britun N, et al. Understanding Microwave Surface-Wave Sustained Plasmas at Intermediate Pressure by 2D Modeling and Experiments. Plasma Process Polym. 2016:n/a-n/a.
[20] Chen G, Silva T, Georgieva V, Godfroid T, Britun N, Snyders R, et al. Simultaneous dissociation of CO2 and H2O to syngas in a surface-wave microwave discharge. Int J Hydrogen Energ. 2015;40:3789-96.
[21] Henriques J, Bundaleska N, Tatarova E, Dias FM, Ferreira CM. Microwave plasma torches driven by surface wave applied for hydrogen production. Int J Hydrogen Energ. 2011;36:345-54.
[22] Nizio M, Albarazi A, Cavadias S, Amouroux J, Galvez ME, Da Costa P. Hybrid plasma-catalytic methanation of CO2 at low temperature over ceria zirconia supported Ni catalysts. Int J Hydrogen Energ. 2016;41:11584-92.
[23] Bongers W, Bouwmeester H, Wolf B, Peeters F, Welzel S, van den Bekerom D, et al. Plasma-driven dissociation of CO2 for fuel synthesis. Plasma Process Polym. 2016:n/a-n/a.
[24] van Rooij G, van den Bekerom D, den Harder N, Minea T, Berden G, Bongers W, et al. Taming microwave plasma to beat thermodynamics in CO2 dissociation. Faraday Discuss. 2015;183:233-48.
[25] Bhattacharya M, Basak T. A theoretical study on the use of microwaves in reducing energy consumption for an endothermic reaction: Role of metal coated bounding surface. Energy. 2013;55:278-94.
[26] Spencer LF. The Study of CO2 Conversion in a Microwave Plasma/Catalyst System. 2012;PhD Thesis University of Michigan.
[27] de la Fuente JF, Moreno SH, Stankiewicz AI, Stefanidis GD. Reduction of CO2 with hydrogen in a non-equilibrium microwave plasma reactor. Int J Hydrogen Energ. 2016;41:21067-77.
[28] Nguyen SVT, Foster JE, Gallimore AD. Operating a radio-frequency plasma source on water vapor. Rev Sci Instrum. 2009;80.
[29] Selby M, Hieftje GM. Taming the Surfatron. Spectrochim Acta B. 1987;42:285-98.
[30] Schluter H, Shivarova A. Advanced technologies based on wave and beam generated plasmas: Springer Netherlands; 1999.

[31] COMSOL, Multiphysics, 5.1. Microwave Plasma Module User's Guide. COMSOL AB. 2015.
[32] Phelps database (www.lxcat.net/Phelps) retrieved from http://jilawww.colorado.edu/~avp/.
[33] Hyman HA. Electron-impact ionization cross sections for excited states of the rare gases (Ne, Ar, Kr, Xe), cadmium, and mercury. Phys Rev A. 1979;20:855-9.
[34] Karoulina EV, Yu AL. Computer simulation of microwave and DC plasmas: comparative characterisation of plasmas. Journal of Physics D: Applied Physics. 1992;25:401.
[35] Lymberopoulos DP, Economou DJ. Fluid simulations of glow discharges: Effect of metastable atoms in argon. J Appl Phys. 1993;73:3668-79.
[36] Ferreira CM, Loureiro J, Ricard A. Populations in the metastable and the resonance levels of argon and stepwise ionization effects in a low-pressure argon positive column. J Appl Phys. 1985;57:82-90.
[37] Jimenez-Diaz M, Carbone EAD, van Dijk J, van der Mullen JJAM. A two-dimensional Plasimo multiphysics model for the plasma-electromagnetic interaction in surface wave discharges: the surfatron source. J Phys D Appl Phys. 2012;45:335204.
[38] Baeva M, Bosel A, Ehlbeck J, Loffhagen D. Modeling of microwave-induced plasma in argon at atmospheric pressure. Phys Rev E. 2012;85:056404.
[39] Xiao W, Huang KM, Zhang WC, Lin Y. Modeling of Argon Plasma Excited by Microwave at Atmospheric Pressure in Ridged Waveguide. Ieee T Plasma Sci. 2016;44:1075-82.
[40] Obrusnik A, Bonaventura Z. Studying a low-pressure microwave coaxial discharge in hydrogen using a mixed 2D/3D fluid model. J Phys D Appl Phys. 2015;48.
[41] de la Fuente JF, Moreno SH, Stankiewicz AI, Stefanidis GD. A new methodology for the reduction of vibrational kinetics in non-equilibrium microwave plasma: application to CO2 dissociation. Reaction Chemistry & Engineering. 2016;1:540-54.
[42] Fridman A. Plasma Chemistry: Cambridge: Cambridge University Press; 2008.
[43] Hassouni K, Gicquel A, Capitelli M, Loureiro J. Chemical kinetics and energy transfer in moderate pressure H-2 plasmas used in diamond MPACVD processes. Plasma Sources Sci T. 1999;8:494-512.
[44] Jankowski KJ, Reszke E. Microwave Induced Plasma Analytical Spectrometry: RSCPublishing 2011.
[45] Harmsen J. Industrial Process Scale-up: A practical innovation guide from idea to commercial implementation: Elsevier; 2013.

[46] Dincer I, Acar C. Review and evaluation of hydrogen production methods for better sustainability. Int J Hydrogen Energ. 2015;40:11094-111.
[47] Kaiser M, Baumgartner KM, Mattheus A. Microwave Plasma Sources - Applications in Industry. Contrib Plasm Phys. 2012;52:629-35.
[48] de la Fuente JF, Kiss AA, Radoiu MT, Stefanidis GD. Microwave plasma emerging technologies for chemical processes. Journal of Chemical Technology & Biotechnology. 2017:n/a-n/a.
[49] Chen GX, Silva T, Georgieva V, Godfroid T, Britun N, Snyders R, et al. Simultaneous dissociation of CO2 and H2O to syngas in a surface-wave microwave discharge. Int J Hydrogen Energ. 2015;40:3789-96.
[50] Belmonte T, Noel C, Gries T, Martin J, Henrion G. Theoretical background of optical emission spectroscopy for analysis of atmospheric pressure plasmas. Plasma Sources Sci T. 2015;24.
[51] Miotk R, Jasinski M, Mizeraczyk J. Optical emission spectroscopy of plasma generated by a waveguide-supplied microwave plasma source operated at 915MHz. Phys Scripta. 2014;T161.
[52] Laux CO, Spence TG, Kruger CH, Zare RN. Optical diagnostics of atmospheric pressure air plasmas. Plasma Sources Sci T. 2003;12:125-38.
[53] Belete TT, Van de Sanden MCM, Gleeson MA. Plasma dissociation of water for CO2 conversion. 22nd International Symposium on Plasma Chemistry. 2015.
[54] O'Connor N, Humphreys HH, Daniels S. Oxygen line ratio method for the determination of plasma parameters in atmospheric pressure discharges using air as the working gas. 31st ICPIG, Granada, Spain. 2013.
[55] Leins M, Walker M, Schulz A, Schumacher U, Stroth U. Spectroscopic Investigation of a Microwave-Generated Atmospheric Pressure Plasma Torch. Contrib Plasm Phys. 2012;52:615-28.
[56] Silva T, Britun N, Godfroid T, Snyders R. Optical characterization of a microwave pulsed discharge used for dissociation of CO2. Plasma Sources Sci T. 2014;23:025009.
[57] Kozak T, Bogaerts A. Splitting of CO2 by vibrational excitation in non-equilibrium plasmas: a reaction kinetics model. Plasma Sources Sci T. 2014;23:045004.
[58] Hassouni K, Silva F, Gicquel A. Modelling of diamond deposition microwave cavity generated plasmas. J Phys D Appl Phys. 2010;43.
[59] Leins M, Kopecki J, Gaiser S, Schulz A, Walker M, Schumacher U, et al. Microwave Plasmas at Atmospheric Pressure. Contrib Plasm Phys. 2014;54:14-26.

[60] den Harder N, van den Bekerom DCM, Al RS, Graswinckel MF, Palomares JM, Peeters FJJ, et al. Homogeneous CO2 conversion by microwave plasma: Wave propagation and diagnostics. Plasma Process Polym. 2016:n/a-n/a.
[61] Kwak HS, Uhm HS, Hong YC, Choi EH. Disintegration of Carbon Dioxide Molecules in a Microwave Plasma Torch. Sci Rep-Uk. 2015;5:18436.
[62] Choi DH, Chun SM, Ma SH, Hong YC. Production of hydrogen-rich syngas from methane reforming by steam microwave plasma. J Ind Eng Chem. 2016;34:286-91.
[63] Kopecki J. Developement and spectroscopic investigastions on a microwave plasma torch for the deposition process with powders. 2012;Doctoral Thesis University of Stuttgart.

4

A new methodology for the reduction of vibrational kinetics in non-equilibrium microwave plasma: application to CO_2 dissociation

This chapter is published as:

de la Fuente JF, Moreno SH, Stankiewicz AI and Stefanidis GD, A new methodology for the reduction of vibrational kinetics in non-equilibrium microwave plasma: application to CO_2 dissociation. *Reaction Chemistry & Engineering* **1**: 540-554 (2016).

Abstract

Plasma reactor technologies have the potential to enable storage of green renewable electricity into fuels and chemicals. One of the major challenges for the implementation of these technologies is the energy efficiency. Empirical enhancement of plasma reactors performance has proven to be insufficient in this regard. Numerical models are becoming therefore essential to get insight into the process for optimization purposes. The chemistry in non-thermal plasmas is the most challenging and complex part of the model due to the large number of species and reactions involved. The most recent reaction kinetic model for carbon dioxide (CO_2) dissociation in non-thermal microwave plasma considers more than one hundred species and thousands of reactions. To enable the implementation of this model into multidimensional simulations, a new reduction methodology to simplify the state-to-state kinetic model is presented. It is based on four key elements; 1) all the asymmetric vibrational levels are lumped within a single group, or fictitious species, CO_2*, 2) this group follows a non-equilibrium Treanor distribution, 3) an algebraic approximation is used to compute the vibrational temperature from the translational temperature based on the Landau-Teller formula and 4) weighted algebraic expressions are applied, instead of complex differential equations, to calculate the rates of the most influencing reactions; this decreases substantially the calculation time. Using this new approach, the dissociation and vibrational kinetics are captured in a reduced set of 44 reactions among 13 species. The predictions of the reduced kinetic model regarding the concentrations of the heavy species in the afterglow zone are in good agreement with those of the detailed model from which the former was derived. The methodology may also be applied to other state-to-state kinetic models in which interactions of vibrational levels have the largest share in the global set of reactions.

4.1. Introduction

Two major environmental and scientific challenges faced nowadays are energy storage and greenhouse gas emissions [1-5]. The pressing need in employing renewable energy sources has brought up new challenges regarding electricity storage, which need to be overcome before the current energy mix can be upgraded to one based on renewable energy sources [3]. Various alternatives are being investigated such as mechanical, chemical, electromagnetic and thermal storage [3-6]. The valorisation of carbon dioxide (CO_2) to produce synthetic fuels has been identified as one of the approaches to convert renewable electricity surplus into easy-to-store chemicals [6]. In this regard, plasma-based systems combine the opportunity of utilizing both electricity surplus as well as greenhouse gases, as feedstock, for the conversion process. Plasma reactor technology offers potential benefits, such as compactness, robustness and fast response time to temporal variations at the reactor inlet [7,8]. Therefore, it is a suitable technology to cope with the intermittent and fluctuating pattern of renewable energy supply (e.g., solar and wind energy) [2,9]. Moreover, the characteristics of non-thermal plasma are particularly favourable for the dissociation and utilization of CO_2, making it a very promising technology for chemical process intensification.

One of the major drawbacks to commercialize plasma technology is the high energy consumption [10]. Despite the extensive research conducted experimentally to optimize plasma reactor performance [11,12], there are still a lot of uncertainties that need to be addressed in order to fully understand the reaction mechanisms in non-thermal plasma conditions and optimize plasma processes [13]. Therefore, there is a need to develop reliable plasma chemistries that can be implemented in plasma reactor models for evaluation of different reactor configurations and process optimization [1]. Predictive plasma reactor models are inherently multiphysics models describing electromagnetic wave propagation, mass conservation, electron and fluid dynamics, heat transfer and plasma chemical kinetics [14-16]. When detailed kinetic models, including all the elementary steps, are taken into account, the model becomes highly complex due to the large number of reactions and species needed to describe the plasma reactive system. Large chemical kinetic models require solution of a large number of transport equations in addition to estimating the chemical source terms, often governed by stiff ordinary differential equations (ODEs) [17]. Hence, to enable the applicability of plasma kinetic models in multidimensional simulations, a simplification approach to reduce complex kinetic models is presented in this work.

Several attempts have been made to develop reaction kinetic models for CO_2 chemistry. In [18], a numerical model for the plasma-chemical reactions taking place in a pure CO_2 glow discharge was developed, albeit vibrational kinetics were not included. In [19], a high temperature non-equilibrium reacting CO_2 flow was studied; although a detailed description of the vibrational kinetics by means of kinetic theory methods was given, the plasma chemistry was missing. More recently, a state-to-state kinetic model including all the relevant chemical reactions in a CO_2 non-thermal microwave discharge was proposed [20]. In a subsequent publication [21], the kinetic model was updated to evaluate the energy efficiency in the discharge. This model consists of 126 species and more than 10000 reactions, including electron impact, neutrals and vibrational energy transfer reactions. In [9], a reduced kinetic model for CO_2 dissociation in dielectric barrier discharges (DBD) was introduced. This model includes the most relevant plasma species and reactions in DBD discharge conditions, but lacks vibrational kinetics. Such a model is then unsuitable for microwave discharges where dissociation through vibrational excitation of the molecule appears to be the most efficient dissociation mechanism [11,22].

Up to date, a practical and manageable kinetic model for CO_2 dissociation in non-thermal microwave plasma has not been reported. In this work, a novel two-step approach for reduction of vibrational kinetics is presented and applied to CO_2 dissociation in non-equilibrium microwave discharges. Two different simplification techniques are coupled to carry out the reduction process: i) chemical lumping of species, where several species are grouped into a single pseudo-species, in combination with ii) a skeletal reduction approach, which includes identification and selection of the most influencing species in the dissociation process without loss of qualitative potential [1,19,23]. The novelty of the presented model lies in four key elements; 1) all the asymmetric vibrational levels are lumped within a single group instead of several groups as reported in [24-26], 2) this group follows the non-equilibrium Treanor distribution, 3) an algebraic approximation is used to compute the vibrational temperature from the translational temperature based on the Landau-Teller formula and 4) weighted algebraic expressions are applied, instead of complex differential equations, to calculate the rates of the most influencing reactions. The obtained kinetic model comprises 13 species and 44 reactions whereby all the relevant chemical reactions influencing the CO_2 dissociation process are accounted for. The comparison of the results given by the detailed and reduced kinetic models shows good agreement. In particular, the best match is obtained in the afterglow zone, where the species concentrations represent those at the

outlet of the reactor. It is important to remark that the purpose of the work is to explore and validate a new methodology for the reduction of vibrational plasma kinetics, exemplified herein for a CO_2 non-thermal microwave discharge, rather than performing self-consistent multidimensional simulations, a task that has not been carried out yet.

4.2. Description of the model

To properly evaluate non-equilibrium reaction kinetics, state-to-state (STS) kinetic models are developed accounting for all the internal excited states and their interactions. This approach leads to reaction mechanisms with a large number of species (in the order of dozens to hundreds) and reactions (in the range of hundreds to thousands), which are not practical for multidimensional simulations. Therefore, the application of STS kinetic models have been mostly limited to zero and one-dimensional simulations. The STS kinetic model reported in [21] was taken as starting point in this work. In the following subsection, a detailed description of the plasma chemical reactive system and also the simplification methodology is given.

4.2.1. Reduced plasma kinetic model: species and reactions

The species considered in the reduced kinetic model are displayed in Table 4.1. As stated in [12,27], the CO_2 molecule presents three normal vibrational modes, the symmetric bending mode, the symmetric stretch mode and the asymmetric stretch mode. The symmetric modes of vibration of this molecule are herein denoted as CO_2v_a, CO_2v_b and CO_2v_c (Table 4.1). The asymmetric stretch mode is found to be the most energy efficient dissociation channel due to its capacity to store vibrational energy. In this mode, 21 vibrational excited levels are considered up to the dissociation limit of the molecule [20]. The reduction potential of the model is based on the lumping of all the asymmetric vibrational excited levels into a fictitious species, referred to as CO_2*. This leads to a substantial simplification of the STS kinetic model, as most of the reactions come from the state-to-state interactions of vibrational levels [28].

Table 4.1. Chemical species included in the reduced kinetic model. CO_2v_a, CO_2v_b and CO_2v_c are symmetric modes of vibration whereas CO_2* represents a fictitious species accounting for all the asymmetric vibrational levels.

Type	Species
Neutral ground states	CO_2, CO, O, O_2
Vibrationally excited states	CO_2v_a, CO_2v_b, CO_2v_c, CO_2*
Charged species	CO_2^+,CO^+,O_2^+,O^+,e

The reactions included in the reduced kinetic model are shown in Tables 4.2, 4.3, 4.4 and 4.5. In this model, four different types of reactions are included; these are electron impact reactions, reactions of neutral species, vibrational energy exchange reactions and surface reactions, which are presented in Tables 4.2, 4.3, 4.4 and 4.5, respectively.

Electron impact reactions form the driving force of the plasma. The electrons gain kinetic energy from the electromagnetic field, which is further transferred to other species through collisions. The generation of new electrons occurs via ionization reactions, which are responsible for sustaining the plasma.

Table 4.2. Electron impact reactions (RX) considered in the reduced kinetic model.

Nº	Process	Reaction	Cross section
RX1	CO_2 Elastic scattering	$e + CO_2 \rightarrow e + CO_2$	[29]
RX2	CO_2* Elastic scattering	$e + CO_2^* \rightarrow e + CO_2^*$	Same as RX1
RX3	CO Elastic scattering	$e + CO \rightarrow e + CO$	[30,31]
RX4	O Elastic scattering	$e + O \rightarrow e + O$	[31]
RX5	O_2 Elastic scattering	$e + O_2 \rightarrow e + O_2$	[32]
RX6	CO_2 Ionization	$e + CO_2 \rightarrow e + e + CO_2^+$	[29]
RX7	CO_2 Ionization from CO_2*	$e + CO_2^* \rightarrow e + e + CO_2^+$	Same as RX6
RX8	CO Ionization	$e + CO \rightarrow e + e + CO^+$	[30]
RX9	O Ionization	$e + O \rightarrow e + e + O^+$	[33]
RX10	O_2 Ionization	$e + O_2 \rightarrow e + e + O_2^+$	[32]
RX11	Vibrational (de) excitation to CO_2v_a	$e + CO_2 \leftrightarrow e + CO_2v_a$	[29]
RX12	Vibrational (de) excitation to CO_2v_b	$e + CO_2 \leftrightarrow e + CO_2\ v_b$	[29]
RX13	Vibrational (de) excitation to CO_2*	$e + CO_2 \leftrightarrow e + CO_2^*$	Section "Simplification approach"

Reactions of neutral species play an important role in the formation of reactive species to promote chemical reactions. At favourable dissociation conditions, a fraction of the energy transferred from the electrons to the CO_2 molecule is stored as internal energy in high vibrational levels of the asymmetric mode, which can either facilitate its dissociation or be transferred to the bulk gas as heat.

Table 4.3. Reactions of neutrals (RN) included in the model. M = CO_2, CO or O_2. Gas temperature (T_g) in K and rate constants in cm^3/s and cm^6/s for binary and ternary reactions, respectively.

Nº	Process/Reaction	Rate constant
RN1	CO_2* Dissociation by collisions with CO_2, CO and O_2 $CO_2^* + M \rightarrow CO + O + M$	$9.59 \times 10^{-16} (T_g/300)^{2.92} \exp(639/T_g)$
RN2	CO_2* Dissociation by collisions with O $CO_2^* + O \rightarrow CO + O_2$	$3.35 \times 10^{-14} (T_g/300)^{1.47} \exp(-271/T_g)$
RN3	Three-body CO and O recombination $CO + O + M \rightarrow CO_2 + M$	$8.2 \times 10^{-34} \exp(-1510/T_g)$
RN4	Two-body CO and O_2 recombination $CO + O_2 \rightarrow CO_2 + O$	$1.23 \times 10^{-12} \exp(-12800/T_g)$
RN5	Three-body O recombination $O + O + M \rightarrow O_2 + M$	$1.27 \times 10^{-32} (T_g/300)^{-1} \exp(-170/T_g)$

Vibrational energy transfer reactions are responsible for the energy exchange between vibrationally excited molecules and the vibrational energy loss to ground state molecules. In this model, these reactions mainly lead to generation of heat by transferring the energy to the bulk gas via vibrational-translational (VT) relaxation reactions. Note that the parameters v_{s2} and v_{s3} represent the stoichiometric coefficients of the symmetric excited states for reactions RV2 and RV3, whereas v_{l2} and v_{l3} indicate the stoichiometric coefficients of the lumped excited state for the same reactions (RV2 and RV3).

Table 4.4. Vibrational energy transfer reactions (RV) considered in the model. M = CO_2, CO or O_2. Gas temperature (T_g) in K. v_{s2}, v_{s3}, v_{l2} and v_{l3} represent the stoichiometric coefficients of the symmetric excited states (s) and the lumped excited state (l), respectively, for the reactions RV2 and RV3.

Nº	Process/Reaction	Rate constant
RV1	VT Relaxation of symmetric vibrationally excited states x = a,b,c	
	$CO_2v_x + M \rightarrow CO_2 + M$	$7.14 \times 10^{-8} \exp(-177T_g^{-1/3} + 451T_g^{-2/3})$
	$M = CO_2$	x 1
	$M = CO, O_2$	x 0.7
RV2	VT Relaxation of the lumped asymmetric vibrationally excited state	
	$CO_2^* + M \rightarrow v_{l2}\ CO_2^* + v_{s2}\ (CO_2v_a + CO_2v_b + CO_2v_c) + M$	
	$M = CO_2$	$4.72 \times 10^{-17} (T_g/300)^{6.55} \exp(1289/T_g)$
	$M = CO$	$1.47 \times 10^{-17} (T_g/300)^{6.53} \exp(1282/T_g)$
	$M = O_2$	$1.95 \times 10^{-17} (T_g/300)^{6.53} \exp(1282/T_g)$
RV3	VV' Relaxation between symmetric and asymmetric vibrationally excited states	$3.99 \times 10^{-15} (T_g/300)^{4.46} \exp(398/T_g)$
	$CO_2^* + CO_2 \rightarrow v_{l3}\ CO_2^* + v_{s3}\ (CO_2v_a + CO_2v_b)$	

The charged species, electrons and ions, diffuse together toward the walls by the effect of ambipolar diffusion, where electrons and ions are recombined via collisions on the reactor wall.

Table 4.5. Surface reactions (RS) included in the reduced kinetic model

Nº	Process	Reaction	Sticking coefficient (γ)
RS1	CO_2^+ Neutralization	$CO_2^+ \rightarrow CO_2$	1
RS2	CO^+ Neutralization	$CO^+ \rightarrow CO$	1
RS3	O^+ Neutralization	$O^+ \rightarrow O$	1
RS4	O_2^+ Neutralization	$O_2^+ \rightarrow O_2$	1

Using the simplification approach, which is described in the following sections, the STS model has been significantly reduced to 44 reactions among 13 species accounting for the most relevant processes that dominate the dissociation of CO_2 in non-equilibrium microwave plasma. A schematic representation of the reaction pathway is presented in Fig. 4.1.

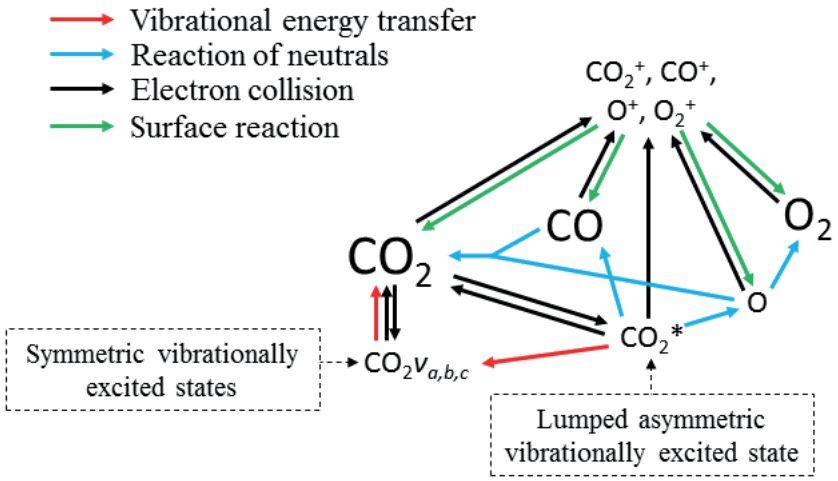

Fig. 4.1. Reaction pathway of the reduced kinetic model.

4.2.2. Simplification approach

Up to date, various approaches have been adopted to reduce STS kinetic models. For instance, in [28], the Principal Component Analysis (PCA) is applied to the CO_2 dissociation process driven by vibrational kinetics; in this approach, a large database of results obtained with the STS kinetic model is required to identify the principal components. One can also make use of commercially available software, such as CHEMKIN-PRO [34], which is mainly used for combustion processes, and PumpKin [35], which employs algorithms to identify key components and group large set of reactions in reduced reaction pathways; the latter is mostly used in plasma chemical models. The approaches in [36] and [37] are closer to the one presented here; specifically, the kinetics are described by the vibrational and translational temperatures for the dissociation and recombination regimes of N_2 + N in non-equilibrium hypersonic flows. Approaches where internal modes of molecules are divided into several groups have been reported as well [24-26]. Such a multigroup lumping method was recently applied to reduce the vibrational kinetics of CO_2 [38]. In this method, the vibrational levels of the asymmetric mode are lumped into various groups, each characterized by an internal Boltzmann equilibrium distribution given by its own vibrational temperature.

In this work, a new reduction approach is introduced to simplify the STS kinetic model proposed in [21] for the dissociation of CO_2 in non-equilibrium microwave discharges. As opposed to [24-26], our approach is based on lumping

all the asymmetric vibrational levels within a single group. In addition, a non-equilibrium distribution, the so-called Treanor distribution, is considered in the lumping process instead of the commonly used Boltzmann distribution. It is known that the Treanor distribution overestimates the population of high energy levels, yet, this is balanced by the high VT and VV' rates obtained for the group (see section Simplification approach). The complexity of multi-temperature approaches, widely used up to now, is reduced by the introduction of an algebraic approximation linking the vibrational and translational temperatures. Another advantange of this methodology is the implementation of weighted algebraic expressions to compute rate constants, instead of solving the complex differential equations used in [24-26], thereby enabling a faster calculation of the reaction rates. The application of this technique results in significant simplification regarding the number of reactions and species to describe the dissociation of CO_2. Few methods have succeeded in the reduction of detailed plasma kinetic models, which concern mainly diatomic molecules. In the case of more complex molecules, the development of practical and manageable approaches is subject to ongoing research in order to enable multidimensional modeling of non-equilibrium plasma processes.

As stated before, the main reduction in the presented approach is achieved by grouping the asymmetric vibrationally excited states of CO_2, which represent the main dissociation channel of the molecule in this type of discharges. Hence, the 21 vibrational levels considered in the detailed kinetic model [21] to describe the dissociation processes are lumped into a single asymmetric vibrational excited state. The fictitious species (CO_2*) is the representation of all asymmetric vibrational excited states that are not in thermal equilibrium with the translational energy mode of the molecule. An illustration of the lumped species is outlined in Fig. 4.2.

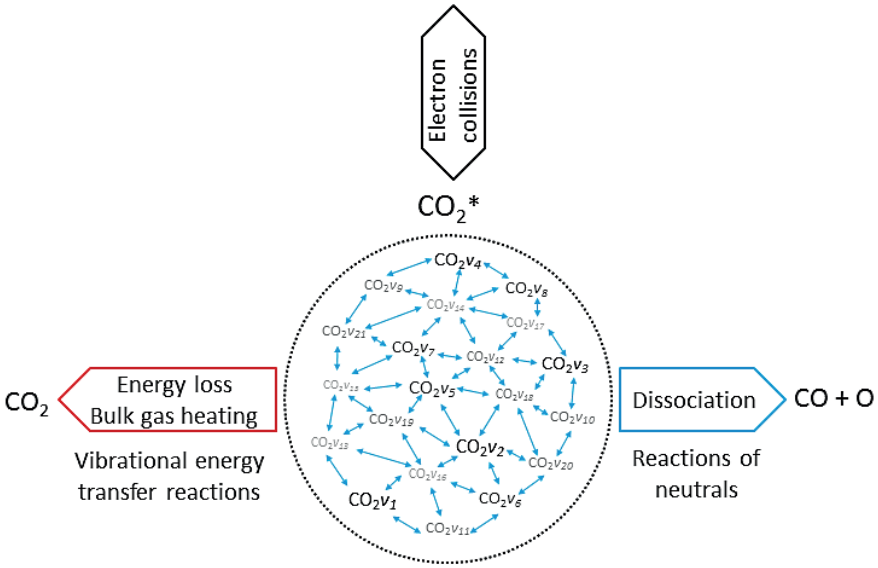

Fig. 4.2. Lumping of 21 asymmetric vibrational levels into a fictitious species CO_2*.

High CO_2 dissociation rates can be attained when the high vibrational levels of CO_2 remain far from equilibrium [21]. In low temperature plasmas, the highest relaxation rate is the (vibrational-vibrational) VV relaxation, i.e. the interaction of CO_2 molecules that are excited in the same vibrational mode. When the temperature of the gas increases, the (vibrational-translational) VT relaxation rate is boosted, thus leading to a high energy loss by heating up the gas. It is assumed that the vibrational levels lumped into the fictitious species CO_2* solely exchange energy through VV relaxation. Although, as a group, they can either dissociate or lose energy via VT relaxation as shown in Fig. 4.2. One of the major assumptions taken in the presented model is that the excited states follow the so-called Treanor non-equilibrium distribution [39], which allows for the calculation of the population densities of all asymmetric vibrationally excited states. The reason behind this assumption is the dominant vibrational energy transfer mechanism in the discharge: electron impact vibrational excitation (0→1) followed by VV relaxation. Hence, the energy used in the dissociation is mainly transferred through this mechanism, which also results in a Treanor vibrational distribution. For simplicity, a good approximation is to fit their energy levels to a diatomic anharmonic oscillator model and compute an effective anharmonicity coefficient so that the Treanor distribution can be calculated. The Treanor distribution enables the evaluation of the departure from thermal equilibrium given by the Boltzmann

distribution. Fig. 4.3 shows this concept more in detail by plotting the vibrational distribution functions considering different approaches: 1) Boltzmann distribution, 2) STS kinetic model [20] (microwave discharge, power density = 25 W cm^{-3} and 0.8 ms time) and 3) Treanor distirbution. The T_v/T_g value shown in Fig. 4.3 do not correspond to the values used to carry out the validation of the model, instead it shows the qualitative difference of the various VDF's. At low T_v/T_g values, the Treanor distribution approaches the Boltzmann distribution (becoming equal when $T_v/T_g = 1$), whereas at high T_v/T_g values the highly non-equilibrium nature of the discharge is noticeable. The departure from thermal equilibrium observed for both the STS and Treanor vibrational distributions represents the stored vibrational energy in the asymmetric mode. In comparison to the Treanor distribution the high levels of the STS distribution are depleted due to VT relaxation and dissociation. Herein, the overpopulation of the Treanor distribution is used to compute effective rates for vibrational relaxation and dissociation.

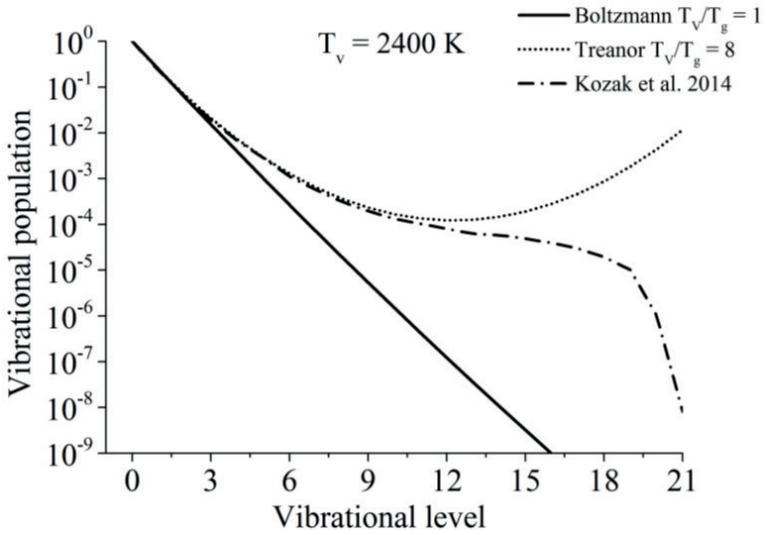

Fig. 4.3. Comparison of the vibrational distributions functions considering the approaches: 1) Boltzmann distribution, 2) STS kinetic model [20] (microwave discharge, power density = 25 W cm^{-3}) and 0.8 ms time) and 3) Treanor distribution.

The vibrational and bulk gas temperatures (T_v and T_g) are required to calculate the Treanor distribution, which reads [39]:

$$n_v = n_0 \exp\left(-\frac{vE_1}{T_v} + \frac{vE_1 - E_v}{T_g}\right) \quad (1)$$

where n_v is the population density and E_v the energy in eV of the vibrational level v, n_0 is the population density of the CO_2 ground state and T_g and T_v are the bulk gas and the vibrational temperatures (both in eV), respectively. The vibrational temperature in the previous equation is based on the population density of the first vibrational level and it is computed as follows

$$T_v = \frac{E_1}{\ln\left(\frac{n_0}{n_1}\right)} \quad (2)$$

The discharge can be characterized by the T_v/T_g ratio, which should be high enough at low bulk gas temperatures to achieve efficient dissociation. For multidimentional models this mean or characteristic value of the discharge could be used for the calculations, instead of considering spatial variations of the T_v/T_g values throughout the discharge. Considering the conditions studied in [21], T_v/T_g values lie in the range of 5.2 to 7. A sensitivity analysis carried out to study the effect of this value on the kinetics yielded the best agreement with a value of 6 (see Validation of the model section). On the other hand, at temperatures beyond the characteristic vibrational temperature, the VT and VV relaxation processes become comparable, even for the lowest vibrational levels [39]. In this case, the non-thermal effect is not attained and the discharge is completely thermalized, $T_v/T_g=1$. The conditions at which a plasma reaches thermal equilibrium vary depending on the type and duration of the discharge. Since it is rather complex to determine when a microwave plasma reaches thermal equilibrium (between 4000 to 5000 K [12]), a value of 5070 K is assumed. This temperature is 1.5 times the characteristic vibrational temperature of CO_2 and is above 5000 K, which ensures thermal equilibrium conditions of the plasma (dominance of VT over VV relaxation). Moreover, as found in [40], the gas temperature in a pure CO_2 microwave plasma torch is about 5000 K, which is consistent with our assumption. For further clarification, a comparison of the influence of these two parameters is given in the subsequent section, in which it is shown that the gas temperature at which quasi-equilibrium plasma conditions are reached barely has any influence on the results, while the high T_v/T_g value affects the calculations to a higher degree. The accuracy of the values chosen to compute the Treanor distribution is of secondary importance for the scope of this work, which is to demonstrate the validity of the reduction methodology.

Another point of discussion is the shape of the curve to estimate the T_v/T_g ratio. An exponential dependence is proposed as an initial approximation based on the Landau-Teller temperature dependence of vibrational-translational relaxation (VT), which becomes more relevant as temperature increases. Besides, a simple expression is preferred so that only two points are required for the fitting (see Fig. 4.4). For the considered range of temperatures the following expression gives a reasonable agreement of the temperature dependence with STS calculations of CO_2 vibrational kinetics

$$T_v/T_g = a \exp\left(\frac{b}{T_g^{1/3}}\right) \times \frac{1}{T_g} = 10937 \exp\left(\frac{-12.05}{T_g^{1/3}}\right) \times \frac{1}{T_g} \quad (3)$$

An accurate description of T_v and T_g would require the full set of reactions, which is not practical, or even possible, for multidimensional simulations. The coefficients a and b were computed by fitting this function to the proposed values of T_v/T_g. By following this approach, the Treanor distribution becomes exclusively a function of the gas temperature, thereby facilitating the calculation of the distribution. The Treanor distribution at various gas temperatures enables the estimation of rate constants for reactions involving the fictitious species CO_2*. These parameters are obtained by adding the individual contributions of the vibrational levels, which are computed from their populations and individual rate constants.

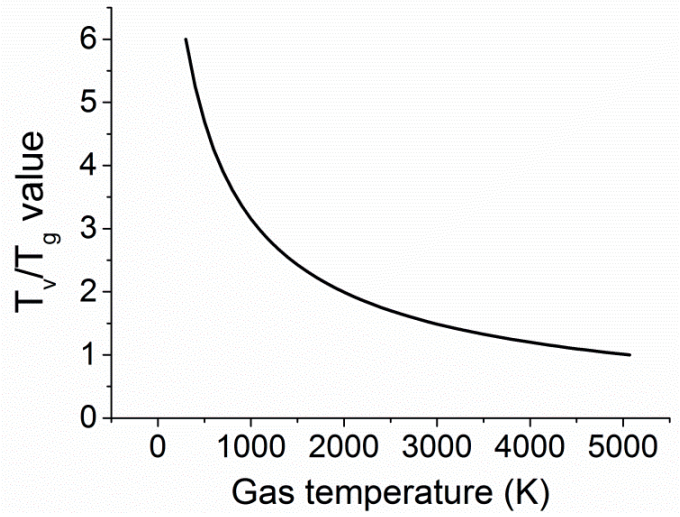

Fig. 4.4. T_v/T_g ratio-gas temperature dependence according to equation (3).

4.2.2.1. Electron impact reactions

One of the major simplifications in the reduced kinetic model is accomplished by assuming a Maxwellian electron energy distribution function (EEDF) This approximation is commonly accepted for typical microwave discharges as shown in [41], where a comparison between Maxwellian and non-equilibrium EEDFs is carried out. The studied microwave discharges present typical electron temperature values in the range 0.5 to 2 eV, in which the Maxwellian EEDF is rather similar to the non-equilibrium EEDF. Nevertheless, careful consideration should be given to this assumption, as reported in [42], where it was shown that non-equilibrium distributions can present an overpopulation in the tail, i.e. at high electron energies, as compared to a Maxwellian EEDF. These overpopulated tails are caused by superelastic collisions with electronically excited states and can influence high-threshold electron impact processes, resulting in increase in their reaction rates.

At low electron energies, the highest reaction rates are expected for elastic scattering and vibrational excitation since these reactions show the largest collisional cross sections [43]. On the other hand, at high electron energies, the EEDF is considerably smaller, meaning that the rate constants are orders of magnitude smaller than processes taking place at low energies. For instance, for an electron temperature of 2 eV, the rate coefficient of the electron impact CO_2 dissociation, which takes place at relatively high electron energies, is 3 orders of magnitude smaller than the rate coefficient of vibrational excitation. Therefore, only reactions with large cross sections are considered in the high electron energy range. In particular, besides elastic scattering, the largest cross section and the lowest energy threshold is attributed to the single charge ionization of CO_2 [29]. In fact, the ionization rate due to single charge ionization is at least two orders of magnitude larger than other ionization processes, such as dissociative ionization or multiple charge ionization. In conclusion, three types of collision processes (elastic scattering, vibrational excitation and non-dissociative single charge ionization) are taken into account for the reduced kinetic model.

Concerning collisions of electrons with the main neutral products of CO_2, i.e. CO, O, O_2 and O_3, these species take part in important processes of the reactive system, thus displaying high population densities. Based on the results given in [21], the population density of O_3 is at least two orders of magnitude less than that of O_2 and three orders of magnitude less than the one of CO_2. Moreover, O_3 is mainly a product formed in the afterglow and does not have a major influence on the dissociation kinetics of CO_2. For this reason, the O_3

species is not included in the model. By analysing the cross section data reported [30-33, 43, 44], it can be concluded that the same type of reactions (elastic scattering, vibrational excitation and ionization) should be considered for the neutral species.

It is noted that the electronic excitation process has been neglected for neutral species in the reduced kinetic model, as it barely influences the CO_2 dissociation kinetics at low electron energies. Furthermore, assuming quasi-neutrality of plasma and an ionization degree of about 10^{-5}, [21] the mass fractions of the charged species are ~5 orders of magnitude lower than the neutrals. Therefore, reactions with charged species are not included in the model.

With regard to electron collisions with vibrationally excited species, vibrational excitation reactions are considered for CO_2 and neglected for other neutrals as the energy transfer to vibrational modes of these species is considerably lower [21]. While the symmetric vibrational modes of CO_2, CO_2v_a and CO_2v_b, in combination with the lumped asymmetric vibrational mode CO_2*, are included, higher symmetric levels, such as the CO_2v_c and CO_2v_d are not added, as the cross sections for multiquantum vibrational jumps are smaller than single quantum vibrational jumps. Reverse processes of vibrational excitation, called de-excitation reactions, are also included in the model by using the detailed balancing principle [45].

The black arrows in Fig. 4.1 show the electron impact reactions included in the reduced kinetic model. A total of 16 electron impact reactions are included; we refer to Table 4.2 for more information.

*4.2.2.2. Cross section calculations for vibrational excitation from CO_2 to CO_2**

An overall vibrational excitation cross section is computed by lumping the vibrational excitation processes in the asymmetric vibrational mode, from the CO_2 ground state to the higher states within CO_2*. Vibrational de-excitation cross sections are obtained from the overall cross section by applying the detailed balancing principle. The calculation is carried out by scaling the cross sections using the Fridman's approximation. Then, the computed cross sections are added to estimate the overall cross section. The total electron impact

vibrational excitation rate for CO_2 is the sum of the vibrational excitation rates from level 0 to all higher levels, thus:

$$n_0 n_e \sum_{j=1}^{21} k_{0,j} = n_0 n_e \gamma \int_0^{\infty} \varepsilon \sigma_V(\varepsilon) f(\varepsilon) d\varepsilon \tag{4}$$

where n_0 is the population density of the vibrational level 0 (CO_2); n_e is the population density of electrons; $k_{0,j}$ is the rate coefficient for the vibrational excitation from level 0 to level j; ε is the electron energy; $\sigma_{0,j}$ (ε) is the cross section for the vibrational excitation from level 0 to level j; f(ε) is the electron energy distribution; γ is a conversion units constant and σ_V (ε) is the cross section for the excitation of CO_2 to CO_2* (reaction RX13 in Table 4.2) and is computed as follows:

$$\sigma_V(\varepsilon) = \sum_{j=1}^{21} \sigma_{0,j}(\varepsilon) \tag{5}$$

Not all the cross sections for the transitions from any level i to a higher level j are available. Hence, they are computed using the Fridman's approximation [12]. Specifically, the cross section of the lowest transition, from level 0 to level 1 ($\sigma_{0,1}$), is scaled to higher transitions by applying the following expression:

$$\sigma_{i,j}\left(\varepsilon + E_{i,j} - E_{0,1}\right) = \sigma_{0,1}(\varepsilon)\, exp\left(\frac{-\alpha(j-i-1)}{1+\beta i}\right) \tag{6}$$

where $E_{i,j} = E_j - E_i$ is the energy difference between levels j and i and α and ß are scaling factors. For the specific case of CO_2, the α factor takes the value of 0.5 and the ß factor is assumed to be 0 [12,20]. This approximation is used to compute all the transitions from level 0, which are subsequently added to obtain σ_v. The cross section's magnitude increases as a consequence of adding the cross sections of multiquantum vibrational jumps, while the discrete energy levels explain the presence of multiple peaks. The values of $\sigma_{0,1}$ used in the calculations are taken from [29].

In Fig. 4.5, a comparison between the cross section for the transition from level 0 to level 1 and the cross section for the excitation from CO_2 to CO_2* is presented. The energy threshold of the process is the minimum energy required to put a CO_2 molecule into vibration, which in this case is $E_1 - E_0 = 0.29$ eV.

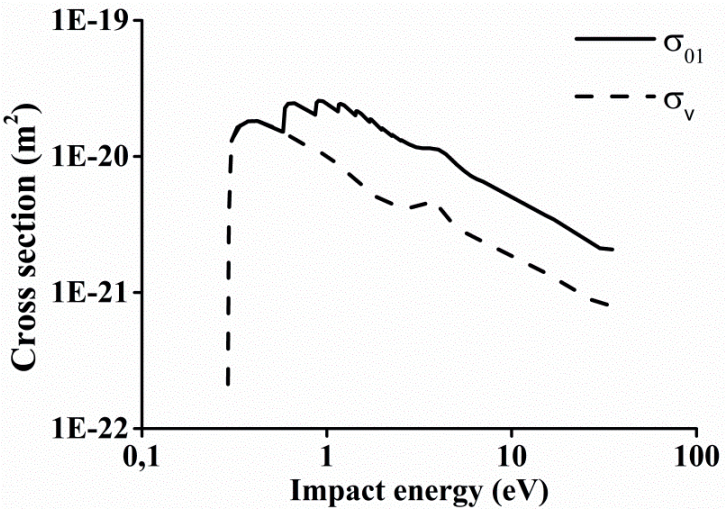

Fig. 4.5. Cross section for the vibrational excitation from CO_2 to CO_2*.

4.2.2.3. Reaction of neutral species

As mentioned in the previous section, a large portion of the energy is transferred from the electrons to the vibrational modes of the CO_2 molecule. Once the asymmetric mode is energized, the stored vibrational energy can be utilized to dissociate the molecule. A total of 11 dissociation and recombination reactions with neutrals are included in the reduced kinetic model (see blue arrows in Fig. 4.1 and Table 4.3). When compared to the STS kinetic model, three neutrals species (C, C_2O and O_3) are disregarded. The reason to neglect these species is the low net production rates and therefore the very low population densities (5 orders of magnitude smaller than CO_2) displayed in the overall reaction scheme. Moreover, these species show a minor influence on the dissociation kinetics. The reactions of neutral species are then restricted to the ones involving CO_2, CO, O and O_2.

In Fig. 4.1, it can be observed that the lumped excited species CO_2* is considered in the dissociation processes as dissociation reactions involving CO_2 ground state (v = 0) present the highest activation energies leading to very low reaction rates.

Due to the change in the activation energy of the dissociation reactions, as a consequence of the stored vibrational energy, the rate constants of reactions RN1 and RN2 must be computed. To estimate the efficiency in the reduction of

the activation energy due to vibrational excitation, the Fridman-Macheret α-model is applied [12]. The following expression is used [46]:

$$k_v(E_v, T_g) = A \exp\left(-\frac{E_a - \alpha E_V}{T_g}\right) \tag{7}$$

where A is the conventional pre-exponential factor, E_a is the activation energy of the reaction in K, E_v is the vibrational energy of level v in K (energy levels given in [20]), T_g is the bulk gas temperature in K and α is the efficiency of the vibrational energy in reducing the activation energy. The α values for RN1 (α = 1) and RN2 (α = 0.5) are taken from [20].

The rate constants of each level are then multiplied by the population densities obtained from the Treanor distribution. For the dissociation reaction RN1, the following equation is apllied [37]:

$$k(T_g) = \sum_{v=1}^{21} n_v(T_g) k_v(E_v, T_g) \tag{8}$$

For the dissociation reaction RN2, a different expression is used. RN1 is an endothermic reaction with a high activation energy, which virtually vanishes at the highest vibrational levels, whereas RN2 is a thermoneutral reaction with an activation energy that vanishes at vibrational levels above v = 10. Hence, the form of the rate constant is divided into two groups: 1) vibrational levels from 0 to 10 and 2) levels from 11 to 21.We propose the following expression to compute the rate constant for RN2:

$$\ln k(T_g) = \frac{v_1}{v_2} \ln k_1(T_g) + \frac{v_2 - v_1}{v_2} \ln k_2 \tag{9}$$

where v_1 is the number of levels in the first group and v_2 the number of levels in the second group; k_1 is the averaged rate constant of the first group and k_2 the one of the second group. Lastly, the averaged rate constant is estimated by adding the individual contributions of the lumped vibrational levels (v = 1 – 21). This process is repeated at various temperatures within the range of interest, 300 – 1500 K. Note that the validity of the rate constant expressions considered for the vibrational energy exchange reactions lies in the range 300 to 1500 K [47], which hinders the evaluation of this model at higher gas temperatures.

In Fig. 4.6, the calculated rate constants for the reactions RN1 and RN2 at different temperatures are displayed. These values are then fitted to a modified Arrhenius type of equation so that a single temperature-dependent expression for the CO_2* dissociation reactions can be implemented (Table 4.3, RN1 and RN2 rate constants).

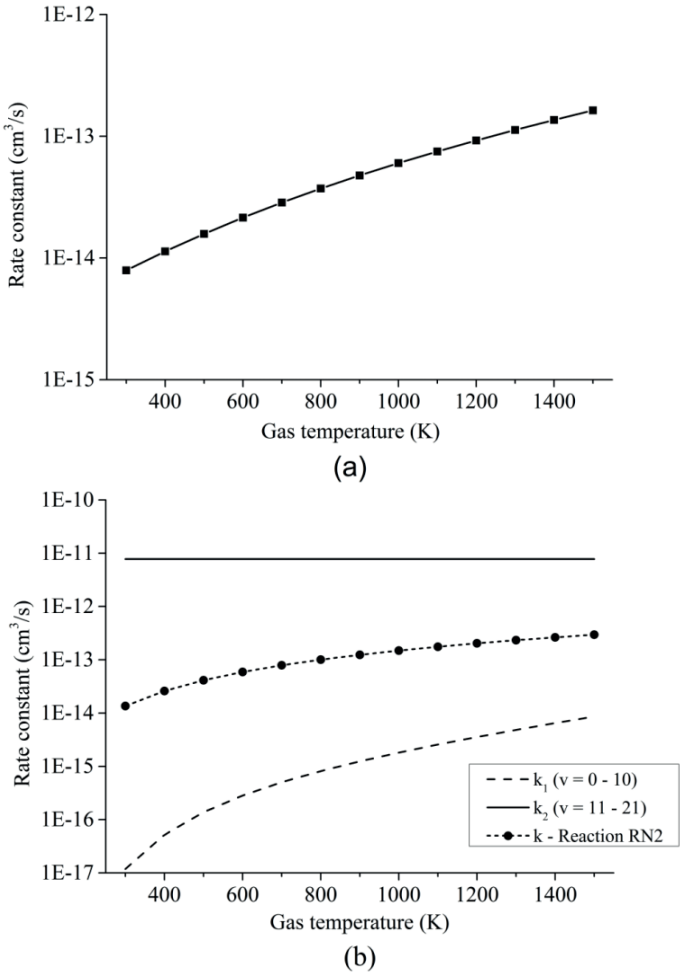

Fig. 4.6. (a) Rate constant of reaction RN1 as function of gas temperature and **(b)** rate constant of reaction RN2 as function of gas temperature (k_1 and k_2 are shown for reference).

4.2.2.4. Vibrational energy transfer reactions

The outcome of these energy exchange processes is mainly related to energy loss from vibrationally excited states to the bulk gas. Two types of relaxation reactions are considered, VT and VV' relaxation. In the VT type, vibrational and translational degrees of freedom exchange energy in which either a symmetric vibrationally excited state loses its energy in a collision with a neutral ground state (RV1) or the lumped asymmetric excited state transfers a fraction of its vibrational energy to the symmetric vibrational modes $CO_2v_{a,b,c.}$(RV2). The VV' relaxation process (RV3) comprises the energy exchange due to collisions between the lumped excited state CO_2* and a CO_2 ground state, thus transferring a portion of its vibrational energy to the symmetric modes of the molecule. A total of 13 vibrational energy exchange reactions are included in the reduced kinetic model (red arrows in Fig. 4.1 and Table 4.4). The following subsections describe how the rate constants for the reactions RV2 and RV3 are calculated. The energy change in the reactions is fitted to diatomic anharmonic oscillator models so that the anharmonicity coefficient can be computed to scale the rate constants from the lowest vibrational state to higher ones at specific gas temperatures [20]. The approach to calculate these rates is rather similar to the one used for the reaction of neutrals with one difference; the stoichiometric coefficients also depend on the Treanor distribution, which then depends on the bulk gas temperature.

4.2.2.5. Rate constant for reaction RV2

The initial step is to compute the rate constants of the VT relaxation reactions for all the asymmetric vibrational levels within CO_2*. In these reactions, a purely asymmetric vibrational level v relaxes into a lower asymmetric level v – 1 with a symmetric sublevel a,b,c. It is assumed that symmetric sublevels relax rapidly via VT relaxation, thus becoming in thermal equilibrium with the asymmetric level. This mechanism is not a direct process and consists of multiple VT relaxation reactions, in which the first process is considered to be the rate limiting step [48]:

$$\left.\begin{matrix} CO_2(0\,0\,v)+M \rightarrow CO_2(0\,1\,v-1)+M \\ \rightarrow CO_2(0\,2\,v-1)+M \\ \rightarrow CO_2(0\,3\,v-1)+M \end{matrix}\right\} \xrightarrow{VT\ Relaxation} CO_2(0\,0\,v-1)+M \quad \left.\begin{matrix} (V2a, Ref.[20]) \\ (V2b, Ref.[20]) \\ (V2c, Ref.[20]) \end{matrix}\right] \qquad (10)$$

The rate constants are scaled by using expressions derived from the SSH theory [49,50]. The scaling of the reaction rates is carried out by fitting the change of energy in the reaction to a diatomic anharmonic oscillator model. The

rate constants of reactions involving higher vibrational levels v > 1 are estimated from the rate constant of the reaction corresponding to the lowest levels (from v = 1 to v = 0). The calculation procedure for scaling the reactions is adapted from [20].

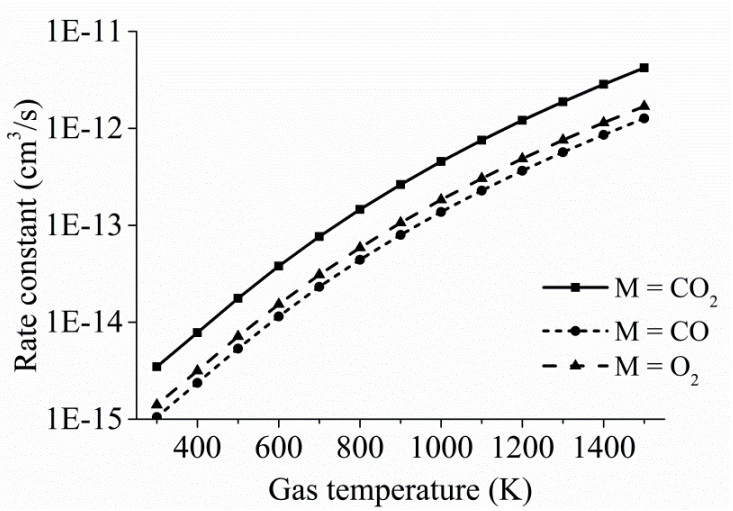

Fig. 4.7. Rate constant of reaction RV2 as function of gas temperature for M = CO_2, CO and O_2.

The reactions V2a,b,c [21] of all asymmetric vibrational levels within CO_2 are multiplied by the corresponding Treanor population and added to obtain three reactions per collision partner M:

$$\sum_{i=1}^{21}(n_i CO_2 v_i + n_i M) \rightarrow \sum_{i=2}^{21}(n_i CO_2 v_{i-1} + n_i M) + n_1 CO_2 v_{a,b,c} + n_1 M \qquad (11)$$

by introducing the fictitious species CO_2* they can be simplified to

$$CO_2{}^* + M \rightarrow (1 - n_1) CO_2{}^* + n_1 CO_2 v_{a,b,c} + M \qquad (12)$$

For a specific collision partner M it is possible to express these reactions in a more general "lumped" expression, which is more convenient for implementation into the model:

$$CO_2{}^* + M \rightarrow v_{l2} CO_2{}^* + v_{s2}(CO_2 v_a + CO_2 v_b + CO_2 v_c) + M$$
$$v_{l2}(T_g) = 1 - n_1(T_g), \quad v_{s2}(T_g) = \frac{1}{3} n_1(T_g) \qquad (13)$$

where v_{l2} and v_{s2} are the stoichiometric coefficients of the lumped excited state and the symmetric levels a,b,c respectively. The coefficients are function of the population density of the first asymmetric vibrational level n_1, which is computed with the Treanor distribution at a specific gas temperature T_g. The total averaged rate constant of the reaction RV2 (see Table 4.4) for a specific collision partner M is estimated by adding the averaged rate constants of the three individual reactions:

$$k_M(T_g) = k_{M,a}(T_g) + k_{M,b}(T_g) + k_{M,c}(T_g) \tag{14}$$

The averaged rate constant of each reaction is computed as in (9), considering that the individual rate constants k_v are scaled to the asymmetric vibrational level v, and depend on the symmetric sublevel and the collision partner M. For each collision partner M, the temperature range of interest (300-1500 K) is evaluated as shown in Fig. 4.7. For each of the reactions with different collision partners, the rate constant is fitted to a modified Arrhenius equation with the aim of using a more practical expression in the model.

4.2.2.6. Rate constant for reaction RV3

The calculation process is similar to the one presented above for RV2. In this case, the energy is transferred between different vibrational modes, i.e. the asymmetric and the first two symmetric modes (a, b). The reaction scheme is represented as

$$\left.\begin{matrix} CO_2(0\,0\,v) + CO_2 \rightarrow CO_2(0\,2\,v-1) + CO_2(0\,1\,0) \\ \rightarrow CO_2(0\,1\,v-1) + CO_2(0\,2\,0) \end{matrix}\right\} \quad \left.\begin{matrix} (V5\ x = a, Ref.[20]) \\ (V5\ x = b, Ref.[20]) \end{matrix}\right] \tag{15}$$

Assuming a rapid VT relaxation of the symmetric sublevels and adding the reactions of all asymmetric levels within CO_2*, the following expression is obtained for V5 x = a:

$$\sum_{i=1}^{21}(n_i CO_2 v_i + n_i CO_2) \rightarrow \sum_{i=2}^{21}(n_i CO_2 v_{i-1} + n_i CO_2 v_a) + n_1 CO_2 v_b + n_1 CO_2 v_a \tag{16}$$

The reaction RV3 included in the model is a result of combining the previous reaction with the analogous reaction V5 for the symmetric level b. Once the two combined reactions are put together, RV3 can be written as:

$$CO_2^* + CO_2 \rightarrow v_{l3}CO_2^* + v_{s3}(CO_2 v_a + CO_2 v_b)$$
$$v_{l3}(T_g) = 1 - n_1(T_g), \quad v_{s3}(T_g) = \frac{1}{2}(n_1(T_g) + 1) \tag{17}$$

The stoichiometric coefficients v_{l3} and v_{s3} are computed as done in the previous section for RV2. The total averaged rate constant of reaction RV3 is estimated by adding the individual averaged rate constants of both reactions:

$$k(T_g) = k_a(T_g) + k_b(T_g) \tag{18}$$

The averaged rate constant of each reaction is computed as in (9), considering that the individual rate constants k_v are scaled to the asymmetric vibrational level v and depend on the symmetric sublevel.

The overall "lumped" rate constant calculated at various temperatures is fitted to a modified Arrhenius equation to obtain a temperature-dependent expression (see Table 4.4).

The results of the rate constant obtained at various temperatures are displayed in Fig. 4.8.

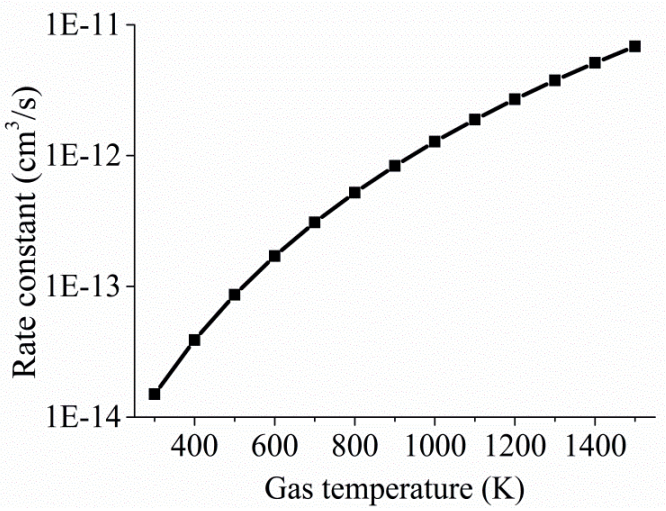

Fig. 4.8. Rate constant of reaction RV3 as function of gas temperature.

4.2.2.7. Surface reactions

These type of reactions take place on the surface of the reactor when chemical species collide with the surface. The rate coefficients for a single species can be determined by the following expression [51]:

$$k_s = \left(\frac{1}{1-\gamma/2}\right)\frac{\gamma}{(\Gamma_{tot})^s}\left(\frac{1}{4}\right)\left(\frac{8k_BT_g}{\pi m}\right)^{\frac{1}{2}} \quad (19)$$

where γ is the sticking coefficient of the reaction, i.e. the probability that the collision results in a reaction. Γ_{tot} is the total surface site density [1/m^2] and the exponent s is the sum of the stoichiometric coefficients of the surface reactants. The square root term is the mean thermal speed of the colliding species, computed from the Boltzmann constant K_B, the bulk gas temperature Tg and the mass of the species m. It is noted that the first term within the brackets is the Motz-Wise correction, which is only included when the sticking coefficient is large, i.e. close to 1 [51].

Various surface reactions can occur in the reactor, such as recombination or vibrational de-excitation reactions. The characteristic diffusion time is orders of magnitude smaller than the residence time of the reactor [21], thus recombination reactions on the wall can be neglected. In the latter, the collision frequency is high enough to ensure a dominant vibrational de-excitation through VT relaxation processes. For the abovementioned reasons, neither recombination nor vibrational de-excitation reactions are included in the model. The included surface reactions are related to recombination or neutralization processes through which ions are grounded (green arrows in Fig. 4.1 and Table 4.5) and restore the neutral charge. Due the low temperatures of heavy species, a unity sticking coefficient is assumed for these low energy collisions of ions with the walls [52,53]. Moreover, ions are consumed in these reactions and thus are needed to avoid their accumulation inside the reactor. The expression presented to calculate the rate coefficients can be simplified to the one shown below as no surface species are involved in the reactions:

$$k_s = \left(\frac{1}{1-\gamma/2}\right)\left(\frac{k_BT_g}{2\pi m}\right)^{\frac{1}{2}} \quad (20)$$

4.3. Results and discussion

In this section, a comparison of the results obtained from the proposed reduced model and the detailed STS kinetic model is performed. A qualitative study of the key model parameters is also carried out to identify which parameter displays the highest influence on the reduced model predictions. A simple reactor model was built in the COMSOL Multiphysics-plasma module [54] for this purpose. Spatially uniform quasi-neutral plasma is assumed throughout the reactor volume.

In the previous section, a description of the calculation process to estimate the rate constants for highly relevant chemical reactions in the dissociation kinetics of CO_2 is provided. In this regard, the computed rate constants for reactions involving the lumped excited species CO_2* are shown in Fig. 4.9. Two different zones are distinguished in this Figure. At low temperatures, below 700-800 K, the rate constants for the reactions with neutrals are relatively higher than the vibrational energy transfer reactions, thus leading to high dissociation rates of the CO_2 molecule. At high temperatures though, above 800 K, the vibrational reactions become dominant, resulting in a drop of the dissociation rate at the expense of increasing the bulk gas temperature.

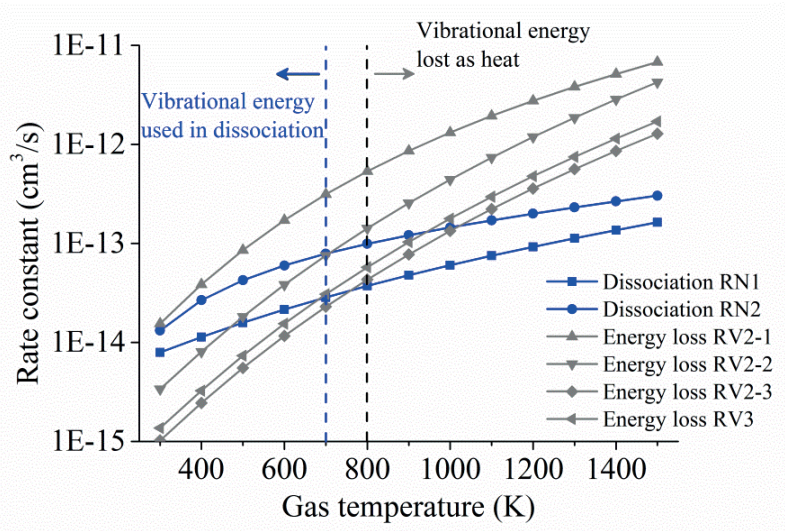

Fig. 4.9. Rate constants of the main reactions leading to dissociation of the CO_2 molecule (blue lines, RN1 and RN2) and the reactions causing energy loss (grey lines, RV2-1, RV2-2, RV2-3 and RV3).

4.3.1. Validation of the model

The simulations to investigate the validity of the reduced kinetic model are carried out at the same conditions as reported in [21]. The discharge takes place at a pressure of 100 torr, reduced electric field of 50 Td, electron density 10^{13} 1/cm^3, specific energy input 0.6 eV/molecule, frequency of the electromagnetic field 2.45 GHz and a residence time of 1.4 x 10^{-5} s. Elastic scattering and ionization reactions are not considered, and CO_2^+ is the only ion included for the quasi-neutrality of the plasma. The initial gas composition is a CO_2 mole fraction of 1; the initial bulk gas temperature is 300 K and the initial electron temperature is 0.39 eV or 4500 K.

In this work, the plasma medium is specified by the electron density and the mean electron energy. In the case of multidimensional simulations, where the spatial distribution and time evolution of the species concentration are to be studied, these parameters should be determined by solving the conservation laws and Boltzmann equation for the electrons. The energy equation is not included in the model. The electron and gas temperatures profiles in the reactor volume are specified as functions fitted to the results given in [21]. Viscosity effects are neglected and the pressure is considered uniform and constant inside the reactor.

Mass conservation equations are solved for the species to validate the reaction kinetics. Diffusion is neglected given its relatively short characteristic time. Thus, for this specific validation model the surface reactions are not included and the charged species densities are constant. This is done for consistency with [21], even though the results are not affected by the kinetics of charged species. Convection is not considered and time dependent simulations are performed based on the residence time value.

The model is divided into two parts describing two spatial zones; these are the plasma zone, where the plasma is active, and the afterglow zone, where the plasma vanishes. In the former, a constant electron density and an increasing electron temperature profile describe the chemically reactive (plasma) zone. In the latter, the electron density is set to zero, whereas a decreasing electron temperature profile is specified to describe the zone where reactive species relax back to equilibrium and radicals recombine. It is known that the electron density is not constant in either zone, but setting a constant electron density seems to be a good approximation to study the influence of chemical reactions in the overall reactive scheme. The total simulation time is fixed to 0.1 s, which is long enough for the relaxation process (VT and VV') to take place. In

conclusion, the inputs required for the model are the electron density, electron temperature, bulk gas temperature and pressure. The comparison of the benchmark STS kinetic model versus the proposed reduced kinetic model is displayed in Fig. 4.10 where the division of both zones can be observed. As expected, the dissociation of CO_2 occurs mainly in the plasma zone, whereas recombination processes take place in the afterglow.

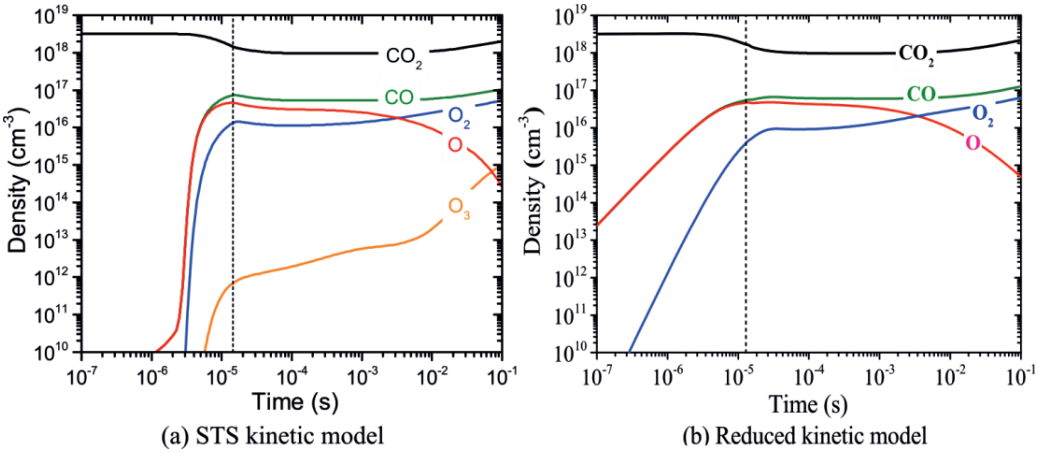

Fig. 4.10. (a) Population densities computed by the STS kinetic model, adapted from [21] **(b)** Population densities calculated by the reduced kinetic model of the most relevant neutral species.

The major difference as for the computed species concentrations is found in the plasma zone. In the afterglow, the species densities are in good agreement with the STS kinetic model. Notably, the predicted CO_2 density is virtually exact in both models, which in turn allows the calculation of the CO_2 dissociation rate. On the other hand, the concentration of CO and O_2 present an error lower than 10% and 20%, respectively. The steep slopes noticed in the time range $10^{-6} – 10^{-5}$ in Fig. 4.10a are the result of the STS kinetic model. The processes by which the energy is transferred from the electrons to the lower levels of the vibrational ladder and then progressively transferred by VV relaxation to higher levels have a time scale of ~10^{-6} s. Once the highest vibrational levels are excited, the dissociation of CO_2 starts taking place until the VT relaxation rates become comparable to the VV relaxation ones at about 10^{-5} s and therefore the dissociation rate declines. In the abovementioned time range, the stored vibrational energy enhances the dissociation processes by lowering the activation energy of the reactions. The rate constants for the dissociation processes are rather high, which explains the sharp increase in the densities of CO and O. The increase in the O_2 concentration is mainly due to the O

recombination reaction (RN5, Table 4.3). Concerning the reduced kinetic model, it is assumed that at low bulk gas temperatures, the lumped excited state CO_2* has a large population of the high vibrational levels, thus initiating the production of CO and O as soon as the species CO_2* is formed by means of electron collisions. This explains the slower dissociation process taking place in the reduced kinetic model in the range 10^{-7} to 10^{-5} s.

It is noticed that the predictions given by the model can be improved by adjusting the assumed value of the T_v/T_g ratio (Section Simplification approach) at low temperature. The value can be experimentally determined by measuring the vibrational and gas temperatures of the discharge, for instance, by optical emission spectroscopy [41]. This fact offers an evident benefit since the STS kinetic model does not enable such tuning due to the large number of reactions. At the very early stage in the plasma zone (10^{-7}-10^{-6} s), the results of the reduced kinetic model do not match the ones from the STS model. Conversely, the densities calculated at the end of the plasma zone and the afterglow do match the predictions of the STS model. To validate other process conditions, the electron dynamics and the energy equation should be included in the model.

4.3.2. Effect of model parameters

The results presented in Fig. 4.10b are calculated using constant values of the following model parameters; scaling factor $\Phi = 1.12$, stoichiometric coefficients $v_{l2} = 0.262$, $v_{s2} = 0.246$, $v_{l3} = 0.262$ and $v_{s3} = 0.869$ for a mean bulk gas temperature of 500 K in the discharge (plasma zone and afterglow). In Section Description of the model, it was shown that these factors are function of the bulk gas temperature. As stated in [21], the gas temperature increases from 300 to 560 K over the residence time in the plasma zone; therefore an alternative mean bulk gas temperature of 300 K is considered to study the effect of these parameters on the model predictions. It was proven that the error induced by keeping the parameters constant is relatively small since the species concentrations follow nearly the same trends. In this regard, the effect of the T_v/T_g ratio at the initial gas temperature (300 K) as well as the assumed gas temperature at which thermal equilibrium is reached are evaluated and displayed in Fig. 4.11.

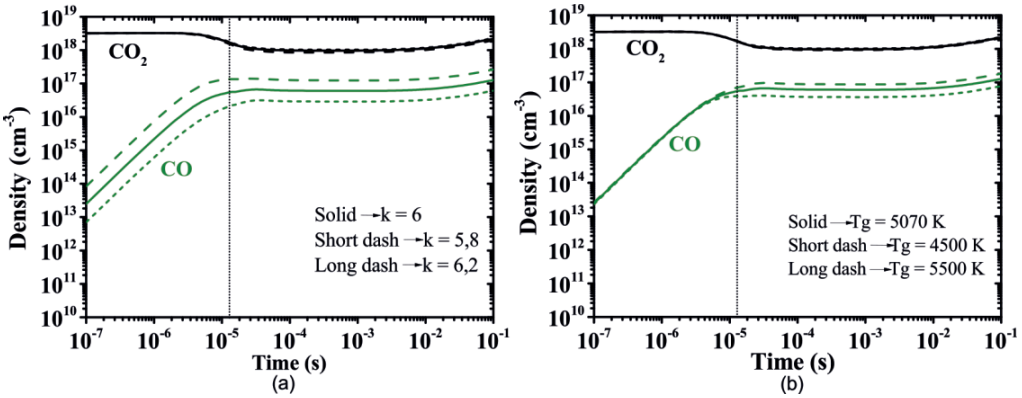

Fig. 4.11. (a) Population densities of CO_2 and CO for different T_v/T_g ratios (T_v/T_g = k) at constant gas temperature of 300 K and **(b)** population densities for constant T_v/T_g ratio (T_v/T_g = 6) considering different gas temperatures at which the plasma becomes thermal.

4

As expected, when the value of T_v/T_g is higher (T_v/T_g = 6,2 – long dash line) the dissociation rate increases and vice versa (T_v/T_g = 5.8 – short dash line). As previously stated, the value of T_v/T_g at low temperatures can be seen as the dissociation potential; the higher the T_v/T_g value the higher the vibrational energy stored in the molecules, thus conducting the process toward higher dissociation rates. The gas temperature at which the plasma becomes thermal seems to be much less influencing than the T_v/T_g ratio at low temperature. Lastly, it is shown that the value of T_v/T_g at low temperature has a higher influence on the predictions of the CO_2 dissociation rate, whereas the gas temperature at which quasi-equilibrium plasma conditions are reached does not have a major effect on the overall process. In this regard, experimental validation of the concept proposed in this work, where the T_v/T_g values are taken from [21], needs to be carried through measurements of the vibrational and gas temperatures in a pure CO_2 microwave discharge via optical emission spectroscopy. However, the experimental determination of these two temperatures is complex and only approximate values can be obtained using current plasma diagnostic techniques. Lastly, the actual implementation of the proposed kinetic model has not yet been done in multidimensional simulations. The computation of local rate constants considering spatial variations of the T_v/T_g ratio can be highly complex. Hence, a better approach is to use a characteristic T_v/T_g value to describe the reactor performance and keep the computational load at its minimum.

4.4. Conclusions

We have introduced a new methodology to simplify detailed plasma vibrational kinetics and applied it to the dissociation of CO_2 in non-equilibrium microwave plasma discharges. In this type of discharges, the dissociation kinetics of the CO_2 molecule are driven by the excitation of the highest vibrational levels of the asymmetric streching mode. The novelty of the proposed model lies in four key elements; 1) the 21 vibrational levels considered for the asymmetric stretching mode are lumped within a single group, or fictitious species, CO_2*, 2) this group follows the so-called non-equilibrium Treanor distribution, 3) an algebraic approximation is used to compute the vibrational temperature from the translational temperature based on the Landau-Teller formula and 4) weighted algebraic expressions are applied, instead of complex differential equations, to calculate the rates of the most influencing reactions. The reduced kinetic model comprises 44 reactions among 13 species, as opposed to our benchmark detailed kinetic model, in which +100 species and +10000 reactions are considered, thus reducing substantially the calculation time to less than a minute. For the validation of the reduced kinetic model, a reactor model was built in COMSOL Multiphysics. The predictions of the reduced kinetic model showed that the neutrals densities are in good agreement with those predicted by the STS kinetic model, notably at the end of the plasma zone and the afterglow, which represent the reactor outlet.

The calculation process for the rate constants of the most influencing chemical reactions in the dissociation kinetics was described. Moreover, it was shown that the bulk gas temperature highly affects the dissociation rate as expected. Remarkably, at temperatures below 700 K, the dissociation rates are faster than the VT relaxation processes, thus resulting in higher conversion. Furthermore, a qualitative analysis of the key model parameters was carried out. The value of the T_v/T_g ratio at low temperature had a considerable effect on the calculation process. This ratio can be used as a fitting parameter to link the presented plasma kinetic model to experimentally measured vibrational and gas temperatures via optical emission spectroscopy. At this stage of development, where current models are in qualitative agreement with experimental data, the introduction of an experimentally obtained parameter describing the non-thermal degree of the discharge can facilitate the transition from STS to more practical models suitable for engineering purposes. Furthermore, this parameter may be used to fit experimental data to the model, improving the overall accuracy of the predictions.

To further assess the influence of plasma/process parameters, the electron dynamics and energy equations should be included in the model. This will be the next step towards development of a self-consistent multidimensional model for non-thermal plasma reactors. As a final note, we believe that the presented approach can also be applied to other plasma chemistries, in which the vibrational kinetics are dominant in the dissociation process.

References

[1] Griffiths JF. Reduced Kinetic-Models and Their Application to Practical Combustion Systems. Prog Energ Combust. 1995;21:25-107.
[2] Amouroux J, Siffert P, Massue JP, Cavadias S, Trujillo B, Hashimoto K, et al. Carbon dioxide: A new material for energy storage. Prog Nat Sci-Mater. 2014;24:295-304.
[3] Sabihuddin S, Kiprakis AE, Mueller M. A Numerical and Graphical Review of Energy Storage Technologies. Energies. 2015;8:172-216.
[4] Hameer S, van Niekerk JL. A review of large-scale electrical energy storage. Int J Energ Res. 2015;39:1179-95.
[5] Mahlia TMI, Saktisandan TJ, Jannifar A, Hasan MH, Matseelar HSC. A review of available methods and development on energy storage; technology update. Renew Sust Energ Rev. 2014;33:532-45.
[6] Amouroux J, Siffert P. Co2--a Future Chemical Fuel: Key Questions About This Project. Spie Eco-Photonics 2011. 2011;8065:80650E.
[7] Wang Q, Spasova B, Hessel V, Kolb G. Methane reforming in a small-scaled plasma reactor - Industrial application of a plasma process from the viewpoint of the environmental profile. Chem Eng J. 2015;262:766-74.
[8] Roth JR. Indutrial plasma engineering IOP Publishing Ltd: British Library; 1995.
[9] Aerts R, Somers W, Bogaerts A. Carbon Dioxide Splitting in a Dielectric Barrier Discharge Plasma: A Combined Experimental and Computational Study. Chemsuschem. 2015;8:702-16.
[10] Kim HH, Ogata A. Nonthermal plasma activates catalyst: from current understanding and future prospects. Eur Phys J-Appl Phys. 2011;55:13806.
[11] Rusanov VD, Fridman AA, Sholin GV. Physics of Chemically Active Plasma with a Non-Equilibrium Vibrational-Excitation of Molecules. Usp Fiz Nauk+. 1981;134:185-235.
[12] Fridman A. Plasma Chemistry: Cambridge: Cambridge University Press; 2008.
[13] Ju YG, Sun WT. Plasma assisted combustion: Dynamics and chemistry. Prog Energ Combust. 2015;48:21-83.
[14] Yang Y, Hua W, Guo SY. Numerical study on microwave-sustained argon discharge under atmospheric pressure. Phys Plasmas. 2014;21:040702.
[15] Baeva M, Bosel A, Ehlbeck J, Loffhagen D. Modeling of microwave-induced plasma in argon at atmospheric pressure. Phys Rev E. 2012;85:056404.
[16] Jimenez-Diaz M, Carbone EAD, van Dijk J, van der Mullen JJAM. A two-dimensional Plasimo multiphysics model for the plasma-electromagnetic

interaction in surface wave discharges: the surfatron source. J Phys D Appl Phys. 2012;45:335204.
[17] Gokulakrishnan P, Joklik R, Viehe D, Trettel A, Gonzalez-Juez E, Klassen M. Optimization of Reduced Kinetic Models for Reactive Flow Simulations. J Eng Gas Turb Power. 2014;136:011503.
[18] Cenian A, Chernukho A, Borodin V, Sliwinski G. Modeling of Plasma-Chemical Reactions in Gas-Mixture of Co2-Lasers .1. Gas Decomposition in Pure Co2 Glow-Discharge. Contrib Plasm Phys. 1994;34:25-37.
[19] Kustova EV, Nagnibeda E. On a correct description of a multi-temperature dissociating CO2 flow. Chem Phys. 2006;321:293-310.
[20] Kozak T, Bogaerts A. Splitting of CO2 by vibrational excitation in non-equilibrium plasmas: a reaction kinetics model. Plasma Sources Sci T. 2014;23:045004.
[21] Kozak T, Bogaerts A. Evaluation of the energy efficiency of CO2 conversion in microwave discharges using a reaction kinetics model. Plasma Sources Sci T. 2015;24:015024.
[22] van Rooij G, van den Bekerom D, den Harder N, Minea T, Berden G, Bongers W, et al. Taming microwave plasma to beat thermodynamics in CO2 dissociation. Faraday Discuss. 2015;183:233-48.
[23] Stagni A, Saggese C, Bissoli M, Cuoci A, Frassoldati A, Faravelli T, et al. Reduced Kinetic Model of Biodiesel Fuel Combustion. Iconbm: International Conference on Biomass, Pts 1 and 2. 2014;37:877-82.
[24] Magin TE, Panesi M, Bourdon A, Jaffe RL, Schwenke DW. Coarse-grain model for internal energy excitation and dissociation of molecular nitrogen. Chem Phys. 2012;398:90-5.
[25] Guy A, Bourdon A, Perrin MY. Consistent multi-internal-temperatures models for nonequilibrium nozzle flows. Chem Phys. 2013;420:15-24.
[26] Le HP, Karagozian AR, Cambier JL. Complexity reduction of collisional-radiative kinetics for atomic plasma. Phys Plasmas. 2013;20:123304.
[27] Spencer LF, Gallimore AD. CO2 dissociation in an atmospheric pressure plasma/catalyst system: a study of efficiency. Plasma Sources Sci T. 2013;22:015019.
[28] Peerenboom K, Parente A, Kozak T, Bogaerts A, Degrez G. Dimension reduction of non-equilibrium plasma kinetic models using principal component analysis. Plasma Sources Sci T. 2015;24:025004.
[29] Itikawa Y. Cross sections for electron collisions with carbon dioxide. J Phys Chem Ref Data. 2002;31:749-67.
[30] Kameta K, Kouchi N, Hatano Y. 4 Cross sections for photoabsorption, photoionization, neutral dissociation of molecules. In: Itikawa Y, editor.

Interactions of Photons and Electrons with Molecules: Springer Berlin Heidelberg; 2003. p. 4001-61.
[31] Zecca A, Karwasz GP, Brusa RS. One century of experiments on electron-atom and molecule scattering: A critical review of integral cross-sections .1. Atoms and diatomic molecules. Riv Nuovo Cimento. 1996;19:1-146.
[32] Itikawa Y. Cross Sections for Electron Collisions with Oxygen Molecules. J Phys Chem Ref Data. 2009;38:1-20.
[33] Laher RR, Gilmore FR. Updated Excitation and Ionization Cross-Sections for Electron-Impact on Atomic Oxygen. J Phys Chem Ref Data. 1990;19:277-305.
[34] Zheng HT, Liu Q. Kinetic Study of Nonequilibrium Plasma-Assisted Methane Steam Reforming. Math Probl Eng. 2014;vol. 2014:938618.
[35] Markosyan AH, Luque A, Gordillo-Vazquez FJ, Ebert U. PumpKin: A tool to find principal pathways in plasma chemical models. Comput Phys Commun. 2014;185:2697-702.
[36] Colonna G, Armenise I, Bruno D, Capitelli M. Reduction of state-to-state kinetics to macroscopic models in hypersonic flows. J Thermophys Heat Tr. 2006;20:477-86.
[37] Colonna G, Pietanza LD, Capitelli M. Recombination-assisted nitrogen dissociation rates under nonequilibrium conditions. J Thermophys Heat Tr. 2008;22:399-406.
[38] Berthelot A, Bogaerts A. Modeling of plasma-based CO 2 conversion: lumping of the vibrational levels. Plasma Sources Science and Technology. 2016;25:045022.
[39] Treanor CE, Rich JW, Rehm RG. Vibrational Relaxation of Anharmonic Oscillators with Exchange-Dominated Collisions. J Chem Phys. 1968;48:1798-&.
[40] Kwak HS, Uhm HS, Hong YC, Choi EH. Disintegration of Carbon Dioxide Molecules in a Microwave Plasma Torch. Sci Rep-Uk. 2015;5:18436.
[41] Silva T, Britun N, Godfroid T, Snyders R. Optical characterization of a microwave pulsed discharge used for dissociation of CO2. Plasma Sources Sci T. 2014;23:025009.
[42] Pietanza LD, Colonna G, D'Ammando G, Laricchiuta A, Capitelli M. Non equilibrium vibrational assisted dissociation and ionization mechanisms in cold CO2 plasmas. Chem Phys. 2016;468:44-52.
[43] Anzai K, Kato H, Hoshino M, Tanaka H, Itikawa Y, Campbell L, et al. Cross section data sets for electron collisions with H-2, O-2, CO, CO2, N2O and H2O. Eur Phys J D. 2012;66:36.

[44] S.J. Buckman JWTC, M.T. Elford, Mitio Inokuti, Y. Itikawa, and Hiro Tawara. Interactions of Photons and Electrons with Atoms: Springer-Verlag, Berlin/Heidelberg; 2000.
[45] Itikawa Y. Molecular processes in plasmas: Springer Series on atomic, optical and plasma physics, Vol. 43 (Springer Berlin Heidelberg); 2007.
[46] Levine RD, Bernstein RB. Thermodynamic Approach to Collision Processes. In: Miller W, editor. Dynamics of Molecular Collisions: Springer US; 1976. p. 323-64.
[47] Blauer JAaNGR. A survey of vibrational relaxation rate data for processes important to CO2-N2-H2O infrared plume radiation. Report Ultrasystems, Inc. 1973.
[48] T. Kozák. Private communication. 2015.
[49] Schwartz RN, Slawsky ZI, Herzfeld KF. Calculation of Vibrational Relaxation Times in Gases. J Chem Phys. 1952;20:1591-9.
[50] Keck J, Carrier G. Diffusion Theory of Nonequilibrium Dissociation and Recombination. J Chem Phys. 1965;43:2284-98.
[51] R. J. Kee MECaPG. Chemically Reacting Flows: John Wiley & Sons, Inc., Hoboken, NJ, USA; 2003.
[52] Hassouni K, Silva F, Gicquel A. Modelling of diamond deposition microwave cavity generated plasmas. J Phys D Appl Phys. 2010;43.
[53] Ryan AJ. Emerging Themes in Polymer Science. The Royal Society of Chemistry2001.
[54] Plasma Module User's Guide COMSOL Multiphysics 44. 2013.

5

Microwave plasma emerging technologies for chemical processes

This chapter is published as:

de la Fuente JF, Kiss AA, Radoiu MT and Stefanidis GD, Microwave plasma emerging technologies for chemical processes. *Journal of Chemical Technology & Biotechnology*: doi:10.1002/jctb.5205 (2017).

Abstract

Microwave plasma (MWP) technology is currently being used in application fields such as semiconductor and material processing, diamond film deposition and waste remediation. Specific advantages of the technology include the enablement of a high energy density source and a highly reactive medium, the operational flexibility, the fast response time to inlet variations and the low maintenance costs. These aspects make MWP a promising alternative technology to conventional thermal chemical reactors provided that certain technical and operational challenges related to scalability are overcome. Herein, an overview of state-of-the-art applications of MWP in chemical processing is presented (e.g. stripping of photo resist, UV-disinfection, waste gas treatment, plasma reforming, methane coupling to olefins, coal/biomass/waste pyrolysis/gasification and CO_2 conversion). In addition, two potential approaches to tackle scalability limitations are described, namely the development of a single unit microwave generator with high output power (> 100 kW), and the coupling of multiple microwave generators with a single reactor chamber. Finally, the fundamental and engineering challenges to enable profitable implementation of the MWP technology at large scale are discussed.

5.1. Introduction

A sustainable and green economy represents one of the major challenges of contemporary society. It involves mostly the reduction of waste generation, but also the optimization of raw material consumption in order to mitigate current alarming pollution problems and lower the energy requirements of industrial conversion processes. In this regard, the process intensification (PI) philosophy [1] has significantly improved such industrial conversion processes. By applying the PI principles [2], various processing advances can be attained such as 1) higher energy efficiency, 2) lower raw material usage, 3) prevention of waste generation (improved product quality) and 4) safer process, as demonstrated in several industrial applications [3-5].

For the chemical industry to progress towards a sustainable economy, novel waste-to-product approaches need to be developed to reduce the dependency on fossil fuels-based raw materials. Carbon Capture & Utilization (CCU) is an emerging concept, which utilizes waste (e.g. greenhouse gases) as chemical feedstock to produce valuable products [6]. In most cases however, the required energy input to transform waste into products tends to be rather high, making the re-utilization process unprofitable. Renewable energy sources, such as wind and solar power, are expected to have an increasing share in the future energy scene as a large fraction of the energy needed for chemical conversion processes can be obtained from these sources during peak electricity production periods. This falls within the so-called power-to-chemicals approach [7], whereby greenhouse gases and/or water are converted into hydrocarbons by means of surplus electric power.

In the context of power-to-chemicals approach, a large variety of electricity-based chemical reactors, such as electrolyzers [8], electrocatalytic reactors [9] and plasma-based reactors [10, 11] have been investigated. The first two reactor types require the use of a catalyst, which potentially introduces problems of thermal degradation and coking at high temperatures [12]. Concerning the use of electrolyzers, even though this technology has reached rather high voltage efficiencies (solid oxide electrolyzers, 80%) [13], the specific energy consumption compared to conventional hydrogen production routes (mainly steam reforming) is still relatively high. Plasma reactors represent a novel alternative technology due to certain processing benefits such as: fast process dynamics, process flexibility, no need for catalyst use in many processes, no need for (bulky and costly) gas-fired furnaces, low maintenance cost, and high quality products (low by-products formation). The performance

of these three reactor types for the production of hydrogen was evaluated by Dincer et al. (2015) [13]. From the cost and energy efficiency point-of-view, they concluded that the plasma-assisted reactor performs better compared to the other electricity-based reactors. In this work, we focus on microwave plasma (MWP)-assisted reactors, which appear to be one of the most promising plasma reactor types as discussed hereafter.

Plasma can be triggered and sustained by different energy sources. MWP in particular is a gas ionized by means of a high frequency (300 MHz – 300 GHz) electromagnetic field. The alternating electric field heats the electrons which provide energy mostly for ionization and excitation of neutral atoms and molecules creating and sustaining the discharge. The principal advantage of MWP over other discharge types is that it does not require electrodes, which must be placed inside the reactor leading to operational issues, such as regular maintenance (replacement) due to erosion caused by contaminants formation. MWP can also be operated in a wide pressure range (from 10^{-5} mbar – 1 bar). Furthermore, the power-to-plasma efficiency can reach up to 90% [14]. Concerning the reactor performance, the high frequencies at which MWP systems are operated produce a much larger fraction of electrons, i.e. higher electron densities, and higher electron temperature (energy) compared to other plasma sources. This results in high concentrations of active species rendering MWP an ideal highly reactive medium for chemical reactions. To date, most research has been carried out at laboratory-scale, while few successful industrial applications have been demonstrated. Some of the limitations that have hindered widespread implementation of MWP at industrial scale include the cost of equipment, challenges related to process scalability, controllability and stability as well as the cost of electric power. For further information on theoretical concepts related to MWP, the reader is referred to the literature [14-19].

In this work, the state-of-the-art of MWP at laboratory stage, existing industrial chemical applications, current technical and operational limitations and an overview of the fundamental and engineering challenges for further development of the MWP technology are presented. Finally, some promising potential applications, which mainly concern high temperature processes, such as pyrolysis, gasification and reforming of organic waste, biomass and fossil fuels are discussed. Overall, this paper intends to set up a roadmap describing the main requirements and the next steps needed for the implementation of the MWP technology in the chemical manufacturing industry.

5.1.1. Microwave plasma technology: state-of-the-art

In this section, the necessary elements to operate MWP reactors are briefly described. Additionally, an overview of the laboratory state-of-the-art applications of MWP in chemical processing is given. Lastly, well-known industrial applications are discussed, showing the potential of the technology for commercial use.

5.1.1.1. Description of the main elements

In conventional chemical reactors, the design is characterized by process variables needing control during operation, such as temperature, pressure, concentrations of chemical species and throughput. With regard to MWP reactors, the waveguide components [20] are predefined and optimized for each particular operating frequency, whereas elements such as reactor sizing/shape/material, reactant inlet(s) (flow pattern) and cooling/control systems are design-related aspects that can be adjusted for optimization of the reactor performance. Table 5.1 and Fig. 5.1 introduce the essential components of MWP systems. The component number 1 described in Table 5.1 (Microwave generator) is identified as the key element to scale up this type of reactors due to its limitation as to the maximum output microwave power. The reader is referred to the microwave generator section for further information.

Table 5.1. Description of the main elements enabling the operation of MWP reactors.

Nº	Element	Function
1	Microwave generator = HV Power supply (switch mode) & Microwave head	Generation of electromagnetic waves Operating frequency 2.45 GHz: Maximum output power of 15 kW Operating frequency 915 MHz: Maximum output power of 100 kW
2	Isolator	Protection of the magnetron from the reflected microwave field
3	Impedance tuner	Reduction of the reflected microwave power ensuring high energy transfer efficiency from the microwave generator to the plasma zone; manual or automatic operation
4	Reactor assembly	Conversion of raw materials into products A plasma column is generated perpendicular to the incoming microwave field
5	Movable plunger	It positions the electromagnetic wave such that a local electric field maximum is located at the center of the plasma zone to maximize the microwave energy transfer from the generator to the plasma zone; manual or automatic operation

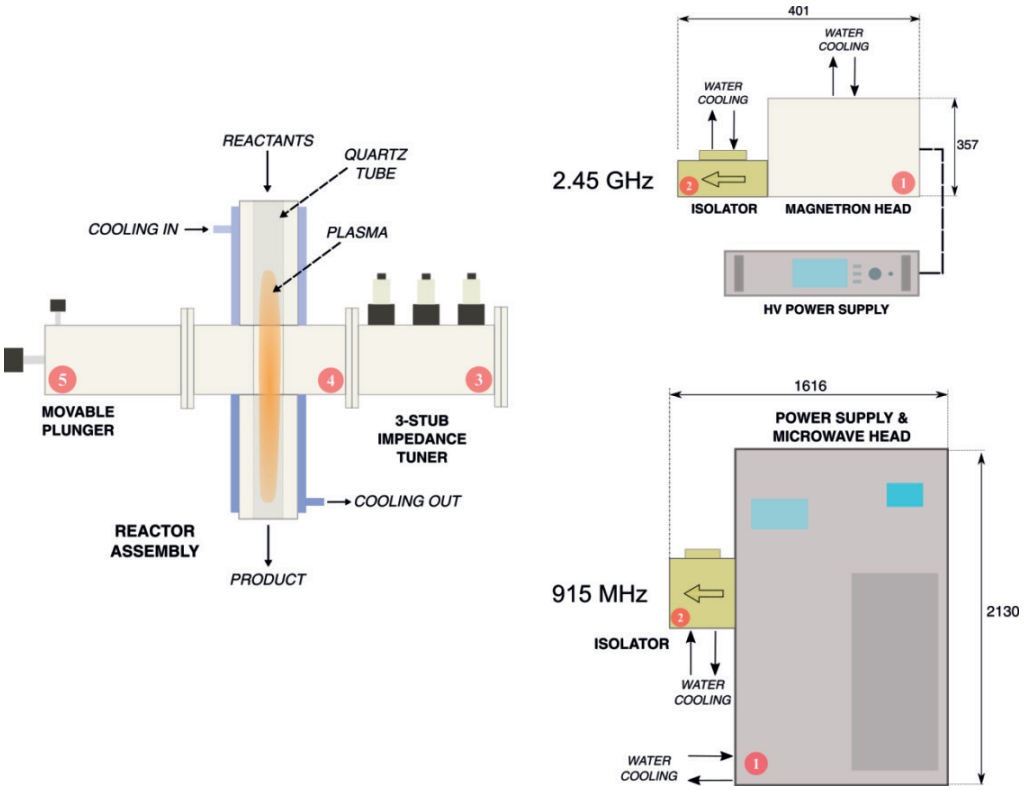

Fig. 5.1. Sketch of the main elements needed to operate MWP reactors. Note that the two commercially available microwave generators for plasma applications (2.45 GHz - 15 kW and 915 MHz – 100 kW) are outlined including the relevant dimensions (mm); both generators consist of switch-mode HV power supplies. Circled numbers refer to the element numbers in Table 5.1; in this example, manually operated 3-stub tuner (3) and manually operated movable plunger (5).

5.1.1.2. State-of-the-art at laboratory stage

A remarkably broad range of chemical applications at laboratory-scale have been explored in different MWP systems with the exception of biomass gasification for syngas production, which has been investigated both at laboratory scale[21] and in medium-scale plants.[22, 23] Concerning chemical manufacturing applications, several processes are highlighted due to the large number of research studies (see Table 5.2), such as: plasma-assisted reforming, biomass gasification and pyrolysis, H_2 production, and CO_2 utilization. We should note that the MWP technology is also used for other applications, including: production of *carbon nanostructures* of high quality (nanotubes,

graphene), production of *synthetic diamond* for gemstones and technical applications, *surface modification* for deposition of thin films to improve material properties, *water purification* (ozone/UV radiation), *photoresist stripping* for removal of polymeric photoresists in semiconductor manufacturing, and *medicine* (cancer treatment, sterilization of medical instruments and disinfection of living tissue).

Table 5.2 presents an overview of MWP-assisted processes for chemical applications. It is noticeable that the research focus has been on the production of synthesis gas or hydrogen. Herein, certain processes should be acknowledged due to the notably good performance shown in MWP reactors. As reported by Jasinski et al.,[24, 25] H_2 generation via plasma-assisted dry reforming of methane can be carried out at a specific energy consumption of ~3 kWh/m^3 H_2 and a H_2 generation cost ~2.3 \$/kg H_2 (assuming 0.06 \$/kWh). This value is close, within a factor 2, to the reported industrial cost of H_2 production (representative value: 1.5 \$/kg H_2)[26, 27] through the mature and highly integrated and optimized process of steam reforming of natural gas in high temperature furnaces. Another example is reported by Uhm et al. (2014),[22] in which the gasification of brown coal in a pilot-scale setup was studied, obtaining cold gas efficiency (CGE, calorific power of produced synthetic gas divided by the total input power to the system) values up to 84%, while conventional gasifiers, more specifically entrained flow gasifiers, have CGE values between 70-80%.[28] Additionally, one should take into account the evident gain in economy of scale and particularly the increase in the energy efficiency when microwave power above 1 kW is used to sustain the plasma chemical reactions, as displayed in Table 5.2.

Table 5.2. Summary of reported MWP processes for chemical applications.

REACTANT MIXTURE	DESIRED PRODUCT	REACTOR TYPE	PRESSURE	POWER (kW)	FLOW RATE/ THROUGHPUT	CONVERSION	SELECTIVITY (%)	ENERGY EFFICIENCY	REF
PLASMA ASSISTED REFORMING									
$CH_4 + H_2O_g$	Syngas	2.45 GHz	1 bar	5 (3-5)	27 l/min H_2O_g + 3-9 l/min CH_4	95%	70 (H_2) & 19 (CO)	300 l syngas/kWh	[29]
$CH_4 + CO_2$	H_2	2.45 GHz	1 bar	4	6000 l/h CH_4 + 6000 l/h CO_2	1100 l/h H_2	-	350 l H_2/kWh	[25]
$C_2H_5OH + N_2$	H_2	915 MHz	1 bar	5	2700-3900 l/h N_2 0.4-1.2 kg/h C_2H_5OH	1150 l/h H_2	100 (H_2)	267 l H_2/kWh	[30]
$C_3H_7OH + CO_2$	H_2	915 MHz	1 bar	5	2700 l/h CO_2 2.4 kg/h C_3H_7OH	1116 l/h H_2	37 (H_2)	223 l H_2/kWh	[30]
$C_6H_{14} + H_2O_g$ + Ar	Syngas	2.45 GHz	1 bar	2	34.6 mol/h H_2O_g 5 mol/h C_6H_{14}	36 mol/h H_2 14.4 mol/h CO	-	0.24 kg syngas/kWh	[31]
$C_8H_{18} + H_2O_g$ + Ar	Syngas	2.45 GHz	1 bar	2	34.6 mol/h H_2O_g 4.3 mol/h C_8H_{18}	21.6 mol/h H_2 10.8 mol/h CO	-	0.17 kg syngas/kWh	[31]
C_2H_6 + Ar	C_2H_4	2.45 GHz	20-73 mbar	2 (0.1-0.8)	-	95%	50 (C_2H_4)	-	[32]
C_5H_{12} + Ar	C_2H_4	2.45 GHz	0.1 mbar	2 (0.45)	25 ml/min Ar + 7 ml/h C_5H_{12}	65%	40 (C_2H_4)	0.44 g C_2H_4/kWh	[33]
C_6H_{14} + Ar	C_2H_4	2.45 GHz	0.1 mbar	2 (0.45)	25 ml/min Ar + 7 ml/h C_6H_{14}	72%	65 (C_2H_4)	0.75 g C_2H_4/kWh	[33]
C_7H_{16} + Ar	C_2H_4	2.45 GHz	0.1 mbar	2 (0.45)	25 ml/min Ar + 7 ml/h C_7H_{16}	75%	55 (C_2H_4)	0.56 g C_2H_4/kWh	[33]
$C_8H_{18} + O_2$ + Ar	Syngas	2.45 GHz	1 bar	0.10	0.2 ml/min C_8H_{18} + 7 lpm Ar	68.4 g/h syngas	-	0.68 kg syngas/kWh	[34]
Gasoline + O_2 + Ar	Syngas	2.45 GHz	1 bar	0.10	0.2 ml/min gasoline + 7 lpm Ar	84.6 g/h syngas	-	0.85 kg syngas/kWh	[34]
$CH_4 + O_2$ + Ar	Syngas	2.45 GHz	1 bar	0.10	140 ml/min CH_4 + 7 l/min Ar	46.8 g/h syngas	-	0.47 kg syngas/kWh	[34]
$CH_4 + O_2$	CH_3OH	2.45 GHz	31 mbar	0.02	30 ml/min CH_4 + 50 ml/min O_2	97%	4.4 (CH_3OH)	1.3 kg CH_3OH/kWh	[35]
METHANE COUPLING TO OLEFINS									
CH_4	C_2H_2	2.45 GHz	160 mbar	0.4	500 ml/min	94%	> 90 (C_2H_2)	64 l C_2H_2/kWh	[36]
CH_4	C_2H_2	Pulsed 2.45 GH	15-65 mbar	2 (0.07)	150 ml/min	94%	71 (C_2H_2)	85 l C_2H_2/kWh	[37]
WASTE GAS TREATMENT									
$SF_6 + N_2 + H_2O$		2.45 GHz	1 bar	6 (5.4)	80 l/min N_2 + 12 l/min (H_2O + SF_6)	99.9% decompo.		1 m^3/kWh	[38]
CFC 12 + H_2O_g	-	2.45 GHz	1 bar	2	2 kg/h CFC 12	99.99% decompo.	-	0.5 kg/kWh	[39]
VOC (CCl_4) + Ar + He	-	2.45 GHz	1 bar	1	1 l/min Ar + 5-12000 ppm CCl_4	Reduction to ppb	-	3 kg/kWh	[40]

PYROLYSIS/GASIFICATION									
Brown Coal (Gasification) + H_2O_g + air + O_2	Syngas	915 MHz (2)	1 bar	75 each (70)	90 kg/h coal + 60 kg/h H_2O_g+ 320 l/min N_2 + 410 l/min O_2	99.8% CCE	40 (H_2) & 32 (CO)	84% CGE	[22]
Charcoal (Gasification) + H_2O_g + air	Syngas	2.45 GHz	1 bar	6 (5)	1.26 kg/h charcoal + 1.1 kg/h H_2O_g + 20 l/min air	52% CCE	-	43% CGE	[41]
Wood (Pyrolysis) + N_2 + Ar	Syngas	Plasma jet 2.45 GHz	200 mbar	2 (1)	1 l/min N_2 + 1 l/min Ar plasma + 10 g samples	2 l/min syngas	-	-	[42]
Waste paper (Gasification) + air	Fuel gas	2.45 GHz	1 bar	0.8	1-4 l/min air + 5 g sample	3.3 m^3/kg paper	7.7 (H_2) & 8.5 (CO)	2.3 MJ/m^3 LHV	[43]
Rice straw (Pyrolysis) + N_2	Syngas	2.45 GHz	1 bar	2 (0.5)	5 g sample + 50 ml/min N_2	80% mass reduction ratio	55 (H_2) ; 17 (CO_2) 13 (CO) ; 10 (CH_4)	-	[44]
CO_2 UTILIZATION									
CO_2 and H_2O_g	Syngas	Pulsed 915 MHz	40 mbar	1	3-6 l/min CO_2 and H_2O_g	0.72 mol/h CO 0.22 mol/h H_2	-	0.02 kg syngas/kWh	[45]
CO_2	CO	2.45 GHz	10-250 mbar	1 (0.6)	5 l/min	30%	-	0.17 kg CO/kWh	[46]
CO_2 and H_2	Syngas	2.45 GHz	20-50 mbar	0.2	400 ml/min CO_2+H_2	85%	100 (CO_2 → CO)	0.03 kg CO/kWh	[47]
H_2 PRODUCTION									
CH_4	H_2	2.45 GHz	1 bar	6 (1-5)	87.5 l/min CH_4	99.8% (0.87 kg H_2/h)	100 (H_2)	640 g H_2/kWh	[24]
$C_2H_2F_4$	H_2	2.45 GHz	1 bar	6 (1-5)	97 l/min $C_2H_2F_4$	84% (0.7 kg H_2/h)	99.9 (H_2)	670 g H_2/kWh	[24]
CO + H_2O_g	H_2	Reverse Vortex 2.45 GHz	1 bar	3	27 l/min H_2O_g + 3 l/min CO	85% (CO)	36 (H_2)	3.40 g H_2/kWh	[48]
C_2H_5OH/CH_3 OH + Ar + H_2O_g	H_2	2.45 GHz	1 bar	0.2-0.7	2 l/min Ar + CH_3OH + H_2O_g 0.5 l/min Ar + C_2H_5OH + H_2O_g	100% (CH_3OH)	-	0.41 g H_2/kWh	[49]
CH_3OH + N_2	H_2	2.45 GHz	1 bar	5 (1.4)	12.4 l/min N_2 (5% CH_3OH)	99%	85 (H_2)	2 g H_2/kWh	[50]
PFO (pyrolysis fuel oil) + Ar	H_2	2.45 GHz	1 bar	2 (0.85)	5 l/min Ar	446.3 ml/min H_2 27.4 ml/min C_4	92 (H_2) & 5 (C_4)	2.8 g H_2/kWh	[51]
CH_3OH/C_2H_5 OH/ C_3H_7OH + Ar + H_2O_g	H_2	Tornado-type 2.45 GHz	1 bar	2 (0.45)	1 l/min Ar + 9 ml/min (CH_3OH) 1 l/min Ar + 13.5 ml/min (C_2H_5OH) 1 l/min Ar + 8.5 ml/min (C_3H_7OH)	0.10 g H_2/h 0.24 g H_2/h 0.18 g H_2/h	> 95 (H_2)	0.24 g H_2/kWh 0.53 g H_2/kWh 0.45 g H_2/kWh	[52]

5.1.1.3. Capital cost

The capital cost of conventional chemical reactors is mainly determined by the reactor dimensions (volume) and material of construction. In the case of MWP reactors, the main driver of the total capital investment is the microwave generator in combination with the waveguide components required to operate the plasma reactor. Fig. 5.2 gives an estimation of the commercial price of MWP equipment (generator + components, see Table 5.1) as well as the commercial equipment cost per kW microwave power, as function of the total output power of the microwave generator. For the particular case of 100 kW, the equipment cost amounts to ~1400 €/kW microwave power. This value is calculated as the ratio between the MWP equipment price and the total output power of the generator (e.g. 1.4 10^5 €/100 kW). The prices given in Fig. 5.2 include switch mode HV power supplies, which are required in the case of atmospheric pressure plasmas; the switch mode has low ripple and better control on the magnetron including the rise time or time needed for the magnetron to increase the power from 0 W to the requested power for plasma ignition. It is observed that the higher the output power of the microwave generator, the lower the equipment cost per kW microwave power as shown in Fig. 5.2 (black line, square markers). Therefore, the development of single unit microwave sources with higher power (> 100 kW) should significantly reduce the high capital cost of MWP equipment.

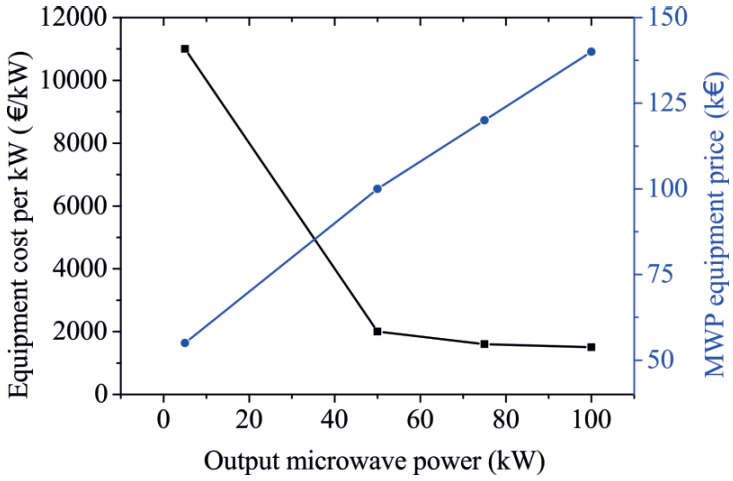

Fig. 5.2. Commercial MWP equipment price (generator + components, see Table 5.1) and commercial equipment cost per kW microwave power (MWP equipment price (k€) divided by output microwave power (kW)) as function of the total output power of the microwave generator for equipment at 915 MHz frequency (microwave generator based on a switch-mode HV power supply).

5.1.1.4. Industrial applications of MWP technology

The applications of MWP at industrial-scale have been previously discussed in the literature [16]. In summary, the main industrial applications include: photoresist stripping in semiconductor manufacturing, deposition of barrier layers in PET bottles, high rate deposition process of quarts on polycarbonate windows, plasma photo curing of paintings applied to the automotive industry, UV disinfection for water treatment, waste gas treatment for decomposition of fluorine-based components such as CF_4, C_2F_6, CHF_3, and SF_6 [38, 53] or ammonia, and plasma reforming to increase efficiency in wood gas engines. In the past few years, few advancements have been reported on the industrial application of this technology, although there are some novel processes that should be added to the existing list. Table 5.3 presents these applications together with a brief description of the main features of the process. Most of the future industrial applications of the MWP technology will be relevant to high temperature processes for chemical synthesis and (oxygenated) fuels conversion including pyrolysis, gasification and reforming of organic waste, biomass, and fossil fuels. Other application fields in which MWP will play a role are water and air purification, material synthesis (nano-particle production, diamonds, textiles) and biomedicine (cancer treatment, wound healing, disinfection).

Table 5.3. Summary of novel MWP processes for chemical applications.

PROCESS/(COMPANY)	DESCRIPTION	MAIN FEATURES
BIOMASS GASIFICATION (Plasma2Energy) [23]	- Medium-scale plant for biomass gasification. - It runs for four years. - It exploited the concept of coupling multiple microwave generators to a single gasification chamber. - The plant consumed only 20% of the energy generated.	▪ Input microwave power = 30 kW (plasmatrons) ▪ Pressure (bar) = 1 ▪ Annual Biomass Capacity = 3.3 kton ▪ Selectivity (H_2) = 50-52% ▪ Annual Production = 1830 m^3 ethanol & 253 m^3 diesel fuel ▪ Maintenance: 5 years ▪ Lifetime: 25 years
CARBON FIBER MANUFACTURING (RMX Technologies) [54]	- Low-pressure microwave plasma enhanced the oxidation and carbonization steps. - Reduction in the residence time and the equipment size by 1/3. - Energy requirements were reduced by 75% and manufacturing costs by 20% compared to conventional one.	▪ Input MW power = 30 kW (915 MHz) ▪ Pressure (mbar) = 10 ▪ Reactor size: Diameter = 0.05 m & Length = 4 m ▪ Energy efficiency = 17 kWh/kg carbon fiber
PECVD OF Si_3N_4 ON MULTI-CRYSTALLINE SILICON SOLAR CELLS [55]	- Deposition of silicon nitride anti-reflective layers on solar cell wafers by plasma enhanced carbon vapour deposition (PECVD).	▪ Input microwave power = 2 x 4 kW (pulsed-type) ▪ Pressure (mbar) = 0.01-1 ▪ Reactor size: Diameter = 0.02 m & Length = 1.5 m ▪ Production = 1500 solar cells wafers per hour
TREATMENT OF CHRONIC WOUNDS (Adtec Europe SteriPlas) [56]	- Wound healing by reduction of microbial load and by modifying the wound microenvironment. - Working gas is Argon, which ensures the reproducibility of generated active agents.	▪ Input microwave power = 200 W ▪ Working gas = Argon, purity 99.95% ▪ Operating temp range = 10-30 °C
PRODUCTION OF SYNTHETIC DIAMOND MPECVD (ASTeX)[57]	- Synthetic diamond growth from the gas phase by microwave-plasma enhanced vapor chemical deposition (MPECVD). - Synthesis diamonds are presented as a much affordable option over naturally mined diamonds.	▪ Frequency = 915 MHz & Power = 90 kW ▪ Pressure (torr) = 180 & Gas temperature = 4000 K ▪ Working gas = H_2 + 1-5% CH_4 ▪ Deposition rate = 1 g/h ▪ Annual production rate = 214300 carats (10 reactors) ▪ Diamond production cost = 14 $/carat

5.2. State of development and outlook

5.2.1. Current status of the technology

In this section, the technical and operational limitations of the technology are discussed. The different possibilities to scaling up MWP technology are also addressed. Finally, the most relevant scientific and engineering challenges as for the implementation of this technology to commercial scale are presented in the form of a timeline.

5.2.1.1. Microwave generator

The largest single-unit continuous wave (CW) microwave generator, so-called magnetron, presents a limitation of maximum output power of 15 kW at a frequency of 2450 MHz and 100 kW at 915 MHz. There are magnetrons, operating at 15 kW max power, which are used for diamond synthesis at very low pressure; however, their performance seems to be quite poor and their lifetime rather short (few thousand hours range). In contrast, 15 kW generators work relatively well for laboratory applications, as those do not involve 24h operation. From an economic and regulatory point-of-view, there are two commercially preferable frequencies on the ISM bands, 915 MHz (L-band) and 2450 MHz (S-band) [54] that can be used for MWP reactors. The emissions at other frequencies can create electromagnetic interference and disrupt radio communications. To date, most of the work with MWP has been done at the standard microwave frequency of 2450 MHz. Microwave generators at this frequency, which have been largely produced for decades (e.g. domestic microwave ovens), offer various benefits such as relatively high power capability, durability, low cost and compact size of MWP elements. In the case of the 915 MHz frequency, the waveguide components are characterized by larger sizes (about three times larger than those of one at 2450 MHz), which makes these microwave generators more costly compared to 2450 MHz generators. There are also devices operating at non-standard frequencies (20-250 GHz), known as travelling wave tubes or gyrotrons, with maximum output powers of 1-2 MW. These high power sources are mostly used in nuclear fusion and their evaluation is out of the scope of this paper.

5.2.1.2. Plasma ignition, stability and uniformity

Plasma is ignited when the applied electric field strength overcomes the breakdown voltage of the working gas, which is called electric breakdown. Data for the breakdown voltage for different atomic and molecular gases as a function of the pressure and distance between two parallel electrodes, termed the Paschen curves, are well documented in the literature [11]. When low pressure MWP is considered, the required field strength to ignite and maintain the plasma is less demanding compared to MWP at atmospheric pressure where a rather high electron collision frequency is needed to energize the plasma. For large scale chemical applications, uniformity and stability become imperative in the production process, as it is highly important to ensure a constant and reproducible product composition. One of the major challenges for use of the MWP technology is its inherent instability, which has implications in reproducibility of the results. When operating MWP at atmospheric pressure and high power conditions, plasma stability depends mostly on the interplay between input microwave power and flow dynamics (working gas flow rate, feed gas composition, swirl flow). To obtain stable plasmas, it is important that the input power is adapted to the flow conditions. If the input power is excessive in relation to the gas flow, it can cause arcing and overheating of the quartz tube,[30] whereas if the power is too low, the degree of ionization along with gas bulk temperature will decrease resulting in plasma extinction. For high power equipment, a motorized sliding short circuit and automatic tuner can be used to compensate for variations of the reflected power, which represents a measure of plasma stability. However, operating at a minimum reflected power implies operation very close to or at unstable conditions that can lead to plasma loss or fluctuations (non-uniform).[58, 59] Another reason of instability is small fluctuations in the microwave frequency, which causes variations in the electron density, largely influencing the plasma frequency [60]. In this regard, there are a number of practical measures to improve plasma stability: 1) addition of a carrier/working gas; argon, helium, nitrogen, air and water are the most commonly used gases, 2) design of a novel reactor configuration such as "Vortex/Tornado-type"[48], [61] or multi-point microwave coupling [62], 3) combination of microwave and other fields (e.g. radio-frequency) [15] and 4) insulation of the reactor, which plays an important role in enhancing the stability by reducing heat losses.

5.2.1.3. Cooling of the plasma reactor

MWP is characterized by high power densities, which enable MWP reactors to achieve energy efficiencies up to 90%. As a result, one of the major technical challenges is the cooling of the reactor due to the high values of power input per unit wall area (W/cm^2), which increases significantly the chance of reactor melting (quartz tube). Hence, MWP reactors require carefully designed cooling systems to ensure a continuous operation. The most common cooling techniques are forced-air/N_2 in combination with cooling water jacket-type [47] or, in more demanding cases, cooling oil, surrounding the plasma reactor. The area with the highest risk for reactor puncturing is the one found within the ignition plasma zone, i.e. where the waveguide crosses the quartz tube, which also presents the highest electric field strength. Frequently, MWP reactors are characterized by a one-sided incoming microwave field, meaning that the plasma is mostly energized on one side. This causes non-homogeneous plasma formation, which leads to hot spot formation [62]. When the power input per unit wall area becomes relatively high (> 40 W/cm^2),[14] a common measure of protection of the reactor wall is the use of high-speed tangential gas injection (swirl flow) to confine the plasma at the core of the reactor by creating a tornado/vortex gas motion, which isolates the reactor wall from the plasma column. Another alternative is the addition of an inert gas such as helium with high heat conductivity to increase the dissipation of heat generated in the plasma, thus reducing the possibility of reactor failure. Therefore, thermal management is one of the key engineering challenges to continuously operate this type of systems at large scale. Note that MWP reactors can be run under two different conditions: a) non-thermal/low pressure MWP and b) thermal/atmospheric pressure MWP. In the latter, the cooling requirements are rather demanding, as the temperature of the gas gets close to the temperature of the electrons – all species are close to thermal equilibrium – whereas in non-thermal MWP, the bulk gas remains rather cold (near room temperature) while having high kinetic electron temperature.

5.2.1.4. Reactor material

As already stated, one of the main features provided by MWP is the high energy density, which also implies high temperatures inside the reactor. In this regard, the material of the reactor is a crucial aspect in MWP operation and must fulfill three requirements: 1) have high melting point to provide resistance to high temperature operation, 2) have thermal shock resistance and 3) be transparent to microwaves, i.e. it should not absorb or reflect microwaves.

At lab-scale, the most commonly used material is quartz, which seems unsuitable for commercial applications due to its fragility. Therefore, other materials such as ceramics (alumina-based), aluminium oxynitride (melting point above 2000 °C) or silicon carbide can be used to build large size MWP reactors. The latter has already been used in a plasma gasification unit [63]. Moreover, in the pilot-scale setup developed by Uhm et al. 2014 [22] alternative materials such as HACT180 (fire-resistance ceramic) and INCT120 (insulating-cement) were used to form the inner and outer layers of the MWP reactor respectively, showing great performance at temperatures up to 1800 °C.

5.2.1.5. Process control and safety

MWP-based processes show remarkably fast dynamics, in which most of the events take place in the micro/milli-second range. Such dynamics require demanding continuous process control tools that are capable of adjusting process parameters within a response time of milliseconds. Various control parameters are critical during MWP operation: 1) net input microwave power, 2) input gas flow rate, 3) operating pressure and 4) cooling flow rate.

The input power is the most important process variable, as it influences directly the absorbed energy by the plasma and consequently the temperature of the reactor. A practical way to control the forward power, while assuring reactor stability is by measuring the reactor wall temperature. This value is then compared to a setpoint that guarantees no reactor puncturing. The input power is then regulated based on the temperature difference between the readings and the setpoint.

The gas flow rate largely affects reactor stability as low flow rates can lead to severe increase in the specific energy input (SEI, J/m^3), i.e. the ratio between the input power and the inlet flow rate, causing rupture of the reactor. When the flow rates are excessive, plasma is extinguished due to the drop of SEI. The study of operating flow rate range should therefore be carefully assessed in MWP reactors.

Control of the operating pressure is particularly important when working with low-pressure MWP, as it influences both plasma ignition and sustenance. When pressure is increased, the number of collisions between electrons and other species also increases, implying that more input power is needed to sustain plasma.

Finally, as discussed, the cooling system (flow rate) requires a suitable design in which sufficient heat is removed from the plasma reactor to ensure proper function and stability of the system.

With respect to safety, the primary concern is related to exposure of operators and/or fuel to microwave radiation. Thus, the installation of microwave leak detectors is highly recommended when operating MWP equipment. In this regard, it is critical to assure good microwave shielding to eliminate any possibility of microwave radiation. If openings along the cavity are present, common practice is the installation of a metal mesh as an additional shield. Furthermore, considering the possible risk of reactor breaking, it is advisable to operate MWP reactors within a properly ventilated area to contain the hazard of a gas leakage.

5.2.2. Scalability

When evaluating the development of a new process, the production capacity represents the main design guideline, thus dictating the equipment requirements. Bulk chemicals are commonly produced on a very large scale, implying the need to operate at considerably high throughput and therefore demanding high energy input. As an example, a common methanol manufacturing plant [64] with a production rate of 100 kton/year and electricity usage of 550 kWh/ton is herein considered. The largest MWP unit developed so far was able to handle 3.3 kton biomass/year resulting in a production of 1.5 kton ethanol/year [23]. Hence, to meet the expected capacity for bulk chemical manufacturing, the current MWP reactors should be scaled up by a factor of 66 for this particular process, which is challenging.

Another pilot-scale MWP gasification unit was developed by Uhm et al. (2014) [22]. In their work, two microwave generators of 75 kW output each were attached to the gasification chamber and enabled inlet flow rates of 2.2 ton coal/day with respective throughput of 1.9 ton syngas/day corresponding to a total calorific value of 0.5 MW_{th}. To date, the use of MWP reactors in bulk chemical manufacturing processes has been hampered mostly because the input microwave power required to sustain the plasma at rather high throughput cannot be directly delivered by the existing microwave generators. To our knowledge, there are two possibilities to address this technical limitation: 1) coupling multiple microwave generators to a single reactor chamber or 2) developing single unit microwave sources with > 100 kW output power at lower frequencies (e.g. 433 MHz).

The first approach has already been explored for a medium-scale gasification plant as shown in Sanchez A.L. (2010) [23]. To increase the capacity, multiple 20 kW microwave plasmatrons were arranged around and along a single MWP gasification chamber. In a plasmatron, plasma is formed as an axial, cylindrical extension of the inner conductor of a coaxial line; microwave power is fed from a standard waveguide and a waveguide-to-coaxial transition carries out the wave mode conversion and impedance matching functions. A general advantage of these plasma sources is homogeneous plasma heating from all sides [62, 65]. A schematic representation is presented in Fig. 5.3. When multiple microwave sources are to be combined, one should take into account the minimization of cross-coupling between generators, as this can cause a drastic reduction of the generator life and also non-uniformity of the energy delivered to the plasma. A more detailed description regarding design and application of multiple microwave generators is discussed in references [14, 62, 66]. As a final remark, the MWP gasification system reported in Sanchez A.L. (2010) [23] was designed to have maintenance every 5 years and a lifetime of 25 years, which is common practice in the chemical process industry.

The second alternative envisages the development of single unit microwave sources with > 100 kW output power. Within the microwave ISM frequencies for industrial processing, the frequency band 433.05 – 434.79 MHz (central frequency 433.92 MHz) appears to be the most interesting one for scale-up. Currently, there are no reported industrial applications operating at 433.96 MHz. However, according to magnetron manufacturers, CW magnetrons operated at this frequency can be designed to deliver much higher microwave power levels than the L-band (896 MHz, 915 MHz, 922 MHz and 929 MHz) magnetrons namely, between 0.5 and 1 MW. The design of high power 433.96 MHz equipment should consider the development not solely of the magnetron and the HV DC power supply, but also all the high power rated WR2100 waveguide components (isolators, impedance tuners etc.) required to run industrial applications.

Fig. 5.3. Schematic representation of multiple microwave generators attached to a single reactor [23]. Note that each of the black elements represents a 20 kW microwave plasmatron.

5.2.3. Potential of MWP for commercial chemical applications

At the current technological state of MWP, the concept of modularized production seems to be the most promising approach to respond to: (1) the decentralized electricity generation via renewable energy sources, and (2) the present volatile markets due to frequent fluctuations in factors such as demand, economic uncertainties, depletion of natural resources, demographic trends and oil and gas prices among others [67]. In this regard, the development of modular MWP units powered by locally generated renewable electricity for distributed manufacturing may, at least partially, change the current model of very large scale centralized industrial processing and also form an attractive strategy to overcome rapid changes in the market demand [68]. Therefore, the production of syngas, hydrogen, acetylene and localized waste treatment represent some of the opportunities that MWP technology can address at present.

As for bulk chemical manufacturing, the first steps to bring MWP technology to commercial scale have been taken, although some technical and operational

challenges still need to be tackled before MWP can be extensively used in the chemical industry. Fig 5.4 presents in the form of a timeline, the main scientific and engineering challenges to be addressed. These challenges mainly concern: 1) development of higher than 100 kW microwave power sources and of effective plasma reactor designs that can be powered by multiple microwave generators to attain wide throughput range, 2) development of suitable reactor materials for MWP operation, 3) improvement of process reliability (controllability, stability and uniformity) and 4) development of chemical kinetic models that can be implemented into multidimensional multiphysics models for process design, optimization, and control.

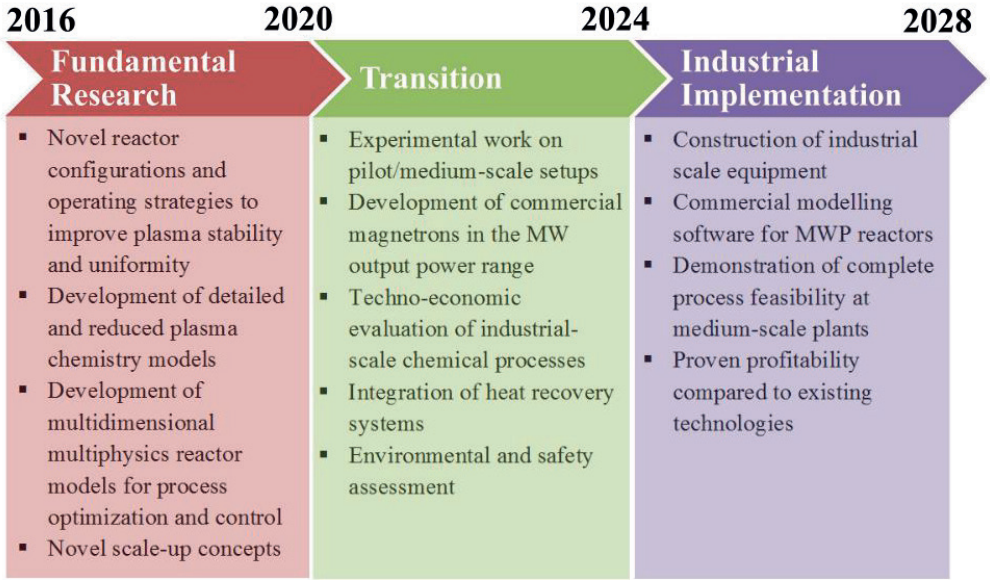

Fig 5.4. Timeline for the implementation of MWP technology in chemical manufacturing industry.

5.3. Conclusions

Microwave plasma (MWP) is one of the most promising enabling technologies for electricity-based reactors as regards the future partial electrification of the chemical industry. In this work, we have summarized the extensive research carried out on MWP at laboratory-scale combined with some successfully demonstrated industrial applications. Concerning chemical processing applications, high temperature processes, such as pyrolysis, gasification and reforming of organic waste, biomass and fossil fuels have the highest potential to benefit from MWP. However, it is imperative to perform research with

medium-scale setups to quantitatively demonstrate the profitability, reliability and operational benefits of the technology, as already shown for biomass gasification. In parallel, work on development of a) single-unit microwave sources with >100 kW output power (0.5-1 MW), b) suitable reactor materials that can withstand harsh operating conditions and c) reaction kinetic models that can be implemented into multidimensional multiphysics reactor models appear to be key scientific and engineering challenges that need to be addressed to promote wider application of the technology to large scale operations.

References

[1] Stankiewicz A, Van Gerven T. The Fundamentals of Process Intensification: Wiley; 2015.
[2] Van Gerven T, Stankiewicz A. Structure, Energy, Synergy, Time-The Fundamentals of Process Intensification. Ind Eng Chem Res. 2009;48:2465-74.
[3] Kiss AA. Distillation technology-still young and full of breakthrough opportunities. J Chem Technol Biot. 2014;89:479-98.
[4] Chen JF. The Recent Developments in the HiGee Technology, http://inpact.inp-toulouse.fr/GPE-EPIC2009/images/presentation_chen.pdf. (accessed 05-10-2016).
[5] Lavric D, Woehl P. Advanced-FlowTM glass reactors for seamless scale-up. Chemistry Today. 2009;27:45-8.
[6] Styring P, Jansen D. Carbon Capture and Utilisation in the green economy. The centre for Low Carbon Futures 2011.
[7] Mennicken L, Janz A, Roth S. The German R&D Program for CO2 Utilization-Innovations for a Green Economy. Environ Sci Pollut R. 2016;23:11386-92.
[8] Wang MY, Wang Z, Gong XZ, Guo ZC. The intensification technologies to water electrolysis for hydrogen production - A review. Renew Sust Energ Rev. 2014;29:573-88.
[9] Hu B, Guild C, Suib SL. Thermal, electrochemical, and photochemical conversion of CO2 to fuels and value-added products. J Co2 Util. 2013;1:18-27.
[10] Boulos MI. The Role of Transport Phenomena and Modeling in the Development of Thermal Plasma Technology. Plasma Chem Plasma P. 2016;36:3-28.
[11] Fridman A. Plasma Chemistry: Cambridge: Cambridge University Press; 2008.
[12] Argyle MD, Bartholomew CH. Heterogeneous Catalyst Deactivation and Regeneration: A Review. Catalysts. 2015;5:145-269.
[13] Dincer I, Acar C. Review and evaluation of hydrogen production methods for better sustainability. Int J Hydrogen Energ. 2015;40:11094-111.
[14] Ferreira CM, Moisan M. Microwave Discharges Fundamentals and Applications: NATO ASI Series; 1993.
[15] Lebedev YA. Microwave discharges: generation and diagnostics. 25th Summer School and International Symposium on the Physics of Ionized Gases - Spig 2010. 2010;257.
[16] Kaiser M, Baumgartner KM, Mattheus A. Microwave Plasma Sources - Applications in Industry. Contrib Plasm Phys. 2012;52:629-35.

[17] Schulz A, Buchele P, Ramisch E, Janzen O, Jimenez F, Kamm C, et al. Scalable Microwave Plasma Sources From Low to Atmospheric Pressure. Contrib Plasm Phys. 2012;52:607-14.
[18] Uhm HS, Hong YC, Shin DH. A microwave plasma torch and its applications. Plasma Sources Sci T. 2006;15:S26-S34.
[19] Jankowski KJ, Reszke E. Microwave Induced Plasma Analytical Spectrometry: RSCPublishing 2011.
[20] Stefanidis GD, Munoz AN, Sturm GSJ, Stankiewicz A. A helicopter view of microwave application to chemical processes: reactions, separations, and equipment concepts. Rev Chem Eng. 2014;30:233-59.
[21] Sturm GSJ, Munoz AN, Aravind PV, Stefanidis GD. Microwave-Driven Plasma Gasification for Biomass Waste Treatment at Miniature Scale. Ieee T Plasma Sci. 2016;44:670-8.
[22] Uhm HS, Na YH, Hong YC, Shin DH, Cho CH. Production of hydrogen-rich synthetic gas from low-grade coals by microwave steam-plasmas. Int J Hydrogen Energ. 2014;39:4351-5.
[23] Sanchez AL. Method and apparatus for plasma gasification of carbonic material by means of microwave radiation. US Patent. 2010:2010/0219062.
[24] Jasinski M, Dors M, Nowakowska H, Nichipor GV, Mizeraczyk J. Production of hydrogen via conversion of hydrocarbons using a microwave plasma. J Phys D Appl Phys. 2011;44.
[25] Jasinski M, Czylkowski D, Hrycak B, Dors M, Mizeraczyk J. Atmospheric pressure microwave plasma source for hydrogen production. Int J Hydrogen Energ. 2013;38:11473-83.
[26] Dincer I, Zamfirescu C. Sustainable Hydrogen Production: Elsevier; 2016.
[27] Banerjee S, Musa MN, Jaafar AB. Economic assessment and prospect of hydrogen generated by OTEC as future fuel. Int J Hydrogen Energ. 2016.
[28] Grabner M. Industrial Coal Gasification Technologies Covering Baseline and High-Ash Coal: Wiley-VCH; 2014.
[29] Choi DH, Chun SM, Ma SH, Hong YC. Production of hydrogen-rich syngas from methane reforming by steam microwave plasma. J Ind Eng Chem. 2016;34:286-91.
[30] Miotk R, Hrycak B, Czylkowski D, Dors M, Jasinski M, Mizeraczyk J. Liquid fuel reforming using microwave plasma at atmospheric pressure. Plasma Sources Sci T. 2016;25.
[31] Nakanishi S, Sekiguchi H. Comparison of reforming behaviors of hexane and isooctane in microwave steam plasma. J Jpn Petrol Inst. 2005;48:22-8.
[32] Fall M, Bowlin R, Shulman H. Microwave enhanced cracking of ethane for ethylene production. AIChE Spring Meeting and Global Congress on Process Safety. 2012:1-12.

[33] Mora M, Garcia MD, Jimenez-Sanchidrian C, Romero-Salguero FJ. Transformation of light paraffins in a microwave-induced plasma-based reactor at reduced pressure. Int J Hydrogen Energ. 2010;35:4111-22.
[34] Kim TS, Song S, Chun KM, Lee SH. An experimental study of syn-gas production via microwave plasma reforming of methane, iso-octane and gasoline. Energy. 2010;35:2734-43.
[35] Huang J, Badani MV, Suib SL, Harrison JB, Kablauoi M. Partial Oxidation of Methane to Methanol through Microwave Plasmas - Reactor Design to Control Free-Radical Reactions. J Phys Chem-Us. 1994;98:206-10.
[36] Shen CS, Sun YZ, Sun DK, Yang HS. A study on methane coupling to acetylene under the microwave plasma. Sci China Chem. 2010;53:231-7.
[37] Heintze M, Magureanu M. Methane conversion into acetylene in a microwave plasma: Optimization of the operating parameters. J Appl Phys. 2002;92:2276-83.
[38] Radoiu M, Hussain S. Microwave plasma removal of sulphur hexafluoride. J Hazard Mater. 2009;164:39-45.
[39] Masahiro B. Development of CFCs Decomposition System Using Microwave Plasma. Mitsubishi Heavy Industries, Ltd. 2000;37:83-7.
[40] Rubio SJ, Quintero MC, Rodero A, Rodriguez JMF. Assessment of a new carbon tetrachloride destruction system based on a microwave plasma torch operating at atmospheric pressure. J Hazard Mater. 2007;148:419-27.
[41] Yoon SJ, Lee JG. Hydrogen-rich syngas production through coal and charcoal gasification using microwave steam and air plasma torch. Int J Hydrogen Energ. 2012;37:17093-100.
[42] Lupa CJ, Wylie SR, Shaw A, Al-Shamma'a A, Sweetman AJ, Herbert BMJ. Experimental analysis of biomass pyrolysis using microwave-induced plasma. Fuel Process Technol. 2012;97:79-84.
[43] Paris Knongkrapan NT, and Tanongkiat Kiatsiriroat. Thermochemical Conversion of Waste Papers to Fuel Gas in a Microwave Plasma Reactor. Journal of Clean Energy Technologies. 2013;1:80-3.
[44] Huang YF, Kuan WH, Lo SL, Lin CF. Total recovery of resources and energy from rice straw using microwave-induced pyrolysis. Bioresource Technol. 2008;99:8252-8.
[45] Chen GX, Silva T, Georgieva V, Godfroid T, Britun N, Snyders R, et al. Simultaneous dissociation of CO2 and H2O to syngas in a surface-wave microwave discharge. Int J Hydrogen Energ. 2015;40:3789-96.
[46] van Rooij G, van den Bekerom D, den Harder N, Minea T, Berden G, Bongers W, et al. Taming microwave plasma to beat thermodynamics in CO2 dissociation. Faraday Discuss. 2015;183:233-48.

[47] de la Fuente JF, Moreno SH, Stankiewicz AI, Stefanidis GD. Reduction of CO2 with hydrogen in a non-equilibrium microwave plasma reactor. Int J Hydrogen Energ.
[48] Ma SH, Choi DH, Chun SM, Yang SS, Hong YC. Hydrogen Production by the Water-Gas Shift Reaction Using an Atmospheric Steam Plasma Torch System with a Reverse Vortex Reactor. Energ Fuel. 2014;28:7721-5.
[49] Dias FM, Bundaleska N, Henriques J, Tatarova E, Ferreira CM. Microwave plasma torches used for hydrogen production. 4th International Workshop & Summer School on Plasma Physics 2010. 2014;516.
[50] Wang YF, You YS, Tsai CH, Wang LC. Production of hydrogen by plasma-reforming of methanol. Int J Hydrogen Energ. 2010;35:9637-40.
[51] Khani MR, Guy ED, Gharibi M, Shahabi SS, Khosravi A, Norouzi AA, et al. The effects of microwave plasma torch on the cracking of Pyrolysis Fuel Oil feedstock. Chem Eng J. 2014;237:169-75.
[52] Tatarova E, Bundaleska N, Dias FM, Tsyganov D, Saavedra R, Ferreira CM. Hydrogen production from alcohol reforming in a microwave 'tornado'-type plasma. Plasma Sources Sci T. 2013;22.
[53] Radoiu MT. Studies on atmospheric plasma abatement of PFCs. Radiat Phys Chem. 2004;69:113-20.
[54] Terry LW. System to continuously produce carbon fiber via microwave assisted plasma processing. US Patent. 2014:8 679 592.
[55] Schlemm H, Mai A, Roth S, Roth D, Baumgartner KM, Muegge H. Industrial large scale silicon nitride deposition on photovoltaic cells with linear microwave plasma sources. Surf Coat Tech. 2003;174:208-11.
[56] Adtec. SteriPlas, http://www.adtecplasma.com/products.html#home. (accessed 25-09-2016).
[57] Dischler B, Wild C. Synthetic Diamond: Manufacturing and Applications: Springer-Verlag; 1998.
[58] Rummel P, Grotjohn TA. Methods for modeling microwave plasma system stability. Journal of Vacuum Science & Technology a-Vacuum Surfaces and Films. 2002;20:536-43.
[59] Samukawa S, Hori M, Rauf S, Tachibana K, Bruggeman P, Kroesen G, et al. The 2012 Plasma Roadmap. J Phys D Appl Phys. 2012;45.
[60] Bogdankevich IL, Loza OT, Pavlov DA. Frequency stability in plasma relativistic microwave oscillators. Tech Phys Lett+. 2007;33:629-31.
[61] Bundaleska N, Tsyganov D, Tatarova E, Dias FM, Ferreira CM. Steam reforming of ethanol into hydrogen-rich gas using microwave Ar/water "tornado" - Type plasma. Int J Hydrogen Energ. 2014;39:5663-70.
[62] Reszke E. Split energy delivery to material heating at RF and microwave frequencies. Prz Elektrotechniczn. 2012;88:354-8.

[63] Willis KP, Osada S, Willerton KL. Plasma Gasification: Lessons Learned at EcoValley WTE Facility. 18th Annual North American Waste-to-Energy Conference. 2010.
[64] Kiss AA, Pragt JJ, Vos HJ, Bargeman G, de Groot MT. Novel efficient process for methanol synthesis by CO2 hydrogenation. Chem Eng J. 2016;284:260-9.
[65] Schluter H, Shivarova A. Advanced technologies based on wave and beam generated plasmas: Springer Netherlands; 1999.
[66] Metaxas AC, Meredith RJ. Industrial Microwave Heating, Volume 1: IEE Power Engineering Series 4; 1993.
[67] ATKearney. Chemical Industry Vision 2030: A European Perspective, https://www.atkearney.nl/documents/10192/536196/Chemical+Industry+Vision+2030+A+European+Perspective.pdf/7178b150-22d9-4b50-9125-1f1b3a9361ef. (accessed 05-01-2017).
[68] Hessel V, Cravotto G, Fitzpatrick P, Patil BS, Lang J, Bonrath W. Industrial applications of plasma, microwave and ultrasound techniques: Nitrogen-fixation and hydrogenation reactions. Chem Eng Process. 2013;71:19-30.

6

Conclusions and Recommendations

6.1. Conclusions

The world population is expected to grow from 7 billion today to 9 billion by 2050, and to over 11 billion by the end of the century. Certainly, we all aim to have better living standards, which will lead to consuming more energy. To ensure the increasing demand of energy, it is highly probable that the energy system will end up doubling in size by the end of the century. Undeniably, the production of additional energy cannot be supported by the exploitation of more fossil fuels. Therefore, the world's transition to a lower-carbon energy system will require the development and implementation of extraordinary solutions along with a great amount of innovation. It is time to invest in alternative energy technologies that can promote the sustainable growth of our society.

In this thesis, the application of microwave plasma technology is explored as a promising alternative to tackle two major issues in the energy transition process: the storage of renewable energy and the conversion of carbon dioxide (CO_2) into added-value products. In this context, two reaction processes relevant to the conversion of CO_2, i.e. splitting of pure CO_2 and reduction of CO_2 with a hydrogen source (H_2), have been studied in a bench-scale microwave plasma reactor (*Chapter 2 and 3*). In particular, the focus of this work has been put into the latter reaction system (reduction of CO_2 with H_2) due to its potential to become a technically and economically feasible solution in the short-term. This reaction enables the production of synthesis gas (mixture of H_2 and CO), which can be further processed to manufacture liquid fuels. In addition to experimental research, the use of modelling tools for design and optimization purposes of microwave plasma reactors has been assessed in this thesis. Three different approaches have been proposed based on the level of difficulty to reproduce the kinetics of the studied reactions: (1) 0-D isothermal model for the reduction of CO_2 with H_2 (*Chapter 2*), (2) 1-D kinetic model for the dissociation of CO_2 in non-equilibrium microwave plasma conditions (*Chapter 4*), and (3) 2-D axisymmetric model for the bench-scale microwave plasma reactor considering a much simpler chemistry such as argon; the CO_2 chemistry cannot yet be implemented in multidimensional simulations under the studied conditions (*Chapter 3*). Lastly, a technological roadmap of microwave plasma is presented where the possibilities for scale up are explored together with the scientific and engineering challenges in order to facilitate the transition of this technology to commercial scale (*Chapter 5*).

Most of the research as regards the reduction of CO_2 with H_2, the so-called reverse water-gas shift (RWGS) reaction, has been carried out in thermal

catalytic reactors operating at high temperatures due to the endothermicity of the reaction. The best catalyst performance for the conversion of CO_2 to CO (~60%) was experimentally found to be given by a Cu/Al_2O_3 catalyst under highly diluted conditions (H_2:CO_2 = 60:1). The RWGS reaction has also been studied, to a much lesser extent, in plasma-assisted reactors. The highest conversion of CO_2 to CO (~26%) was achieved in a glow discharge-type reactor. In this thesis, we have shown experimentally that a CO_2 conversion value up to ~80% can be achieved in a non-equilibrium microwave plasma reactor under high microwave power input (~150 W), high feed gas composition ratio (H_2:CO_2=3) and low operating pressure (20-25 mbar) conditions (*Chapter 2*). In a future commercialization of this technology to perform the RWGS reaction, it is required to minimize the use of reducing agents (H_2) as the production cost of H_2 via non-fossil fuel processes still remains relatively high. In this regard, we have proposed a novel modified downstream section of the microwave plasma reactor that enables increase in the absorption of microwave energy by plasma at low feed ratios (H_2:CO_2) (*Chapter 3*). In fact, we have shown that the conversion of CO_2 to CO can be increased by 50%, from 40 to 60%, at a feed ratio of H_2:CO_2 = 1. Concerning the energy efficiency, we have observed values in a low range (~6%); however, it should be emphasized that laboratory-scale microwave plasma equipment is commonly characterized by poor performance as regards energy efficiency. This is mainly due to the low attainable specific energy input, i.e. the ratio between microwave energy and flow rate, compared to pilot/medium-scale units where much higher throughputs can be handled. Besides RWGS, we have experimentally explored the splitting of pure CO_2 for which a maximum CO_2 conversion to CO of 60% and energy efficiency of 8% have been obtained (*Chapter 2*).

The study of three different chemistries (CO_2, CO_2 + H_2, argon) has been performed by distinct approaches that suit each of the reaction systems, i.e. RWGS and CO_2 splitting, the best. With regard to the gas mixture CO_2 + H_2, an isothermal zero dimensional (0-D) reactor model has been considered, given the high complexity to reproduce the RWGS reaction under non-equilibrium microwave plasma conditions (*Chapter 2*). This model has shown that reaction temperatures in the range of 2000 to 2500 K are required to achieve CO_2 conversions of around 80% in a thermally-driven reactor. As proven by optical emission spectroscopy measurements, the gas temperature in the core of the plasma column is around 2500 K, thus demonstrating the validity of the model's predictions. In the case of argon microwave plasma, a two-dimensional (2-D) axisymmetric reactor model has proven the feasibility of using modelling tools (COMSOL Multiphysics) to optimize the performance of microwave

discharges (*Chapter 3*). This model enabled us to investigate the influence of assembling two different downstream reactor configurations in critical process parameters (net input microwave power, gas temperature) and plasma parameters (electron density and temperature). Finally, the dissociation of pure CO_2, a much more complex chemistry compared to argon, has been evaluated in non-equilibrium microwave plasma conditions by a one-dimensional (1-D) simplified kinetic model (*Chapter 4*). The benchmark, a state-to-state kinetic model in which 10000+ reactions among 100+ species are included in order to simulate the dissociation of CO_2, represented an unsuitable option to run multidimensional multiphysics simulations. By applying the concept of chemical lumping, we reduced the original model to solely 44 reactions among 13 species, taking therefore the first step to enable the implementation of complex plasma chemistries into multidimensional multiphysics simulations for optimization purposes.

Even though the limitless possibilities of the plasma technology has been subject of research for the last five decades, the extensive implementation of this technology in the chemical and other branches of the industry is yet to come. The last part of this work is focused on the microwave plasma technology and a roadmap is presented to describe the main requirements and next steps for the implementation of this technology in the chemical industry (*Chapter 5*). We have summarized the state-of-the-art applications of microwave plasma at laboratory- and pilot-scale combined with successfully demonstrated industrial processes. We have shown that high temperature processing applications, such as pyrolysis, gasification and reforming of organic waste, biomass and fossil fuels, have the highest potential to make it through into the chemical industry. At the current technological state of microwave plasma, the development of modular units powered by locally generated renewable electricity seems to be the most appealing option in the category of electricity-driven processes. However, microwave manufacturers believe that more powerful single-unit microwave sources can be made compared to the ones that are currently available (frequency: 915 MHz and output power: 100 kW). In particular, the frequency of 433 MHz might enable the development of microwave sources with an output power in the range of 0.5 to 1 MW. This advancement will certainly have a notably positive impact on further scalability of the microwave plasma technology, which is likely the main barrier to promote wider application of this technology to larger scale operations.

6.2. Recommendations

In this thesis, a detailed parametric study of the reduction of CO_2 with H_2 in a non-equilibrium microwave plasma reactor has been carried out. On the one hand, this work is of significant importance to the scientific community providing sufficient information for future researchers to follow up the study and applicability of the microwave plasma technology in the chemical industry. On the other hand, it only gives a broad insight as to the potentially attainable performance of this type of reactors at larger scale. Therefore, the recommendations are divided into two types: the first type (1-4) focuses on the further investigation of microwave plasma at laboratory/pilot-scale whereas the second type (5-6) highlights important suggestions towards the commercialization of the microwave plasma technology.

1) Although high CO_2 conversions to CO (80%) are reported in this work, the energy efficiency still remains low (6%). Therefore, the RWGS reaction should be studied under thermal plasma conditions (atmospheric pressure), which may result in an increase of the energy efficiency. In fact, we conducted preliminary experiments of the RWGS reaction in an atmospheric pressure microwave plasma unit built in the Process & Energy Department (Delft). The unit consists of a microwave generator (frequency: 2.45 GHz and maximum output power: 6 kW) that enables ignition of plasma at atmospheric pressure and higher throughputs (~100 times larger than the bench-scale unit). Although the results are not included in the thesis, we obtained a H_2 conversion of nearly 100% at a total flow rate = 30 l/min, a feed gas ratio CO_2:H_2 = 2.6, and a net input microwave power = 1.6 kW. The continuation of this experimental work would surely be an interesting scale-up study with respect to microwave energy input, flow rate (throughput), and operating pressure.

2) Similar to the previous recommendation, additional research not only in the realization of experimental energy balances but also in understanding the energy distribution (major energy loss mechanisms) along the studied bench-scale microwave plasma reactor is highly advisable in order to improve the overall energy efficiency. In this work, an experimental energy balance was also attempted. However, due to a large number of uncertainties, mostly relevant to the measurement of temperatures such as the cooling system along with the plasma column axially and radially, a good agreement between the

measured microwave energy input and the calculated total energy output was not achieved.

3) Currently, there is a great amount of effort put into the development of simpler kinetic models (e.g. CO_2 plasma chemistry) that can be implemented in multidimensional multiphysics simulations. Nevertheless, most of the work has mainly been approached from a theoretical point-of-view, which results in quantitative disagreement between computed estimations and experimental results. Hence, it is encouraged to continue the work on reduction of complex kinetic models via more practical approaches. For example, the introduction of one or more experimental parameters into the model is an appealing option, as such parameters can be adjusted based on each particular system and operating conditions.

4) An interesting area of research is the development of hybrid systems, i.e. the combination of two or more technologies to attain a better reactor performance than that obtained by using a single technology. In the context of process intensification, microwave plasma reactors may potentially be combined with other technologies, such as plasma catalysis, laser-plasma hybrid technology, and plasma catalysis combined with solid oxide electrolyser cells (SOEC). For instance, in the latter case, Shinsuke Mori et al. (2015) reported that the synthesis of carbon nanotubes can be performed with a CO_2 conversion of nearly 100% by combining plasma, catalyst, and SOEC. The use of the SOEC allowed the removal of oxygen formed during the reaction, which suppressed the recombination of CO to CO_2, and therefore it increased the overall CO_2 conversion.

5) In the field of plasma technology, the chemistry and reactor performance have been the main focus of research, while the interest in process technology development has been rather limited. If this technology is to be used at industrial scale, most of the processing applications will most likely require to be run in continuous operation. To do so, microwave plasma reactors should be highly automated, which is not a straightforward task given the extremely fast dynamics of plasma. Therefore, the development of control models and strategies that not only allow to regulate process parameters (microwave power input, throughput, gas temperature), but also to control plasma parameters (electron density and temperature) in-situ are required to

succeed in completing the last given recommendation (no. 6). An example of an interesting measurement and control device would be a spectrometer that measures the emission intensity of active species and directly translates those measurements into temperature and/or density values, which may notably speed up the optimization process.

6) Last, but equally important with the previous recommendations, it should be noted that microwave plasma is strictly related to each individual reaction system. As a result of the high amount of research done at laboratory scale, there is seldom relevant information to evaluate the feasibility of this technology at larger (commercial) scale. It is imperative to demonstrate the complete process feasibility at medium-scale to convince industry to invest in the microwave plasma technology. Thus, the construction of medium-scale plants at technology readiness levels (TRL) 4-7 should be one of the main lines of research hereafter. Afterwards, validated scale up rules of (microwave) plasma units should be developed.

List of publications

Journal articles

1. de la Fuente JF, Moreno SH, Stankiewicz AI and Stefanidis GD, A new methodology for the reduction of vibrational kinetics in non-equilibrium microwave plasma: application to CO_2 dissociation. *Reaction Chemistry & Engineering* 1: 540-554 (2016).

2. de la Fuente JF, Moreno SH, Stankiewicz AI and Stefanidis GD, Reduction of CO2 with hydrogen in a non-equilibrium microwave plasma reactor. *International Journal of Hydrogen Energy* 41: 21067-21077 (2016).

3. de la Fuente JF, Kiss AA, Radoiu MT and Stefanidis GD, Microwave plasma emerging technologies for chemical processes. *Journal of Chemical Technology & Biotechnology*: doi:10.1002/jctb.5205 (2017).

4. de la Fuente JF, Moreno SH, Stankiewicz AI and Stefanidis GD, On the improvement of chemical conversion in a surface-wave microwave plasma reactor for CO_2 reduction with hydrogen (The Reverse Water-Gas Shift reaction). *International Journal of Hydrogen Energy* 42: 12943-12955 (2017).

Conference Proceedings

Selected oral presentations

de la Fuente JF, Sturm GSJ, Stankiewicz AI and Stefanidis GD, Reduction of CO_2 with H_2 in a microwave-driven plasma reactor. 3GCMEA, Cartagena (Spain, 2016).

de la Fuente JF, Sturm GSJ, Stankiewicz AI and Stefanidis GD, Microwave-driven plasma for CO_2 chemical utilization. AMPERE, Krakow (Poland, 2015).

Selected poster presentations

de la Fuente JF, Sturm GSJ, Stankiewicz AI and Stefanidis GD, Study of catalytic properties of microwave-induced plasma in CO_2 utilization reactions. ECCE, Nice (France, 2015).

de la Fuente JF, Sturm GSJ, Stankiewicz AI and Stefanidis GD, Study of microwave-driven plasma reactors in CO_2 chemical utilization. ISPC, Antwerp (Belgium, 2015).

de la Fuente JF, Sturm GSJ, Stankiewicz AI and Stefanidis GD, Gas phase reactions under microwave-driven plasma for CO_2 utilization. NPS14, Utrecht (The Netherlands, 2014).

de la Fuente JF, Sturm GSJ, Stankiewicz AI and Stefanidis GD, Study of catalytic properties of microwave plasma in CO_2 utilization reactions. DPTI, Rotterdam (The Netherlands, 2014).

Curriculum vitae

Javier Fernandez was born in Valladolid, Spain. He was awarded as one of the best students of the year (2006) in high school by graduating within the top 5% of the class. In 2012, he completed his M.Sc. degree in Chemical Engineering at Valladolid University (Spain). He graduated in the top 10% of his year. He has broad experience as a R&D engineer, mostly focused on the production of liquid fuels through innovative and sustainable technologies. He has worked on projects such as (1) the design of a pervaporation unit, based on membranes, to separate butanol from acetone-butanol-ethanol (ABE) mixture as an alternative to distillation, and (2) the start-up and optimization of an ammonia fiber expansion pilot plant to pre-treat wheat straw for the production of ethanol. Moreover, he explored a new approach to produce MCM-41 for the encapsulation of ibuprofen by ultrasound-assisted supercritical CO_2 during his stage at Ruhr University of Technology in Germany (2011-2012). He joined Delft University of Technology (March 2013) as PhD researcher to work on the application of microwave plasma technology to convert CO_2 into high value-added products. In September (2017), he joined the Pipeline Development Program for chemical engineers at Hexion.

For more information:

Linkedin
https://www.linkedin.com/in/javierfdelafuente

Email
javier.f.delafuente@gmail.com

Acknowledgements

This important chapter of my life, the doctoral studies, has come to an end. In preparation for writing this final section, I have realized that there are thousands, if not millions, of thoughts coming to my mind about all the experiences that I lived throughout this PhD journey. When reflecting on the decision I took almost 5 years ago to pursue a PhD, I still feel it is unclear as to why I chose this pathway. I can only find an answer by recalling one of the most sounded John F. Kennedy speeches in 1961: "*We choose to go to the Moon in this decade and do the other things, not because they are easy, but because they are hard; because that goal will serve to organize and measure the best of our energies and skills, because that challenge is one that we are willing to accept, one we are unwilling to postpone, and one we intend to win".*

From beginning to end, one must be prepared to face difficult challenges and adversities that cannot be expressed by words. Fortunately, I was lucky enough to have the support and encouragement of great people who always made me push forward into finishing this book. I would like to take this opportunity to express my most sincere gratitude to all of those who helped me during my doctoral journey.

In first place, I would like to thank my promotor, Professor Andrzej Stankiewicz, who has been a supportive figure throughout my PhD. He was always there when I needed his encouragement and inspiration to carry on with my work. I will never forget all the progress meetings we had to discuss rather complex issues and how to deal with them. Moreover, I cannot miss the opportunity to thank you once again for giving me the chance to celebrate your 60th birthday in Poland, your home country, which was an unforgettable experience. Tip: if you are reading this book and have never been to Poland, you should certainly consider spending few days off visiting Krakow and Warsaw.

I am equally thankful to my co-promotor and now promotor, Professor Georgios Stefanidis, who made all of this possible. He gave me the chance to join one of the best technical universities in Europe and pursue my dream of becoming a doctor in the field of Chemical Engineering. Even though the journey has been long and bumpy, he was always the compass of my PhD thesis. He guided me through windstorms that, without him, I would have never survived. He helped me improve not only as a researcher, but also as

a writer by significantly contributing to the correction of our publications. Thank you Georgios.

I would also like to thank Professor Herman Kramer, with whom I shared a significant number of hours working on the preparation of assignments, case studies, Aspen tutorials, and exams for the course Process Plant Design. I think we have learned a lot from each other, especially when struggling with AspenPlus.

A special appreciation should be given to the DEMO staff, our beloved technicians, for helping with the design, engineering, procurement, construction and start-up of the systems used in this work. Back in the old P&E building, I would like to thank Andre van den Bosch and Gerard van de Sande for your technical support. Concerning the new P&E building, I sincerely thank Gerard once more, Lennart Middelplaats, with whom I worked on design and controllability issues of the microwave plasma reactor, Bas Overtoom and Martijn Karsten, who helped me with all the technical and electrical issues in the construction of the unit. Last but not least, I am grateful to Guido Sturm, who actively participated in the design and construction phase of the system, Michel van den Brink for making sure that safety goes first, and finally Jaap van Raamt and Aad Beeloo for managing the lab facilities.

Leslie van Leeuwen and Helma Duijndam-Nieuwpoort, you are the best secretaries ever. You were always willing to help me whenever I needed something, always keeping a very positive attitude with a smile on the face. Thank you for making our life's so much easier.

I would also like to acknowledge some of the industrial partners, Dr. Marilena Radoiu and Dr. Louis Latrasse from Sairem, who greatly supported me when I encountered difficulties understanding the complex subject of microwave plasma. Marilena, thank you for accepting my invitation to collaborate in one of my publications. Thank you Dr. Tony Kiss from AkzoNobel, for sparking very interesting scientific discussions, and also for bringing into the project your industrial experience, which led to the publication of a technological roadmap on microwave plasma technology.

When I started my PhD journey back in 2013, I found an amazing group of people at the P&E department that, luckily for me, made the adaption process very enjoyable. What great memories I have from my first office-

mates at the old P&E building: Rohit Kacker, Cristian Brunchi, and Alvaro Fernandes. Not only my office-mates were great, also colleagues in my group (IRS) and in the whole P&E department were always friendly with me. I still remember as if it was yesterday every Thursday late afternoon enjoying a cool beer in Delft city centre with George Krintiras, Rohit Kacker, George Tsalidis, Onursal Yakaboylu, Gerasimos Sarras, Konstantinos Anastasakis, and others. I also remember all our IRS progress meetings having well-deserved drinks & snacks afterwards. Daniel Irimia, Cristian Brunchi, Anamaria Soare, Marloes Reus, David Branco, Rohit Kacker, Guido Sturm, Lalit Gangurde, WeiWei Li, Fatemeh Anisi, Maryam Khodadadian, and Samir Kulkarni, thank you all for making these meetings memorable. I should also thank my office-mates at the new P&E building, Sergio Moreno, Tim Becker, Meng Wang, Farnaz Eghbal, and Xuan Tao, who supported me during the final phase of my PhD.

I would also like to thank the graduate school for organizing the PhD start-up course, where I had the pleasure to meet the start-up crew (Vallin, Tophi, Matija, Alexey, and of course Rohit). All the experiences, especially at night, that we enjoyed together helped me make it to the point where I am today. Without you guys probably I would have never made it.

I would also like to acknowledge some of my gym buddies, the ones that did not last long, Cristian and George, and the ones who still keep it up, Vallin and Rohit. Vallin, tío muchas gracias por estar ahí cuando más lo he necesitado, por los buenos momentos en el gimnasio motivándonos uno a otro para ser mejores.

There are two colleagues who deserve my most sincere gratitude, Rohit Kacker and Sergio Moreno. Rohit, what can I say? Thank you so much for being always there when I needed someone to talk to, I wish you all the best in your life and hope we keep in touch in the future. Sergio, thank you from the bottom of my heart for everything. Muchas gracias por tu apoyo y constante ayuda, sobre todo en discusiones sobre plasma y papers.

Hanaa El Hilali, thank you very much for translating the summary in such a short notice. It was very kind of you.

To all my friends who somehow have also been part of this amazing journey, I would also like to thank you, Enrique, Ricardo, Robin, Laura, Javier, Anshuman, Ethan, Luismi, Alessandro and many others.

Particularly I would like to thank my family, Pirulo, Mamu, Chuchi y Angelines, muchísimas gracias por todo lo que me habéis dado, por vuestro apoyo incondicional, y aunque ahora no estemos juntos, siempre os llevo y os llevare en mi corazón. I am grateful to my friends in Spain, especially Carlos, Ruben, Ricardo, Alfonso, Casqueta, and Hugo, siempre seréis mis mejores compis de fiesta golfos.

I would like to end by thanking the most important person in my life, Alexandra, my soulmate, my driving force, my compass in life, the person who has changed my life and the way I feel about the meaning of love. Alexandra, you know better than anyone that without you I would have never finished this book. I will be eternally thankful to you. I could not ask more from you, I love you Bu&Me. Lastly, your family Alexandra, you are lucky to have such a nice family who has always accepted me as one of your own, obrigado Felismina, Ana, Fernando, Ricardo and Carlos.

Javier Fernández,
Delft, June 2017